The Dissertation Committee for Dong Eun Seo
certifies that this is the approved version of the following dissertation:

Noncertainty Equivalent Nonlinear Adaptive Control and its Applications to Mechanical and Aerospace Systems

Committee:

Maruthi R. Akella, Supervisor

David G. Hull

Robert H. Bishop

Glenn Lightsey

S. Joe Qin

Noncertainty Equivalent Nonlinear Adaptive Control and its Applications to Mechanical and Aerospace Systems

by

Dong Eun Seo, B.S.M.E., M.S.

Dissertation

Presented to the Faculty of the Graduate School of

The University of Texas at Austin

in Partial Fulfillment

of the Requirements

for the Degree of

Doctor of Philosophy

The University of Texas at Austin

August 2007

To my wife and family

Acknowledgments

I would like to thank my advisor, Professor Maruthi R. Akella for his advices and encouragements during the dissertation research. He is the person who not only led me to the field of control theory but guided me while I lost in study. I am sure that what he taught me of philosophical way of thinking with his comprehensive knowledge will be in my mind for the rest of my life.

I also would like to thank all my committee members, Professor David G. Hull, Professor Robert H. Bishop, Professor Glenn Lightsey, and Professor S. Joe Qin. They provided the foundation of my knowledge and gave me inspiration of how to approach problems from various perspectives by lectures, seminars and classes. There are other people that I want to express my gratitude. My friends and staffs in ASE/EM department who supported my academic life and encouraged me in doing my best.

I am always thankful to Professor Sang-Yong Lee in Korea Advanced Institute of Science and Technology (KAIST) who was my mentor and gave me a chance to study aborad.

Finally, I want to give my sincere appreciation to my wife, Dr. Jiwon Kim, who became my soul mate always standing beside me, and my family who made all that I have possible. I wish to thank my father, mother, and sister for their love and support. I wish I can do the same things to my son, Ryan, who was born during my wife's dissertation.

The present work was partially supported by the National Science Foundation and NASA Goddard Spaceflight Center.

Dong Eun Seo

The University of Texas at Austin
August 2007

Noncertainty Equivalent Nonlinear Adaptive Control and its Applications to Mechanical and Aerospace Systems

Publication No. _____

Dong Eun Seo, Ph.D.
The University of Texas at Austin, 2007

Supervisor: Maruthi R. Akella

Adaptive control has long focused on establishing stable adaptive control methods for various nonlinear systems. Existing methods are mostly based on the certainty equivalence principle which states that the controller structure developed in the deterministic case (without uncertain system parameters) can be used for controlling the uncertain system along by adopting a carefully determined parameter estimator. Thus, the overall performance of the regulating/tracking control depends on the performance of the parameter estimator, which often results in the poor closed-loop performance compared with the deterministic control because the parameter

estimate can exhibit wide variations compared to their true values in general. In this dissertation, we introduce a new adaptive control method for nonlinear systems where unknown parameters are estimated to within an attracting manifold and the proposed control method always asymptotically recovers the closed-loop error dynamics of the deterministic case control system. Thus, the overall performance of this new adaptive control method is comparable to that of the deterministic control method, something that is usually impossible to obtain with the certainty equivalent control method. We apply the noncertainty equivalent adaptive control to study application arising in the n degree of freedom (DOF) robot control problem and spacecraft attitude control. Especially, in the context of the spacecraft attitude control problem, we developed a new attitude observer that also utilizes an attracting manifold, while ensuring that the estimated attitude matrix confirms at all instants to the special group of rotation matrices $SO(3)$. As a result, we demonstrate for the first time a separation property of the nonlinear attitude control problem in terms of the observer/controller based closed-loop system. For both the robotic and spacecraft attitude control problems, detailed derivations for the controller design and accompanying stability proofs are shown. The attitude estimator construction and its stability proof are presented separately. Numerical simulations are extensively performed to highlight closed-loop performance improvement vis-a-vis adaptive control designs obtained through the classical certainty equivalence based approaches.

Contents

List of Figures

Chapter 1

Introduction

This chapter is devoted to basic concepts of adaptive control for further discussion on the main results. At the beginning, two conventional adaptive control design methods are explained, both of which are based on the certainty equivalence principle. The following section discusses about noncertainty equivalence control based on the analysis of differential topology. Motivation of the research is placed at the end of this chapter.

1.1 Adaptive Control Principle

The control method that is able to adjust itself to unknown system parameters (circumstances) without sacrificing system stability is defined as the adaptive control. Thus, adaptive control requires a systematic design tool for automatic adjustment of itself in real time in order to achieve or maintain a desired control performance when the system parameters are uncertain or varying in time. Because of the property of the adaptive control, it has attracted increasing attention by both researchers and practitioners. Since every system has unknown structure/parameters or disturbances/defects in its dynamics virtually, verified and robust adaptive control

methods are always requested from diverse applications such as industrial robots, aeromechanical systems, and underwater vehicles.

The definition (or concept) of adaptive control first appeared at 1950's but development of practical control methods (earlier conceptual design of model reference adaptive control) started in 1960's[1], which is followed by an era of meaningful theoretical progress in 1970's and 1980's (starting from Lyapunov theory and use of Barbalat's lemma). Nowadays, adaptive control is one of mature branch in control theories and there exists a large amount of published literature on designing adaptive controllers[2–4]. As a next phase of development, adaptive control confronts many important challenges which include a faster response time for real-time applications, a multi-agent cooperative control for flexible mission designs, a bio-mechanical control for continuously changing interaction with environments, etc. To cope with one of those challenges, a high performance adaptive control is addressed throughout this dissertation.

Based on the adaptation algorithm, conventional adaptive control methods are broadly categorized into two groups: one is a direct adaptive control and the other is an indirect adaptive control scheme. The term 'direct' and 'indirect' are used to differentiate the relationship between the estimator for unknown system parameters and the controller. In the following two sections, the detailed structure of each control scheme is presented. In addition, a noncertainty equivalence adaptive control is explained as a different approach to adaptation.

1.1.1 Model Reference Adaptive Control

Model reference adaptive control (also called a direct adaptive control) consists of one unit which is used for control parameter adaptation and system control simultaneously. In Fig. 1.1, a schematic diagram of MRAC is shown.

A MRAC-type control law is designed as follows. First, the reference model

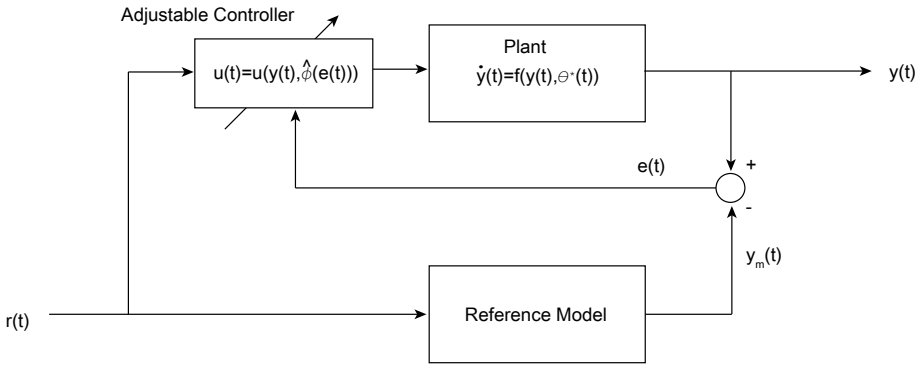

Figure 1.1: MRAC control scheme

system should be identified wherein all the key performance requirements are considered and its feasibility on the actual system is guaranteed. Then, the control structure is defined as if necessary control parameters are known. At this stage, controller is parameterized by stabilizing control parameters $\boldsymbol{\phi}^*$ (usually a constant or considered as a constant with slow-change assumption in time), not by unknown system parameters $\boldsymbol{\theta}^*$. Finally, control parameter update law is designed and estimates from control parameter estimator $\hat{\boldsymbol{\phi}}$ replace actual control parameters $\boldsymbol{\phi}^*$ in the previously designed control law.

For example, consider the following first-order linear time-invariant plant modified from [5]

$$\dot{y}(t) = \theta^* y(t) + bu(t), \quad t > 0 \tag{1.1}$$

where $\theta^*,\ b$ are unknown constant real system parameters, $y(t)$ is a system output, and $u(t)$ is a control input. In addition, we assume $b > 0$ (in fact, this assumption on b can be replaced with the relaxed assumption that the sign of b is known, but here $b > 0$ for the simplicity). Then, the control objective is to design an adaptive control input such that all closed-loop signals are bounded and $y(t)$ tracks, asymptotically,

$y_m(t)$ given by

$$\dot{y}_m(t) = -a_m y_m(t) + r(t), \quad t > 0 \tag{1.2}$$

where $a_m > 0$. The stabilizing control law for the given system is expressed by

$$u(t) = -\frac{\theta^*}{b} y(t) + \frac{1}{b} \left[-a_m y(t) + r(t) \right], \quad t > 0 \tag{1.3}$$

Since both θ^* and b are unknown, the structure of an adaptive controller is given by

$$u_a(t) = \hat{\phi}_1(t) y(t) + \hat{\phi}_2(t) \left[-a_m y(t) + r(t) \right] \tag{1.4}$$

which is designed with an assumption that stabilizing control parameter $\phi_1^* = -\frac{\theta^*}{b}$ and $\phi_2^* = \frac{1}{b}$ are known. Finding update laws for $\dot{\hat{\phi}}_1(t)$ and $\dot{\hat{\phi}}_2(t)$can be done in various ways depending on design philosophies. However, for nonlinear systems (to be handled in this dissertation), not much options are left and each design method is sensitive to the system structure. Consider the following update laws for $\hat{\phi}_1(t)$ and $\hat{\phi}_2(t)$:

$$\dot{\hat{\phi}}_1(t) = -\gamma_1 y(t) e(t) \tag{1.5}$$

$$\dot{\hat{\phi}}_2(t) = -\gamma_2 \left[-a_m y(t) + r(t) \right] e(t) \tag{1.6}$$

where $e(t) \doteq y(t) - y_m(t)$ is a tracking error and $\gamma_1, \gamma_2 > 0$ are learning rates for each update law. Then, we can show that $e(t) \to 0$ as $t \to \infty$ asymptotically by analyzing the following Lyapunov candidate function

$$V = \frac{1}{2} e(t)^2 + \frac{b}{2\gamma_1} \tilde{\phi}_1(t)^2 + \frac{b}{2\gamma_2} \tilde{\phi}_2(t)^2 \tag{1.7}$$

where $\tilde{\phi}_1(t) \doteq \hat{\phi}_1(t) - \left(-\frac{\theta^*}{b}\right)$ and $\tilde{\phi}_2(t) \doteq \hat{\phi}_2(t) - \frac{1}{b}$ are parameter estimation errors. In the subsequent analysis, time argument 't' is dropped off for the notational

simplicity except when there is a need for emphasis. The time derivative of V in Eq. (1.7) along with system trajectories by Eq. (1.1), Eq. (1.2), Eq. (1.4), Eq. (1.5), and Eq. (1.6) leads to the following inequality

$$\begin{aligned}
\dot{V} &= e\dot{e} + \frac{b}{\gamma_1}\dot{\hat{\phi}}_1\tilde{\phi}_1 + \frac{b}{\gamma_2}\dot{\hat{\phi}}_2\tilde{\phi}_2 \\
&= e\left[\theta^* y + bu_a + a_m y - r\right] + \frac{b}{\gamma_1}\dot{\hat{\phi}}_1\tilde{\phi}_1 + \frac{b}{\gamma_2}\dot{\hat{\phi}}_2\tilde{\phi}_2 \\
&= e\left[\theta^* y + b\hat{\phi}_1 y + b\hat{\phi}_2(-a_m y + r) + a_m y - r - a_m(y - y_m)\right] + \\
&\quad \frac{b}{\gamma_1}\dot{\hat{\phi}}_1\tilde{\phi}_1 + \frac{b}{\gamma_2}\dot{\hat{\phi}}_2\tilde{\phi}_2 \\
&= e\left[b\tilde{\phi}_1 y + b\tilde{\phi}_2(-a_m y + r) - a_m e\right] + \frac{b}{\gamma_1}\dot{\hat{\phi}}_1\tilde{\phi}_1 + \frac{b}{\gamma_2}\dot{\hat{\phi}}_2\tilde{\phi}_2 \\
&= -a_m e^2 + bye\tilde{\phi}_1 + b(-a_m y + r)e\tilde{\phi}_2 + \frac{b}{\gamma_1}\dot{\hat{\phi}}_1\tilde{\phi}_1 + \frac{b}{\gamma_2}\dot{\hat{\phi}}_2\tilde{\phi}_2 \\
&= -a_m e^2 \leq 0
\end{aligned} \tag{1.8}$$

Since V is radially unbounded and $\dot{V} \leq 0$, $\lim_{t\to\infty} V(t) \doteq V_\infty$ exists and is finite, which means every closed signal is bounded (i.e., they belong to $\mathcal{L}_\infty$). Thus, $e \in \mathcal{L}_\infty \cap \mathcal{L}_2$ from $V_\infty - V(0) = \int_0^\infty \dot{V}(\sigma)d\sigma$. In addition, $\dot{e} \in \mathcal{L}_\infty$ from its definition. Finally, $\lim_{t\to\infty} e(t) = 0$ by using Barbalat's lemma.

In this simple MRAC example, we may take the following observations:

1. Design of adaptive control law starts from the deterministic control design where there is no uncertainty in system parameters. It is called the certainty equivalence (CE) principle.

2. Based on Eq. (1.5) and Eq. (1.6), parameter update laws are driven by system errors (trajectory tracking errors), not by parameter estimation errors. As a result, parameter estimates deviate from their true values as long as there exist nonzero system errors.

3. The result of Eq. (1.8) tells us only about $e(t)$. To achieve the zero parameter

estimation error, reference trajectory $y_m(t)$ should satisfy certain condition which is called the persistence excitation condition derived from Eq. (1.5) and Eq. (1.6).

Listed characteristics are considered as common to CE-based control designs. In the next section, we show the other adaptive control design philosophy based on the certainty equivalence principle, that is expected to share the preceding properties of CE-based control methods.

1.1.2 Indirect Adaptive Control

Different from MRAC (direct adaptive control), an indirect adaptive control scheme consists of two parts: one is a system controller whose control parameters pretend to be known (i.e., deterministic control design) and the other is a system parameter estimator. Thus, in the indirect adaptive control method, system parameters are estimated explicitly and then they are used to determine control parameters. In Fig. 1.2, we can see an additional estimator between the system controller and the plant in contrast with Fig. 1.1.

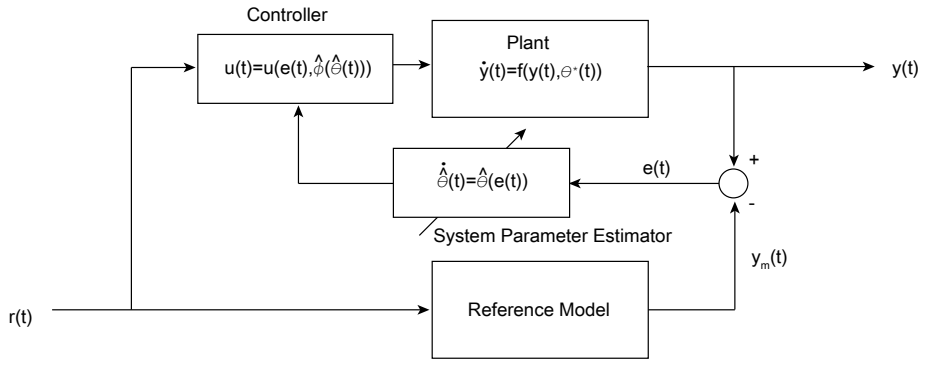

Figure 1.2: Indirect adaptive control scheme

Since this scheme is explicitly estimating the unknown system parameters, we may have an extra information about the plant compared to the MRAC scheme. To highlight the difference between the MRAC and the indirect adaptive control, we use the same equation as Eq. (1.1), Eq. (1.2), and Eq. (1.3) as an example. Since we have two unknown system parameters θ^* and b, $\hat{\theta}(t)$ and $\hat{b}$ are needed. The corresponding adaptive controller is designed as follows

$$u_a(t) = \frac{1}{\hat{b}(t)} \left[-\hat{\theta}(t) y(t) - a_m y(t) + r(t) \right] \tag{1.9}$$

Therefore, in the indirect adaptive control scheme, adaptation is applied to a system parameter and the task is to design both $\dot{\hat{\theta}}(t)$ and $\dot{\hat{b}}(t)$ which stabilize the overall closed-loop system. Consider the following update laws:

$$\dot{\hat{\theta}}(t) = \gamma_1 y(t) e(t) \tag{1.10}$$

$$\dot{\hat{b}}(t) = \gamma_2 u_a(t) e(t) \tag{1.11}$$

where $e(t)$ is the trajectory tracking error defined as before and $\gamma_1, \gamma_2 > 0$ are learning rates for each update law (they play the same role as in MRAC). Next, define the Lyapunov candidate function as follows

$$V = \frac{1}{2} e^2 + \frac{1}{2\gamma_1} \tilde{\theta} + \frac{1}{2\gamma_2} \tilde{b} \tag{1.12}$$

where $\tilde{\theta} \doteq \hat{\theta} - \theta^*$ and $\tilde{b} \doteq \hat{b} - b$ are parameter estimation errors. Then, taking the time derivative of V in Eq. (1.12) along with Eq. (1.1), Eq. (1.2), Eq. (1.9),

Eq. (1.10), and Eq. (1.11) gives us

$$\begin{aligned}
\dot{V} &= e\dot{e} + \frac{1}{\gamma_1}\dot{\hat{\theta}}\tilde{\theta} + \frac{1}{\gamma_2}\dot{\hat{b}}\tilde{b} \\
&= e\left[\theta^* y + b u_a + a_m y_m - r\right] + \frac{1}{\gamma_1}\dot{\hat{\theta}}\tilde{\theta} + \frac{1}{\gamma_2}\dot{\hat{b}}\tilde{b} \\
&= e\left[\theta^* y - \tilde{b} u_a + \hat{b} u_a + a_m y - r - a_m e\right] + \frac{1}{\gamma_1}\dot{\hat{\theta}}\tilde{\theta} + \frac{1}{\gamma_2}\dot{\hat{b}}\tilde{b} \\
&= -a_m e^2 - y e\tilde{\theta} - u_a e\tilde{b} + \frac{1}{\gamma_1}\dot{\hat{\theta}}\tilde{\theta} + \frac{1}{\gamma_2}\dot{\hat{b}}\tilde{b} \\
&= -a_m e^2 \leq 0
\end{aligned} \tag{1.13}$$

If $\hat{b} \neq 0$ for all t, then we may conclude that $\lim_{t\to\infty} e(t) = 0$ following the similar arguments on closed-loop signal boundedness and Barbalat's lemma as in the previous MRAC section. Therefore, following observations are in order

1. As in the MRAC design, the control design is based on the deterministic control case as in Eq. (1.3) for indirect adaptive control scheme. In other words, the indirect adaptive controller also considers the estimated value as the true system parameter. In other words, the indirect adaptive control scheme is also developed based on the certainty equivalence principle.

2. Different from MRAC, each unknown system parameter is estimated explicitly. Thus, the resultant structure of the indirect adaptive control law is identical to the deterministic control law given in Eq. (1.3).

3. To implement Eq. (1.9), we need to guarantee $\hat{b}(t) \neq 0$ for all t. This requires the projection for $\hat{b}$ with an extra information of b (we already know $b > 0$).

Necessity of Projection Mechanism for $\hat{b}(t)$

In addition to $b > 0$, assume that b_o, the lower bound of b, is known (i.e., $b \geq b_o$). Then, the update law for $\hat{b}$ is modified as follows

$$\dot{\hat{b}}(t) = \begin{cases} \gamma_2 u_a(t) e(t), & \hat{b}(t) \geq b_o \\ 0, & \hat{b}(t) = b_o \text{ and } e(t)u_a(t) < 0 \end{cases} \tag{1.14}$$

The modified update law for $\hat{b}(t)$ guarantees that $\hat{b}(t) \geq b_o$ for all t with $\hat{b}(0) \geq b_o$. Corresponding stability proof can be shown from Eq. (1.13). If $\hat{b}(t^*) = b_o$ and $u_a(t^*)e(t^*) < 0$ at some t^* (i.e., $\hat{b}$ is about to be smaller than b_o from Eq. (1.11) after t^*), then $\dot{\hat{b}}(t^*)$ is set to zero until $\hat{b}(t)$ starts increasing again at some $t > t^*$ by Eq. (1.14). Therefore, $\dot{V} = -a_m e^2 - \tilde{b}ue \leq 0$ because $\tilde{b}ue \geq 0$. As shown in the preceding arguments, the projection mechanism helps the parameter estimate stay within the known space where the true parameter value reside. In fact, the method of projection for adaptation is useful when there is an unmodeled dynamics and this will be discussed in the next chapter. Finally, we guarantee that $e(t) \to 0$ as $t \to \infty$ asymptotically in the indirect adaptive control scheme combined with the projection mechanism and may summarize the followings about the projection:

1. The projection method for $\hat{b}(t)$ guarantees the stability of the indirect adaptive control method when there is an unknown high frequency gain b.

2. Although the projection mechanism successfully stabilizes the tracking system and enables us to implement Eq. (1.9), it introduces a nonsmooth parameter estimate and thereby, a potential nonsmooth control signal, which is not desirable in a practical sense.

1.1.3 Noncertainty Equivalence Adaptive Control

Besides MRAC and indirect adaptive control schemes, a different approach to adaptive control problems is suggested[6] and its applications are presented[7–9], which is called an immersion and invariance (I&I) control. Immersion is a mapping between manifolds whose derivative is injective everywhere. In usual, immersion is defined from the higher dimensional manifolds to the lower dimensional manifold for the mapping to be injective (i.e., nonsingular map). In the context of the adaptive control design, immersion is used to transform the given nonlinear system involving parameter estimate into the reduced order dynamics (target dynamics) in terms of system states which is locally/globally stable with respect to the equilibrium points. In spite of benefits from immersion such as smooth control trajectory, there is a major restriction for it to be applied to general nonlinear systems. The nonlinearity of closed-loop dynamics should also have an attractive implicit manifold as well as a proper immersion[6] where the implicit manifold represents the unknown parameter adaptation . By the following example, each concepts in I&I control method are demonstrated. Consider the following nonlinear trajectory tracking control system

$$\dot{y}(t) = \underbrace{y^2(t)}_{f(y(t))}\,\theta^* + u(t), \quad t > 0 \tag{1.15}$$

where θ^* is an unknown system parameter and $f(y)$ is a regressor for the system parameter θ^*. We denote the reference trajectory as $y_m(t)$ as before. Since θ^* is unknown, entire error system including adaptation is represented as follows

$$\Sigma : \begin{cases} \dot{e}(t) &= f(y(t))\theta^* + u(t) - \dot{y}_m(t) \\ \dot{\hat{\theta}}(t) &= \beta_2(t) \end{cases} \tag{1.16}$$

where $e(t) \doteq y(t) - y_m(t)$ and $\beta_2(t)$ will be determined. An I&I controller proposed by [6] is given as

$$u(t) = -e(t) - f(y(t)) \left[\hat{\theta}(t) + \beta_1(y(t))\right] + \dot{y}_m(t) \tag{1.17}$$

If we can find $\beta_1(y)$ satisfying the following

$$\frac{\partial \beta_1(y)}{\partial y} f(y) + \left[\frac{\partial \beta_1(y)}{\partial y} f(y)\right]^T > 0 \tag{1.18}$$

then, $\beta_2(t)$ is determined and the closed-loop system is asymptotically stable. Consider the following Lyapunov candidate function

$$V = \frac{1}{2}e^2 + \frac{1}{2\gamma}z^2 \tag{1.19}$$

where $z \doteq \hat{\theta} + \beta_1 - \theta^*$ and $\gamma > 0$. Then, by taking the time derivative of V in Eq. (1.19) along with Eq. (1.16) and Eq. (1.17), we have

$$\begin{aligned} \dot{V} &= e(-e - y^2 z) + \frac{1}{\gamma} z \left[\dot{\hat{\theta}} + \frac{\partial \beta_1}{\partial y}(-e - y^2 z + \dot{y}_m)\right] \\ &= e(-e - y^2 z) + \frac{1}{\gamma} z \left[\beta_2(t) + \frac{\partial \beta_1}{\partial y}(-e - y^2 z + \dot{y}_m)\right] \end{aligned} \tag{1.20}$$

Now, choose $\beta_1(y)$ as

$$\beta_1(y) = \frac{\gamma}{3} y^3 \tag{1.21}$$

which satisfies Eq. (1.18) obviously. Subsequently, $\beta_2(t)$ is determined as

$$\beta_2(t) = \gamma y^2 (y - y_m - \dot{y}_m) \tag{1.22}$$

Substituting Eq. (1.21) and Eq. (1.22) into Eq. (1.20) leads to the following inequality

$$\begin{aligned}\dot{V} &= -e^2 - ey^2z - y^4z^2 \\ &= -\frac{1}{2}e^2 - \frac{1}{2}y^4z^2 - \frac{1}{2}(e + y^2z)^2 \\ &\leq -\frac{1}{2}e^2 - \frac{1}{2}y^4z^2 \end{aligned} \tag{1.23}$$

Since V is radially unbounded and $\dot{V} \leq 0$, $\lim_{t\to\infty} V(t) \doteq V_\infty$ exists and is finite. Thus, $e, z \in \mathcal{L}_\infty$. From $\int_0^\infty \dot{V}(\sigma)d\sigma = V_\infty - V(0)$, $e, y^2z \in \mathcal{L} \in \mathcal{L}_2 \cap \mathcal{L}_\infty$. In addition, $\dot{e}$, $\frac{d}{dt}(y^2z) \in \mathcal{L}_\infty$. Therefore, by Barbalat's lemma, $\lim_{t\to\infty}[e, y^2z] = 0$. For the given nonlinear system Eq. (1.16), the immersion π is defined as

$$\pi : [e] \to \begin{bmatrix} e \\ \theta^* - \beta_2(e) \end{bmatrix} \tag{1.24}$$

where $\beta_2(e)$ is just coordinate transformation of $\beta_2(t)$. The corresponding implicit manifold is $z = 0$ and its manifold attractivity is given by

$$\dot{z} = -\gamma y^4 z \tag{1.25}$$

Target dynamics for Eq. (1.16) are $\dot{e} = -e$ which can always be achieved since the disturbance term y^2z of the closed-loop dynamics ($\dot{e} = -e - y^2z$) goes to zero.

In fact, solving Eq. (1.18) requires $f^T(y)$ be integrable. Because $f(y)$ is scalar, it is always possible to find such $\beta_1(y)$ that Eq. (1.18) is satisfied. However, Eq. (1.18) is not solvable for general multidimensional nonlinear $f(y)$. For linear systems, these requirements are easily bypassed by adopting state filters[9].

1.2 Research Motivation

Based on the previous research survey, the existing adaptive control methods using a certainty equivalence principle suffer from performance degradation due to the following aspects:

1. As shown in preceding examples for MRAC and indirect adaptive control schemes, both system error dynamics share the following structure

$$\dot{e} = \underbrace{-a_m e}_{\text{target dynamics}} + \text{disturbance} \tag{1.26}$$

   wherein 'disturbance' term converges to zero only when parameter estimates coincide with their true values if $e \neq 0$. Therefore, the overall closed-loop system performance is ultimately determined by the performance of the parameter estimator, which is poor without a persistently exciting reference trajectory (the PE reference trajectory is defined as a signal that can derive parameter estimates to true parameter values in section 1.1.1).

2. The parameter update law involves no estimation error term and is driven by the regulation/tracking error of the system. This leads to the fact that the estimator keeps generating update signals even when estimates are equal to true parameters as long as the regulation/tracking error has nonzero values. In the same context, the parameter update stops whenever the regulation/tracking error becomes zero although parameter estimates are away from true parameters. Consequently, the structure of the adaptation algorithm also degrades the overall closed-loop system performance.

3. The closed-loop dynamics controlled by the certainty equivalence principle are unable to recover the deterministic control system dynamics although the regulation/tracking error converges to zero asymptotically. This recovery of the

error dynamics happens only when estimates are exactly equal to true parameters since the certainty equivalence principle is based on the cancelation of uncertain parameter effects. The exact cancelation of uncertain parameter effects never happens in actual applications. Therefore, the certainty equivalence control never achieves its theoretical best performance in the long run.

4. An attempt to improve the performance of certainty equivalence based control methods by increasing the learning rate results in the large amount of control efforts. Thus, increasing the learning rate is limited by the practical issue on implementation.

5. The I&I control method shows a potential to improve aforementioned problems of the certainty equivalence principle, but it is not applicable to general nonlinear systems because of a strong restriction due to the integrability condition.

Motivated by those observations, we address the high performance adaptive control method by introducing an attracting manifold into adaptation while maintaining global asymptotic stability. The key issue is how to eliminate the integrability restriction and thereby improve the overall system performance with general nonlinearities. To resolve the integrability issue, we introduce a regressor filter. The regressor filter enables us to transform the closed-loop dynamics into the filtered system dynamics wherein states are given by filtering states of the original closed-loop dynamics. Further, the filtered error dynamics make it possible to construct a strict Lyapunov function, which, in turn, helps to provide a separation property for certain classes of nonlinear observer-based adaptive control systems.

The rest of the dissertation is organized as follows. In Chap. 2, the main results and analysis are presented. Then, as an application of the proposed control method, a robot arm trajectory control problem and an attitude tracking control

problem are solved in Chap. 3 and Chap. 4, respectively. Through Chap. 5 and Chap. 6, the attitude tracking problem is addressed more specifically involving a new attitude observer and a separation property for the proposed attitude observer and the controller. Finally, summary and contributions of the present work are presented in Chap. 7.

Chapter 2

A New Adaptive Control with High Performance

In this chapter, we introduce a new control method which is not using the certainty equivalence principle. As mentioned in the previous chapter, certainty equivalence control depends on the cancelation of uncertain parameter effects. Thus, it has limited transient performance because cancelation is not always exact. The proposed control method overcomes this transient performance limitation by adopting an attracting manifold and enables the controlled system to recover the transient performance of deterministic control regardless of unknown parameter effects. This chapter contains the derivation of main theoretical results, stability proof, and discussions about its properties.

2.1 Problem Definition

The generalized system representation in the state space form is given by

$$\dot{\boldsymbol{x}}(t) = F(\boldsymbol{x}(t), \boldsymbol{\theta}^*, \boldsymbol{u}(t)) \tag{2.1}$$

where F describes the vector field, $\boldsymbol{x}(t) \in \mathbb{R}^n$ is a state vector, $\boldsymbol{\theta}^* \in \mathbb{R}^m$ is an m-dimensional constant unknown system parameter vector, and $\boldsymbol{u}(t) \in \mathbb{R}^p$ is a p-dimensional control input. For the simplicity of notation, the time argument t is omitted except when we need to emphasize it in the context. To reduce this general system in Eq. (2.1) into the manageable form, we need the following assumption.

Assumption 1. System equation given in Eq. (2.1) has the parameter affine representation in general sense.

In Assumption 1, "general sense" means that the original system of Eq. (2.1) can have the nonlinearly parameterized representation as long as it can be linearly parameterized using overparametrization. Under Assumption 1, we consider the systems which have the following parameter affine representation throughout this dissertation.

$$\dot{\boldsymbol{x}} = f(\boldsymbol{x})\boldsymbol{\theta}^* + \Phi^* g(\boldsymbol{x})\boldsymbol{u} \tag{2.2}$$

where $f(\boldsymbol{x}) \in \mathbb{R}^{n\times m}$ is a regressor matrix and $g(\boldsymbol{x}) \in \mathbb{R}^{n\times p}$ is a control mapping matrix. In addition to the parameter affine system assumption, we are also in need of the controllability assumption stated as follows:

Assumption 2. $\Phi^* > 0$ and $g(\boldsymbol{x})$ in Eq. (2.2) have a full rank with respect to the control input $\boldsymbol{u}$

In other words, we disregard the uncontrollable system. One more thing need to be mentioned is that linear systems always can be expressed as in Eq. (2.2), we focus only on nonlinear systems hereafter.

2.2 Adaptive Control Utilizing Attracting Manifold

This section contains the new control method and its stability proof for the simplified system with the analysis of the attracting manifold used in the parameter adaptation.

2.2.1 Motivating Problem

To highlight the effect of attracting manifold in adaptation, the controllability condition of Eq. (2.2) for $g(\boldsymbol{x})$ is simplified by replacing $g(\boldsymbol{x})$ with an identity matrix. However, this simplification will not hurt our result because we already assumed that $g(\boldsymbol{x})$ has a full rank with respect to the control input $\boldsymbol{u}$. Thus, the following system equation is considered.

$$\dot{\boldsymbol{x}} = f(\boldsymbol{x})\boldsymbol{\theta}^* + \Phi^*\boldsymbol{u} \tag{2.3}$$

Our control objective is to make the system of Eq. (2.3) follow the reference trajectory $\boldsymbol{x}_m$. Thus, to quantify the error between the system state $\boldsymbol{x}$ and the reference state $\boldsymbol{x}_m$, we define the following error vector $\boldsymbol{e}$ as

$$\boldsymbol{e} = \boldsymbol{x} - \boldsymbol{x}_m \tag{2.4}$$

Then, the control objective rendered in error vector space can be restated as follows: Tracking control objective is to make $\boldsymbol{e}$ go to zero as time passes, where $\boldsymbol{e}$ has the following dynamics.

$$\dot{\boldsymbol{e}} = f(\boldsymbol{x})\boldsymbol{\theta}^* + \Phi^*\boldsymbol{u} - \dot{\boldsymbol{x}}_m \tag{2.5}$$

In followings, we develop a nonlinear controller that ensures the satisfaction of the tracking control objective for $\boldsymbol{e}$ whose dynamics is given by Eq. (2.5).

2.2.2 Transforming Error System Using Filter States

Before we proceed to the synthesis of the proposed controller, following filter states need to be defined.

$$\dot{\boldsymbol{e}}_f = -\alpha \boldsymbol{e}_f + \boldsymbol{e} \tag{2.6}$$

$$\dot{W}_f(t) = -\alpha W_f(t) + W(\boldsymbol{x}, \dot{\boldsymbol{x}}_m) \tag{2.7}$$

$$\dot{\boldsymbol{u}}_f = -\alpha \boldsymbol{u}_f + \boldsymbol{u} \tag{2.8}$$

where $\alpha > 0$ and $W(\boldsymbol{x}, \dot{\boldsymbol{x}}_m)$ is defined from the following relationship.

$$W(\boldsymbol{x}, \dot{\boldsymbol{x}}_m)\boldsymbol{\psi}^* = \Phi^{*-1} f(\boldsymbol{x})\boldsymbol{\theta}^* - \Phi^{*-1}\dot{\boldsymbol{x}}_m + k\Phi^{*-1}\boldsymbol{e} \tag{2.9}$$

with $k > 0$ and a new unknown constant vector $\boldsymbol{\psi}^* \in \mathbb{R}^{n(n-1)(m+1)/2}$ having mixed parameters from both $\boldsymbol{\theta}^*$ and Φ^{*-1}. Since $\dot{\boldsymbol{x}}_m$ is assumed to be known reference information, we denote $W(\boldsymbol{x}, \dot{\boldsymbol{x}}_m)$ as $W(\boldsymbol{x})$ for the notational simplicity. From the definition of filter states, the following observations are in order.

1. Although Φ^* is a constant unknown matrix, we already assumed that it is a positive definite matrix in Eq. (2.1). Thus, the existence of Φ^{*-1} is always guaranteed.

2. In addition to the error filter $\boldsymbol{e}_f$ of Eq. (2.6), a regressor filter W_f of Eq. (2.7) is newly introduced because of the integrability issue mentioned in the previous chapter. This regressor filter enables us to eliminate the integrability conditions posed by [6, 9], which will be explained in the following section.

3. Introduced control filter $\boldsymbol{u}_f$ of Eq. (2.8) does not have to be included for actual implementation for $\boldsymbol{u}$. After $\boldsymbol{u}_f$ is defined in terms of either original states in Eq. (2.5) or filter states, $\boldsymbol{u}$ can be easily recovered using the filter state definition. Thus, the control filter of Eq. (2.8) is used only for the analysis.

4. The dimension of $\boldsymbol{\psi}^*$ in Eq. (2.9) is maximal in a sense that it is derived based on overparametrization. It can be smaller than expected depending on the actual application as presented in the later chapter.

5. α is a filter gain which regulate filter response to system states. By increasing α, we can make filter states converge to the system states more rapidly.

6. k is a proportional gain of the proposed controller described in the next section.

Based on these filter definitions, Eq. (2.6), Eq. (2.7) and Eq. (2.8), we derive the following lemma to synthesize the new control scheme.

Lemma 1 (Dynamics of Filter States)**.** *The following filtered system dynamics are equivalent to the error dynamics of Eq. (2.5) in a sense that if* $\dot{\boldsymbol{e}}_f(t) \to 0$ *as* $t \to 0$*, then* $\lim_{t\to\infty} \boldsymbol{e}_f = 0 \Leftrightarrow \lim_{t\to\infty} \boldsymbol{e} = 0$.

$$\dot{\boldsymbol{e}}_f = -k\boldsymbol{e}_f + \Phi^* \left[W_f(t)\boldsymbol{\psi}^* + \boldsymbol{u}_f\right] \tag{2.10}$$

Proof. Filter states defined from Eq. (2.6) to Eq. (2.8) are used to transform the error dynamics of Eq. (2.5) into the filtered error dynamics of Eq. (2.10). First, we have to rearrange the error dynamics in Eq.(2.5) to get a regressor matrix defined in Eq.(2.9). The error system dynamics of Eq.(2.5) is rewritten as follows:

$$\begin{aligned}\dot{\boldsymbol{e}} &= -k\boldsymbol{e} + \Phi^* \left[\Phi^{*-1} f(\boldsymbol{x})\boldsymbol{\theta}^* - \Phi^{*-1}\dot{\boldsymbol{x}}_m + k\Phi^{*-1}\boldsymbol{e} + \boldsymbol{u}\right] \\ &= -k\boldsymbol{e} + \Phi^* \left[W(\boldsymbol{x})\boldsymbol{\psi}^* + \boldsymbol{u}\right]\end{aligned} \tag{2.11}$$

By substituting each filter definition into Eq. (2.11) and rearranging terms properly, we get the following differential equation.

$$\frac{d}{dt}\left[\dot{\boldsymbol{e}}_f + k\boldsymbol{e}_f - \Phi^* \left(W_f(t)\boldsymbol{\psi}^* + \boldsymbol{u}_f\right)\right] = -\alpha\left[\dot{\boldsymbol{e}}_f + k\boldsymbol{e}_f - \Phi^* \left(W_f(t)\boldsymbol{\psi}^* + \boldsymbol{u}_f\right)\right] \tag{2.12}$$

which is the simple first order differential equation. Since the solution for Eq. (2.12) exponentially converges to zero, the term inside the square bracket can be expressed as follows:

$$\dot{\boldsymbol{e}}_f = -k\boldsymbol{e}_f + \Phi^* \left[W_f(t)\boldsymbol{\psi}^* + \boldsymbol{u}_f \right] + \boldsymbol{\varepsilon}(t) \tag{2.13}$$

where $\boldsymbol{\varepsilon}(t) \doteq \boldsymbol{\varepsilon}(0)e^{-\alpha t}$ represents the exponentially decaying term given by

$$\dot{\boldsymbol{\varepsilon}}(t) = -\alpha\boldsymbol{\varepsilon}(t); \quad \boldsymbol{\varepsilon}(0) = \left[\dot{\boldsymbol{e}}_f + k\boldsymbol{e}_f - \Phi^* \left(W_f(t)\boldsymbol{\psi}^* + \boldsymbol{u}_f \right) \right]_{t=0} \tag{2.14}$$

Thus, Eq. (2.10) is derived by setting $\boldsymbol{\varepsilon}(0) = 0$ because the initial value of each filter state can be chosen arbitrarily. Finally, proof of the stability equivalence between $\boldsymbol{e}_f$ and $\boldsymbol{e}$ is done simply by noticing that both sides of Eq. (2.6) should go to zero as t goes to infinity. □

It is clear from the above result that the control input $\boldsymbol{u}$ should be synthesized to ensure the convergence of both $\dot{\boldsymbol{e}}_f$ and $\boldsymbol{e}_f$ to zero. In other words, $\boldsymbol{u}_f$ need to be designed to make both $\dot{\boldsymbol{e}}_f$ and $\boldsymbol{e}_f$ go to zero as t goes to infinity. Ignoring exponentially decaying additive terms during stability analysis is somewhat standard practice among the adaptive control research community[10, 11] as in Eq. (2.10). However, the previous lemma should be applied carefully in the general case of cascaded systems involving exponentially decaying terms[12].

2.2.3 New Adaptive Control Scheme and Stability Proof

We propose a new adaptive control scheme in this section. The proposed control method performs adaptation on the attracting manifold. As a result, deterministic control system dynamics are recovered by the attracting manifold, not by the cancelation of unknown parameter effects which is the principle of the certainty equivalent control scheme. After we show the structure of the controller, the stability proof is presented.

Theorem 1 (Adaptive Full-state Feedback Control)**.** *Consider the tracking control problem whose error dynamics can be represented by Eq. (2.5). Then, the control input* $\boldsymbol{u}$ *computed by the following update law with filters defined by Eq. (2.6) and Eq. (2.7) guarantees the global stability and the satisfaction of the control objective described by the asymptotic tracking error convergence,* $\lim_{t\to\infty} \boldsymbol{e}(t) = 0$*, for any initial condition.*

$$\boldsymbol{u} = -W(\boldsymbol{x})(\hat{\boldsymbol{\theta}} + \boldsymbol{\beta}) - \gamma W_f(t) W_f^T(t) \left[(k-\alpha)\boldsymbol{e}_f + \boldsymbol{e}\right] \tag{2.15}$$

where $\gamma > 0$ *is an adaptive gain,* k *and* $W(\boldsymbol{x})$ *are from Eq. (2.9), and* α *is the same* α *as in the filter definition. Each* $\hat{\boldsymbol{\theta}}$ *and* $\boldsymbol{\beta}$ *is generated by the following relationships:*

$$\dot{\hat{\boldsymbol{\theta}}}(t) = \gamma(k+\alpha) W_f^T(t)\boldsymbol{e}_f - \gamma W^T(\boldsymbol{x})\boldsymbol{e}_f \tag{2.16}$$

$$\dot{\boldsymbol{\beta}} = \gamma W_f^T(t)\boldsymbol{e}_f \tag{2.17}$$

The estimates of unknown parameters are given by $\hat{\boldsymbol{\theta}} + \boldsymbol{\beta}$*.*

Proof. This stability proof consists of three steps. First, the original tracking error system is transformed into the filtered error system. Second, the proposed control input $\boldsymbol{u}_f$ is synthesized based on the filtered error system. Finally, the global asymptotic stability for the filtered error system is proved using Lyapunov candidate function and the actual control input $\boldsymbol{u}$ is recovered from $\boldsymbol{u}_f$.

Using filter states in Eq. (2.6) and Eq. (2.7), we get the filtered error system Eq. (2.10) in Lemma 1 from Eq. (2.5) along with the regressor $W(\boldsymbol{x})$ in Eq. (2.9). To make sure that $\boldsymbol{\varepsilon}(t) = 0$ for all $t > 0$, we set the filter initial value as $\boldsymbol{e}_f(0) = \boldsymbol{e}(0)/(\alpha - k)$ and $W_f(0) = 0$. Since $\alpha - k$ is the denominator of $\boldsymbol{e}_f(0)$, α and k should be chosen properly. By transforming the error system of Eq. (2.5) into the filtered error system of Eq. (2.10), we can always construct $\boldsymbol{\beta}$ function instead of finding one which is satisfying the condition in Eq. (1.18) because, as mentioned

earlier, a solution to Eq. (1.18) for most of nonlinear regressor matrix $W(\boldsymbol{x})$ is not available in general. Next, control input $\boldsymbol{u}_f$ is designed as follows

$$\boldsymbol{u}_f = -W_f(t)(\hat{\boldsymbol{\theta}} + \boldsymbol{\beta}) \tag{2.18}$$

where $\hat{\boldsymbol{\theta}}$ and $\boldsymbol{\beta}$ are from Eq. (2.16) and Eq. (2.17). By substituting Eq. (2.18) into the filtered error system Eq. (2.10), we obtain the following simplified dynamics for $\boldsymbol{e}_f$.

$$\dot{\boldsymbol{e}}_f = -k\boldsymbol{e}_f - \Phi^* W_f(\boldsymbol{x})\boldsymbol{z} \tag{2.19}$$

where $\boldsymbol{z}$ represents the error vector between the estimates and the true parameters defined by

$$\boldsymbol{z} = \hat{\boldsymbol{\theta}} + \boldsymbol{\beta} - \boldsymbol{\psi}^* \tag{2.20}$$

If we can show that both $\dot{\boldsymbol{e}}_f(t)$ and $\boldsymbol{e}_f(t)$ go to zero as t goes to infinity, then we prove $\lim_{t\to\infty} \boldsymbol{e}(t) = 0$ by Lemma 1. As the final step of our proof, consider the following Lyapunov candidate function.

$$V = \frac{1}{2}\boldsymbol{e}_f^T\boldsymbol{e}_f + \frac{\zeta}{2\lambda_{\min}}\boldsymbol{z}^T\boldsymbol{z} \tag{2.21}$$

where ζ is any positive number that satisfies $\zeta > \frac{1}{2k\gamma}$ and $\lambda_{\min}$ is the smallest eigenvalue of $\frac{1}{2}(\Phi^{*-T} + \Phi^{*-1})$. The time derivative of V evaluated along the trajectory generated from Eq. (2.19) can be simplified together with Eq. (2.16) and Eq. (2.17)

as follows:

$$
\begin{aligned}
\dot{V} &= \boldsymbol{e}_f^T\left(-k\boldsymbol{e}_f - \Phi^* W_f \boldsymbol{z}\right) + \frac{\zeta}{\lambda_{\min}}\boldsymbol{z}^T\left(\dot{\hat{\boldsymbol{\theta}}} + \dot{\boldsymbol{\beta}}\right) \\
&= -k\boldsymbol{e}_f^T\boldsymbol{e}_f - \boldsymbol{e}_f^T\Phi^* W_f\boldsymbol{z} + \frac{\zeta}{\lambda_{\min}}\boldsymbol{z}^T\left[\dot{\hat{\boldsymbol{\theta}}} + \gamma\dot{W}_f^T\boldsymbol{e}_f + \gamma W_f^T\dot{\boldsymbol{e}}_f\right] \\
&\leqslant -k\|\boldsymbol{e}_f\|^2 + \|\boldsymbol{e}_f\|\|\Phi^* W_f\boldsymbol{z}\| - \zeta\gamma\|\Phi^* W_f\boldsymbol{z}\|^2 \\
&\leqslant -\frac{k}{2}\|\boldsymbol{e}_f\|^2 - \frac{\zeta\gamma}{2}\|\Phi^* W_f\boldsymbol{z}\|^2 - \frac{k}{2}\underbrace{\left[\|\boldsymbol{e}_f\|^2 - \frac{2}{k}\|\boldsymbol{e}_f\|\|\Phi^* W_f\boldsymbol{z}\| + \frac{2\zeta\gamma}{k}\|\Phi^* W_f\boldsymbol{z}\|^2\right]}_{>0 \text{ from } \zeta \text{ definition}} \\
&\leqslant -\frac{k}{2}\|\boldsymbol{e}_f\|^2 - \frac{\zeta\gamma}{2}\|\Phi^* W_f(t)\boldsymbol{z}\|^2
\end{aligned} \tag{2.22}
$$

which means that $\dot{V}(t)$ is negative semi-definite. Thus, $V(t) \in \mathcal{L}_\infty$, which imply all signals ($\boldsymbol{e}_f$, $\boldsymbol{z}$, and W_f) are bounded. Based on the structure of each filter, the boundedness of all filtered signals is equivalent to the boundedness of all closed loop signals in Eq.(2.5) since $\boldsymbol{x}_m$ might be assumed as a bounded reference signal without loss of generality. In addition to the boundedness of $V(t)$ for all $t \geq 0$, there exists V_∞ such that $\lim_{t\to\infty} V(t) = V_\infty < \infty$. Since $V_\infty - V(0) = \lim_{t\to\infty}\int_0^t \dot{V}(\sigma)d\sigma$, $\boldsymbol{e}_f \in \mathcal{L}_2$. Therefore, $\boldsymbol{e}_f \in \mathcal{L}_2 \cap \mathcal{L}_\infty$. Furthermore, we see that $\dot{\boldsymbol{e}}_f \in \mathcal{L}_\infty$ and $\ddot{\boldsymbol{e}}_f \in \mathcal{L}_\infty$ from Eq. (2.6) and Eq. (2.19), which implies $\lim_{t\to\infty}[\boldsymbol{e}_f(t), \dot{\boldsymbol{e}}_f(t)] = 0$ by applying Barbalat's lemma recursively. This proves the global asymptotic stability of the proposed control scheme with the help of Lemma 1. The actual control input $\boldsymbol{u}$ is recovered from Eq. (2.8) as follows:

$$
\begin{aligned}
\boldsymbol{u} &= \dot{\boldsymbol{u}}_f + \alpha\boldsymbol{u}_f \\
&= -\dot{W}_f\left[\hat{\boldsymbol{\theta}} + \boldsymbol{\beta}\right] - W_f\left[\dot{\hat{\boldsymbol{\theta}}} + \dot{\boldsymbol{\beta}}\right] - \alpha W_f\left[\hat{\boldsymbol{\theta}} + \boldsymbol{\beta}\right] \\
&= -W(\boldsymbol{x})\left[\hat{\boldsymbol{\theta}} + \boldsymbol{\beta}\right] - W_f\left[\dot{\hat{\boldsymbol{\theta}}} + \dot{\boldsymbol{\beta}}\right]
\end{aligned} \tag{2.23}
$$

which is identical to Eq.(2.15) when Eq.(2.6), Eq.(2.7), Eq.(2.16) and Eq.(2.17) are

substituted into Eq. (2.23). This completes the proof of the main theorem. □

Alternative Proof that Carrying $\boldsymbol{\varepsilon}(t)$

In the previous proof of Theorem 1, the exponentially decaying term $\boldsymbol{\varepsilon}(t)$ in filter dynamics is ignored as in Eq. (2.19) and Lemma 1 is used. In the following alternative proof, we include $\boldsymbol{\varepsilon}(t)$ explicitly.

Alternative proof of Theorem 1. Consider the following Lyapunov candidate function including the exponentially decaying term

$$V = \frac{1}{2}\boldsymbol{e}_f^T\boldsymbol{e}_f + \frac{\zeta}{2\lambda_{\min}}\boldsymbol{z}^T\boldsymbol{z} + \frac{\xi}{2}\boldsymbol{\varepsilon}^T\boldsymbol{\varepsilon} \tag{2.24}$$

where $\lambda_{\min}$ is the same as in Eq. (2.21), $\zeta > \frac{9}{4k\gamma}, \xi > \max\left(\frac{9}{4k\alpha}, \frac{9\zeta\gamma\nu_{\min}}{4\alpha\lambda_{\min}}\right)$, and $\nu_{\min}$ is the smallest eigenvalue of $\frac{1}{2}\left(\Phi^* + \Phi^{*T}\right)$. Differentiating V of Eq. (2.24) with respect to time gives us the followings

$$\begin{aligned}
\dot{V} =& \boldsymbol{e}_f^T\left(-k\boldsymbol{e}_f - \Phi^* W_f\boldsymbol{z} + \boldsymbol{\varepsilon}\right) + \frac{\zeta}{\lambda_{\min}}\boldsymbol{z}^T\left(\dot{\hat{\boldsymbol{\theta}}} + \dot{\boldsymbol{\beta}}\right) - \xi\alpha\boldsymbol{\varepsilon}^T\boldsymbol{\varepsilon} \\
=& -k\boldsymbol{e}_f^T\boldsymbol{e}_f - \boldsymbol{e}_f^T\Phi^* W_f\boldsymbol{z} + \boldsymbol{e}_f^T\boldsymbol{\varepsilon} + \frac{\zeta}{\lambda_{\min}}\boldsymbol{z}^T\left[\dot{\hat{\boldsymbol{\theta}}} + \gamma\dot{W}_f^T\boldsymbol{e}_f + \gamma W_f^T\dot{\boldsymbol{e}}_f\right] - \xi\alpha\boldsymbol{\varepsilon}^T\boldsymbol{\varepsilon} \\
=& -k\boldsymbol{e}_f^T\boldsymbol{e}_f - \boldsymbol{e}_f^T\Phi^* W_f\boldsymbol{z} + \boldsymbol{e}_f^T\boldsymbol{\varepsilon} - \frac{\zeta\gamma}{\lambda_{\min}}\boldsymbol{z}^T W_f^T\Phi^* W_f\boldsymbol{z} + \frac{\zeta\gamma}{\lambda_{\min}}\boldsymbol{z}^T W_f^T\boldsymbol{\varepsilon} - \xi\alpha\boldsymbol{\varepsilon}^T\boldsymbol{\varepsilon} \\
\leqslant& -\frac{k}{3}\|\boldsymbol{e}_f\|^2 - \frac{\zeta\gamma}{3}\|\Phi^* W_f\boldsymbol{z}\|^2 - \frac{\xi\alpha}{3}\|\boldsymbol{\varepsilon}\|^2 \\
& -\frac{k}{3}\|\boldsymbol{e}_f\|^2 + \|\boldsymbol{e}_f\|\|\Phi^* W_f\boldsymbol{z}\| - \frac{\zeta\gamma}{3}\|\Phi^* W_f\boldsymbol{z}\|^2 \\
& -\frac{k}{3}\|\boldsymbol{e}_f\|^2 + \|\boldsymbol{e}_f\|\|\boldsymbol{\varepsilon}\| - \frac{\xi\alpha}{3}\|\boldsymbol{\varepsilon}\|^2 \\
& -\frac{\zeta\gamma}{3\lambda_{\min}\nu_{\min}}\|W_f\boldsymbol{z}\|^2 + \frac{\zeta\gamma}{\lambda_{\min}}\|W_f\boldsymbol{z}\|\|\boldsymbol{\varepsilon}\| - \frac{\xi\alpha}{3}\|\boldsymbol{\varepsilon}\|^2 \\
\leqslant& -\frac{k}{3}\|\boldsymbol{e}_f\|^2 - \frac{\zeta\gamma}{3}\|\Phi^* W_f\boldsymbol{z}\|^2 - \frac{\xi\alpha}{3}\|\boldsymbol{\varepsilon}\|^2
\end{aligned} \tag{2.25}$$

wherein the last inequality comes from ζ and ξ conditions. By following similar signal

chasing procedure described in the previous proof of Theorem 1 and using Barbalat's lemma, we guarantee that $\lim_{t\to\infty}[\boldsymbol{e}_f(t), W_f(t)\boldsymbol{z}(t), \boldsymbol{\varepsilon}(t)] = 0$. In addition, by $\dot{\boldsymbol{e}}_f = -k\boldsymbol{e}_f - \Phi^* W_f \boldsymbol{z} + \boldsymbol{\varepsilon}$, we have $\lim_{t\to\infty} \dot{\boldsymbol{e}}_f(t) = 0$. Finally, we obtain $\lim_{t\to\infty} \boldsymbol{e}(t) = 0$ from Eq. (2.6) as expected. □

In this section, we discussed about the global asymptotic stability of the proposed controller and stability proof was given in two ways. Either of them (with/without $\boldsymbol{\varepsilon}(t)$ in filter dynamics) works fine. However, an attracting manifold used in adaptation is not clearly defined and the role of the attracting manifold is not shown either. In the following section, we clarify the attracting manifold in the adaptive control method presented in Theorem 1 and investigate its properties in the perspective of adaptation.

2.2.4 Attracting Manifold in Adaptation

An attracting manifold for adaptation is defined by the following lemma.

Lemma 2 (Attracting Manifold)**.** *For the given adaptive control system in Eq. (2.10) with the control input $\boldsymbol{u}_f$ of Eq. (2.18) along with Theorem 1, the adaptation error $\boldsymbol{z}$ of Eq. (2.20) has an attracting manifold $\mathcal{S}$ such that*

$$\mathcal{S} = \{\boldsymbol{z} \mid W_f \boldsymbol{z} = 0\} \tag{2.26}$$

Proof. Consider the following Lyapunov candidate function from Eq. (2.21).

$$V_{\boldsymbol{z}} = \frac{\zeta}{2\lambda_{\min}} \boldsymbol{z}^T \boldsymbol{z} \tag{2.27}$$

where ζ and $\lambda_{\min}$ are the same as in Eq. (2.21). Taking the time derivative of

Eq. (2.27) lead us to the following inequality.

$$\begin{aligned}\dot{V}_{\boldsymbol{z}} &= \frac{\zeta}{\lambda_{\min}}\boldsymbol{z}^T\left(\dot{\hat{\boldsymbol{\theta}}}+\dot{\boldsymbol{\beta}}\right)\\ &= \frac{\zeta}{\lambda_{\min}}\boldsymbol{z}^T\left(\dot{\hat{\boldsymbol{\theta}}}+\dot{W}_f^T\boldsymbol{e}_f+W_f^T\dot{\boldsymbol{e}}_f\right)\\ &\leqslant -\zeta\gamma\|\Phi^* W_f\boldsymbol{z}\|^2 \end{aligned} \tag{2.28}$$

Last inequality is obtained by substituting Eq. (2.7), Eq. (2.16), and Eq. (2.19) into Eq. (2.28). In a similar way of proving Theorem 1, we see that $V_{\boldsymbol{z}} \in \mathcal{L}_\infty$ as well as the existence of $V_{\boldsymbol{z}\infty}$ such that $\lim_{t\to\infty} V_{\boldsymbol{z}}(t) = V_{\boldsymbol{z}\infty}$ because $V_{\boldsymbol{z}} \geqslant 0$ and $\dot{V}_{\boldsymbol{z}} \leqslant 0$. Thus, $\boldsymbol{z} \in \mathcal{L}_\infty$. In fact, all closed loop signals are already shown to be bounded by the proof of Theorem 1. From $V_{\boldsymbol{z}\infty} - V_{\boldsymbol{z}}(0) = \lim_{t\to\infty}\int_0^t \dot{V}_{\boldsymbol{z}}(\sigma)d\sigma$, $W_f\boldsymbol{z} \in \mathcal{L}_2$. Therefore, $W_f\boldsymbol{z} \in \mathcal{L}_2 \cap \mathcal{L}_\infty$. In addition, $\dot{W}_f,\ \dot{\boldsymbol{z}} \in \mathcal{L}_\infty$ from the boundedness of closed loop signals. Using Barbalat's lemma for $W_f\boldsymbol{z} \in \mathcal{L}_2 \cap \mathcal{L}_\infty$ and $\frac{d}{dt}(W_f\boldsymbol{z}) \in \mathcal{L}_\infty$, we may conclude that $W_f\boldsymbol{z} \to 0$ as $t \to \infty$. This proves the attractiveness of $\mathcal{S}$. □

Remark 1. Using the attractiveness of $\mathcal{S}$, we may prove the global stability in Theorem 1. First, we prove that $\boldsymbol{e}_f \to 0$ as $t \to \infty$. Then, we may show that $\dot{\boldsymbol{e}}_f \to 0$ as $t \to \infty$ from Eq. (2.19) using Lemma 2. Finally, we claim $\boldsymbol{e} \to 0$ as $t \to \infty$ from Eq. (2.6).

Remark 2. Lemma 2 tells us that $\boldsymbol{e}_f$ dynamics of Eq. (2.19) recovers $\dot{\boldsymbol{e}}_f = -k\boldsymbol{e}_f$ all the time, which results in the improvement of transient responses in $\boldsymbol{e}$. On the other hand, to achieve the control objective, the certainty equivalent controller relies upon the cancelation of unknown parameter effects which is not exact.

Remark 3. $\boldsymbol{z} \in \mathcal{S}$ does not mean $\boldsymbol{z} = 0$ because W_f is not a full rank square matrix. Thus, $\boldsymbol{z}$ on $\mathcal{S}$ may have a nonzero vector.

Remark 4. Although the convergence of $\boldsymbol{z}$ to zero is not guaranteed, $\boldsymbol{z}$ stays at zero after the moment when $\hat{\boldsymbol{\theta}} + \boldsymbol{\beta}$ hit the true parameter vector $\boldsymbol{\psi}^*$. This may be clear

from the $\boldsymbol{z}$ dynamics

$$\dot{\boldsymbol{z}} = -\gamma W_f^T \Phi^* W_f \boldsymbol{z} \tag{2.29}$$

which is different from the certainty equivalent control method where parameter estimates always deviate from true values at the beginning of adaptation. This also helps enhancing the performance of the proposed controller compared with the certainty equivalent scheme because the new control method stops updating parameter estimates after hitting true values while the conventional certainty equivalent method keeps searching true values asymptotically. We must be careful about Eq. (2.29). Eq. (2.29) is obtained only when $\boldsymbol{\varepsilon}(t) = 0$ for all $t \geq 0$. Otherwise, there exists an extra term $\gamma W_f^T \boldsymbol{\varepsilon}$ in R.H.S. of Eq. (2.29) and we loose the nice feature (parameter estimate stays locked at the true value after hitting it as long as $\boldsymbol{\varepsilon}(t) \neq 0$). However, it is always possible to choose the initial filter states such that $\boldsymbol{\varepsilon}(t) = 0$ for all $t \geq 0$ by setting $\boldsymbol{\varepsilon}(0) = 0$ based on Eq. (2.14) using $\boldsymbol{e}_f(0) = \frac{\boldsymbol{e}(0)}{k-\alpha}$ and $W_f(0) = 0$.

2.3 Combination with Smooth Projection Technique

In the foregoing analysis, we do not investigate the robustness property of the proposed control method when there exist unknown exogenous disturbances. It is well known that even small bounded disturbances in the adaptively controlled system may lead to the closed-loop system instability or deteriorate the closed-loop performance significantly[13] because of the parameter drift (i.e., unbounded growth of parameter estimates due to the disturbance). To resolve this problem, robustness modification is applied to the system. Conventional robustness modification for the systems with unknown external disturbances include adding a leakage term (e.g., σ-modification and ϵ-modification)[14] or using projection for estimates to be confined inside a bounded convex set where true parameters reside[13–16]. Since we already present the projection technique in the indirect adaptive control example,

only σ-modification is demonstrated here. Suppose we have the following system equation for regulation (i.e., we want that $y(t) \to 0$ as $t \to \infty$)

$$\dot{y}(t) = \theta^* y(t) + u(t) + d(t) \tag{2.30}$$

where $d(t)$ is either unmodeled or external disturbance and θ^* is unknown. By following the conventional parameter update law and CE-based control design, we have

$$u(t) = -y(t) - \hat{\theta}(t)y(t) \tag{2.31}$$

$$\dot{\hat{\theta}}(t) = \gamma y^2(t) \tag{2.32}$$

Consider the following Lyapunov candidate function

$$V = \frac{1}{2}y^2 + \frac{1}{2\gamma}\tilde{\theta}^2 \tag{2.33}$$

where $\tilde{\theta}(t) \doteq \hat{\theta}(t) - \theta^*$ is a parameter estimation error and $\gamma > 0$. The time derivative of V in Eq. (2.33) along with Eq. (2.31) and Eq. (2.32) leads to the following inequality

$$\begin{aligned} \dot{V} &= y(-y - \tilde{\theta}y + d) + \frac{1}{\gamma}\dot{\hat{\theta}}\tilde{\theta} \\ &= -y^2 + (\frac{1}{\gamma}\dot{\hat{\theta}} - y^2)\tilde{\theta} + dy \\ &= -y^2 + dy \end{aligned} \tag{2.34}$$

which is not negative semidefinite. Thus, we cannot guarantee the convergence of y to zero but the boundedness of $\tilde{\theta}$ (parameter estimate may drift without upper/lower bounds).

σ-modification

By adding a leakage term in the parameter update law, we may fix the unbounded regulation and parameter estimation error (parameter drift) simultaneously. Modify the parameter update law of Eq. (2.32) as follows

$$\dot{\hat{\theta}}(t) = \gamma(-\sigma\hat{\theta}(t) + y^2) \tag{2.35}$$

where $\sigma \doteq \frac{\lambda}{\gamma} > 0$ and $\lambda > 0$ is determined by σ and γ. Then, the time derivative of V in Eq. (2.33) is given by

$$\begin{aligned}
\dot{V} =& -y^2 + dy - \sigma\hat{\theta}\tilde{\theta} \\
=& -y^2 + dy - \sigma(\tilde{\theta} + \theta^*)\tilde{\theta} \\
=& -y^2 + dy - \sigma\tilde{\theta}^2 - \sigma\tilde{\theta}\theta^*
\end{aligned} \tag{2.36}$$

If $0 < \lambda < 1$, then, using $1 = \lambda + (1 - \lambda)$ for all $0 < \lambda < 1$, Eq. (2.36) can be simplified further as follows

$$\begin{aligned}
\dot{V} \leq& -\frac{\lambda}{2}y^2 - \frac{\lambda}{2\gamma}\tilde{\theta}^2 - \frac{(1-\lambda)}{2}y^2 - \frac{1}{2}(y-d)^2 - \frac{\lambda}{2\gamma}(\tilde{\theta} - \theta^*)^2 + \frac{1}{2}(d^2 + \frac{\lambda}{\gamma}\theta^{*2}) \\
\leq& -\frac{\lambda}{2}y^2 - \frac{\lambda}{2\gamma}\tilde{\theta}^2 + \frac{1}{2}(d^2 + \frac{\lambda}{\gamma}\theta^{*2}) \\
\leq& -\frac{\lambda}{2}\left(y^2 + \frac{1}{\gamma}\tilde{\theta}^2\right) + \frac{1}{2}(d^2 + \frac{\lambda}{\gamma}\theta^{*2}) \\
\leq& -\lambda V + \frac{1}{2}(d_{\max}^2 + \frac{\lambda}{\gamma}\theta^{*2})
\end{aligned} \tag{2.37}$$

where $d_{\max} \doteq \max_t(|d(t)|)$ is a bound for $d(t)$. This inequality means V is bounded. If $\lambda \geq 1$, then

$$\begin{aligned}
\dot{V} =& -\frac{1}{2}y^2 - \frac{1}{2\gamma}\tilde{\theta}^2 - \frac{(\lambda-1)}{2\gamma}\tilde{\theta}^2 - \frac{1}{2}(y-d)^2 - \frac{\lambda}{2\gamma}(\tilde{\theta}-\theta^*)^2 + \frac{1}{2}(d^2 + \frac{\lambda}{\gamma}\theta^{*2}) \\
\leq& -\frac{1}{2}y^2 - \frac{1}{2\gamma}\tilde{\theta}^2 + \frac{1}{2}(d^2 + \frac{\lambda}{\gamma}\theta^{*2}) \\
\leq& -\frac{1}{2}\left(y^2 + \frac{1}{\gamma}\tilde{\theta}^2\right) + \frac{1}{2}(d^2 + \frac{\lambda}{\gamma}\theta^{*2}) \\
\leq& -\lambda V + \frac{1}{2}(d_{\max}^2 + \frac{\lambda}{\gamma}\theta^{*2})
\end{aligned} \tag{2.38}$$

which means V is bounded. Therefore, by adding the leakage term $-\sigma\hat{\theta}(t)$ to the update law, we now guarantee that V is bounded and subsequently, y and $\tilde{\theta}$ are bounded.

All the aforementioned robustifying algorithms are able to handle the parameter drift and guarantee the bounded closed-loop signals under unknown disturbances. They have a price to pay for uniform stability though: Leakage modifications may not recover the control performance as disturbances vanish and projection techniques need a priori information on parameter bounds while they maintain the performance of disturbance-free adaptive controllers. In addition, projection-based adaptive controls are nonsmooth in general[13], which means a potential to decrease the actuator lifetime in practical sense. Therefore, smooth projection-based adaptations are studied using a boundary layer around the convex set[17], a differentiable projection operator[18], and a nonlinear reparamterization[19].

In this dissertation, the nonlinear reparameterization technique in [19] is adopted since it provides a $\mathcal{C}^\infty$ projection and can be combined directly with the proposed control method. Further, since the projection algorithm is dependent on the bounding structure (e.g., unknown parameters are positive/negative or belong to an open set), we provide applications for each case in the later sections. Effects of projection on the proposed control scheme are demonstrated through numerical sim-

ulations. To understand the smooth projection mechanism, the following example is given.

Smooth projection

Consider the following system equation

$$\dot{y}(t) = \theta^* y(t) + u(t) \tag{2.39}$$

where θ^* is unknown. Suppose we have additional information on θ^* such that $\theta^* > 0$. Then, instead of using projection illustrated in the indirect adaptive control example of Eq. (1.14), we reparameterize θ^* as $\theta^* \doteq e^{\phi^*}$ and thus, θ^* is always positive regardless of ϕ^*. Corresponding control and parameter update laws are given as

$$u(t) = -y(t) - e^{\hat{\phi}(t)} y(t) \tag{2.40}$$

$$\dot{\hat{\phi}}(t) = \gamma y^2 \tag{2.41}$$

Stability proof is given by considering the following Lyapunov like function

$$V = \frac{1}{2} y^2 + \underbrace{\frac{1}{\gamma}\left(e^{\hat{\phi}} - e^{\phi^*}\right)}_{V_{\hat{\phi}}} \tag{2.42}$$

where $\gamma > 0$. Since $V_{\hat{\phi}}$ is lower bounded by the following conditions:

$$\frac{\partial}{\partial \hat{\phi}} V_{\hat{\phi}} = e^{\hat{\phi}} - e^{\phi^*} \quad (= 0 \text{ only at } \hat{\phi} = \phi^*) \tag{2.43}$$

$$\frac{\partial^2}{\partial \hat{\phi}^2} V_{\hat{\phi}} = e^{\hat{\phi}} \quad (> 0 \text{ for all } \hat{\phi}) \tag{2.44}$$

V is a lower bounded function. Differentiating V in Eq. (2.42) with respect to time, we obtain the inequality as follows

$$\begin{aligned}\dot{V} =& y\left[-y-\left(e^{\hat{\phi}}-e^{\phi^*}\right)y\right]+\frac{1}{\gamma}\dot{\hat{\phi}}\left(e^{\hat{\phi}}-e^{\phi^*}\right)\\ =&-y^2+\left(\frac{1}{\gamma}\dot{\hat{\phi}}-y^2\right)\left(e^{\hat{\phi}}-e^{\phi^*}\right)\\ =&-y^2\end{aligned} \tag{2.45}$$

V is lower bounded and monotone decreasing from $\dot{V}\leq 0$. Thus, $\lim_{t\to\infty}V(t)=V_\infty$ exists and is finite. Then, every closed loop signals are bounded (i.e., $y,(e^{\hat{\phi}}-e^{\phi^*})\in \mathcal{L}_\infty$). From $V_\infty - V(0)=\int_0^\infty \dot{V}(\sigma)d\sigma$, we have $y\in\mathcal{L}_2$. Further, $\dot{y}\in\mathcal{L}_\infty$. Finally, by using Barbalat's lemma, we guarantee that $\lim_{t\to\infty}y(t)=0$.

Chapter 3

Application to Robot Arm Control Problem

In this chapter, the proposed adaptive control scheme is applied to a robot arm trajectory tracking problem to demonstrate the effectiveness of theoretical results which claim the better tracking performance compared to the conventional model reference adaptive controls (MRAC). Since the robot arm control problem shares system properties with mechanical systems represented by an Euler-Lagrange system[20], the results of this chapter may be readily extended to broader mechanical system descriptions.

3.1 Introduction

Problems of designing control methods for rigid robot manipulators with uncertain parameters are now classic examples for adaptive control theory and various control solutions are available for actual applications in order to improve system performance and robustness. Specifically, the performance of an adaptive control under the effects of uncertain parameters or unknown disturbances has been a main focus

of study.

Initiated by the full-state feedback control[21, 22], many useful solutions are developed for the adaptive control of robot manipulators which guarantee the global convergence[23–29]. Those methods are roughly categorized into two groups. The first group is characterized by adaptive inverse dynamics and the other is characterized by passivity properties of closed-loop system[30]. This categorization is based on the structure of deterministic control scheme.

As far as adaptation algorithms are concerned, those methods are on the basis of the certainty equivalence principle in the MRAC framework. Thus, the overall closed-loop trajectory tracking/set-point regulating performance is ultimately dominated by the parameter adaptation performance in a sense that the estimation error does not vanish in general and the effect of uncertain parameters on the closed-loop system needs to be canceled continuously. In fact, certainty equivalence adaptive controllers never recover the deterministic control performance except for the case with the persistent-excitation assumption.

Through the implementation of the proposed adaptive control scheme, we show that the closed-loop dynamics controlled by the new method recover that of the deterministic control system and thus the proposed control matches a deterministic control in the overall tracking/regulating performance. Further, it is proven that the performance matching always happens with no further assumption. In other words, the convergence of estimation error does not affect the performance of the proposed adaptive control scheme.

In the following section, a robot arm control problem is formulated and necessary notations are defined. Then, the adaptive control method presented in the previous chapter is applied and its stability proof is given. Next, a smooth projection technique in [19] is combined with the proposed adaptive control method. Based on them, numerical simulations are performed and compared with a conventional

MRAC method.

3.2 Problem Formulation

The dynamic equations of an n dimensional robot arm control system are given as follows:

$$\begin{aligned} &\dot{\boldsymbol{x}}_1 = \boldsymbol{x}_2 \\ &M(\boldsymbol{x}_1)\dot{\boldsymbol{x}}_2 + C(\boldsymbol{x}_1, \boldsymbol{x}_2)\boldsymbol{x}_2 + R(\boldsymbol{x}_1, \boldsymbol{x}_2) = \boldsymbol{u} \end{aligned} \tag{3.1}$$

where $\boldsymbol{x}_1(t), \boldsymbol{x}_2(t) \in \mathbb{R}^n$ are the generalized position and velocity vectors respectively, $M(\boldsymbol{x}_1) \in \mathbb{R}^{n\times n}$ is the mass matrix, $C(\boldsymbol{x}_1, \boldsymbol{x}_2) \in \mathbb{R}^{n\times n}$ is the matrix composed of Coriolis and centrifugal forcing terms, $R(\boldsymbol{x}_1, \boldsymbol{x}_2) \in \mathbb{R}^n$ involves the gravity and friction effect, and $\boldsymbol{u} \in \mathbb{R}^n$ is the control torque at each joint. The Eq. (3.1) has the following properties:

1. $M(\boldsymbol{x}_1)$ is a positive definite inertia matrix whose matrix norm is bounded by $\lambda_{\min},\ \lambda_{\max} > 0$ as follows.

$$\lambda_{\min} \leqslant \|M(\boldsymbol{x}_1)\| \leqslant \lambda_{\max}, \quad \forall \boldsymbol{x}_1(t) \in \mathcal{L}_\infty \tag{3.2}$$

2. Eq. (3.1) has the parameter affine representation given by

$$M(\boldsymbol{x}_1)\dot{\boldsymbol{x}}_2 + C(\boldsymbol{x}_1, \boldsymbol{x}_2)\boldsymbol{x}_2 + R(\boldsymbol{x}_1, \boldsymbol{x}_2) = Y(\boldsymbol{x}_1, \boldsymbol{x}_2, \dot{\boldsymbol{x}}_2)\boldsymbol{\theta}^* \tag{3.3}$$

   where $\boldsymbol{\theta}^* \in \mathbb{R}^m$ is an unknown constant system parameter vector.

3. The following skew symmetry property holds:

$$\boldsymbol{\eta}^T \left[\dot{M}(\boldsymbol{x}_1) - 2C(\boldsymbol{x}_1, \boldsymbol{x}_2)\right] \boldsymbol{\eta} = 0, \quad \forall \boldsymbol{\eta} \in \mathbb{R}^n \tag{3.4}$$

Based on Eq. (3.1), consider the trajectory tracking control problem where reference trajectory is denoted by $\boldsymbol{x}_m = [\boldsymbol{x}_{m_1},\ \boldsymbol{x}_{m_2}]^T$ whose derivatives are assumed to be bounded known signals satisfying $\dot{x}_{m_1} = x_{m_2}$ (matching condition) without loss of generality. Then, the tracking error dynamics of $\boldsymbol{e} = [\boldsymbol{e}_1,\ \boldsymbol{e}_2]^T$ is derived as

$$\begin{aligned} \dot{\boldsymbol{e}}_1 &= \boldsymbol{e}_2 \\ M(\boldsymbol{x}_1)\dot{\boldsymbol{e}}_2 &= W_s(\boldsymbol{e}_1, \boldsymbol{e}_2, t)\boldsymbol{\theta}^* + \boldsymbol{u} \end{aligned} \tag{3.5}$$

where $\boldsymbol{e}_1 = \boldsymbol{x}_1 - \boldsymbol{x}_{m_1}$, $\boldsymbol{e}_2 = \boldsymbol{x}_2 - \boldsymbol{x}_{m_2}$, and $W_s(\boldsymbol{e}_1, \boldsymbol{e}_2, t)$ is defined by

$$W_s(\boldsymbol{e}_1, \boldsymbol{e}_2, t)\boldsymbol{\theta}^* = -M(\boldsymbol{x}_1)\ddot{\boldsymbol{x}}_m - C(\boldsymbol{x}_1, \boldsymbol{x}_2)\boldsymbol{x}_2 - R(\boldsymbol{x}_1, \boldsymbol{x}_2) \tag{3.6}$$

Eq. (3.6) has the same structure as Eq. (3.3) except that W_s has no $\dot{\boldsymbol{e}}_2$ (or $\dot{\boldsymbol{x}}_2$) dependency because $\dot{\boldsymbol{e}}_2$ is not implementable. The control objective is to achieve $\boldsymbol{e} \to 0$ globally and asymptotically.

3.3 Adaptive Control for Robot Arm System

The following theorem achieves the robot arm tracking control objective addressed in the previous section Eq. (3.5) by applying the proposed control philosophy in Theorem 1, which is one of our main results.

Theorem 2 (Adaptive Robot Arm Control)**.** *For the given robot arm system Eq. (3.1), compute the control input* $\boldsymbol{u}$ *by the following relationships:*

$$\boldsymbol{u} = -W(\hat{\boldsymbol{\theta}} + \boldsymbol{\beta}) - \gamma W_f W_f^T\left[(k_v - \alpha)\boldsymbol{e}_{f2} + k_p\boldsymbol{e}_{f1} + \boldsymbol{e}_2\right] \tag{3.7}$$

$$\dot{\hat{\boldsymbol{\theta}}}(t) = \gamma(\alpha W_f - W)^T\boldsymbol{e}_{f2} + \gamma W_f^T(k_v\boldsymbol{e}_{f2} + k_p\boldsymbol{e}_{f1}) \tag{3.8}$$

$$\boldsymbol{\beta} = \gamma W_f^T\boldsymbol{e}_{f2} \tag{3.9}$$

where $k_v > 0, k_p > 0, \gamma > 0, \alpha > 0$ *are control gains and corresponding filter states are defined by*

$$\dot{\boldsymbol{e}}_{f1} = -\alpha \boldsymbol{e}_{f1} + \boldsymbol{e}_1 \tag{3.10}$$

$$\dot{\boldsymbol{e}}_{f2} = -\alpha \boldsymbol{e}_{f2} + \boldsymbol{e}_2 \tag{3.11}$$

$$\dot{W}_f = -\alpha W_f + W \tag{3.12}$$

Regressor matrix W *satisfies the following with* $\boldsymbol{\theta}^*$ *of Eq. (3.3)*

$$\begin{aligned} W\boldsymbol{\theta}^* = M(\boldsymbol{x}_1)\left[k_v \boldsymbol{e}_2 + k_p \boldsymbol{e}_1 - \ddot{\boldsymbol{x}}_m\right] - C(\boldsymbol{x}_1, \boldsymbol{x}_2)\boldsymbol{x}_2 - \\ \boldsymbol{g}(\boldsymbol{x}_1) + \dot{M}(\boldsymbol{x}_1)\left[(k_v - \alpha)\boldsymbol{e}_{f2} + k_p \boldsymbol{e}_{f1} + \boldsymbol{e}_2\right] \end{aligned} \tag{3.13}$$

Then, the tracking error $\boldsymbol{e}_1$ *and* $\boldsymbol{e}_2$ *are guaranteed to satisfy the control objective; in other words, both* $\lim_{t\to\infty} \boldsymbol{e}_1(t) = 0$ *and* $\lim_{t\to\infty} \boldsymbol{e}_2(t) = 0$ *globally asymptotically.*

Before we proceed to the proof of Theorem 2, we notice that a redefined regressor matrix W is used for the control input $\boldsymbol{u}$ of Eq. (3.7) instead of W_s defined in Eq. (3.6) because W of Eq. (3.13) includes filter states as well as system states. In fact, from the comparison between Eq. (3.6) and Eq. (3.13), we see the following identity

$$\begin{aligned} W\boldsymbol{\theta}^* = W_s\boldsymbol{\theta}^* + \\ \underbrace{M(\boldsymbol{x}_1)\left[k_v \boldsymbol{e}_2 + k_p \boldsymbol{e}_1\right] + \dot{M}(\boldsymbol{x}_1)\left[(k_v - 1)\boldsymbol{e}_{f2} + k_p \boldsymbol{e}_{f1} + \boldsymbol{e}_2\right]}_{\text{added for the control analysis}} \end{aligned} \tag{3.14}$$

This means that W consists of not only states from dynamics, but also control signals designed to achieve the control objective, which is different from conventional regressor matrices. In general, a regressor matrix is made of system states described as in W_s of Eq. (3.6).

Proof. First, by applying filter states Eq.(3.10) and (3.11) to the error dynamics in Eq.(3.5), we can obtain the following dynamics of the error system:

$$\begin{aligned}
&\ddot{\boldsymbol{e}}_{f1} - \dot{\boldsymbol{e}}_{f2} = -\alpha\left(\dot{\boldsymbol{e}}_{f1} - \boldsymbol{e}_{f2}\right) \\
&M(\boldsymbol{x}_1)\left[\ddot{\boldsymbol{e}}_{f2} + k_v\dot{\boldsymbol{e}}_{f2} + k_p\dot{\boldsymbol{e}}_{f1}\right] + \dot{M}(\boldsymbol{x}_1)\left[\dot{\boldsymbol{e}}_{f2} + k_v\boldsymbol{e}_{f2} + k_p\boldsymbol{e}_{f1}\right] \\
&= -\alpha M(\boldsymbol{x}_1)\left[\dot{\boldsymbol{e}}_{f2} + k_v\boldsymbol{e}_{f2} + k_p\boldsymbol{e}_{f1}\right] + \boldsymbol{u} + W\boldsymbol{\theta}^*
\end{aligned} \tag{3.15}$$

Substituting Eq.(3.12) into Eq.(3.15) and introducing a control filter of Eq. (2.8) give us the following system equations:

$$\begin{aligned}
\dot{\boldsymbol{e}}_{f1} &= \boldsymbol{e}_{f2} + \boldsymbol{\varepsilon}_1(t) \\
M(\boldsymbol{x}_1)\dot{\boldsymbol{e}}_{f2} &= -M(\boldsymbol{x}_1)\left(k_v\boldsymbol{e}_{f2} + k_p\boldsymbol{e}_{f1}\right) + \boldsymbol{u}_f + W_f\boldsymbol{\theta}^* + \boldsymbol{\varepsilon}_2(t)
\end{aligned} \tag{3.16}$$

Furthermore, we can set $\boldsymbol{\varepsilon}_1(t) = \mathbf{0}$ and $\boldsymbol{\varepsilon}_2(t) = \mathbf{0}$ for all $t \geqslant 0$ by choosing initial conditions of the filter states as follows:

$$\begin{aligned}
\boldsymbol{e}_{f1}(0) &= \frac{(\alpha - k_v)\boldsymbol{e}_1(0) + \boldsymbol{e}_2(0)}{\alpha(\alpha - k_v) + k_p} \\
\boldsymbol{e}_{f2}(0) &= \frac{k_p\boldsymbol{e}_1(0) + \alpha\boldsymbol{e}_2(0)}{\alpha(\alpha - k_v) + k_p}
\end{aligned} \tag{3.17}$$

where positive control gains $\alpha,\ k_p$, and k_v are chosen to satisfy $\alpha(\alpha - k_v) + k_p \neq 0$. Therefore, the original error system of Eq. (3.5) is transformed into the following filtered error system

$$\begin{aligned}
\dot{\boldsymbol{e}}_{f1} &= \boldsymbol{e}_{f2} \\
\dot{\boldsymbol{e}}_{f2} &= -k_v\boldsymbol{e}_{f2} - k_p\boldsymbol{e}_{f1} + M^{-1}(\boldsymbol{x}_1)\left(\boldsymbol{u}_f + W_f\boldsymbol{\theta}^*\right)
\end{aligned} \tag{3.18}$$

Thus, the objective is to design $\boldsymbol{u}_f$ that guarantees $[\dot{\boldsymbol{e}}_f,\ \boldsymbol{e}_f] \rightarrow 0$ globally and asymptotically. Then, with the aid of Lemma 1, the stability of Eq. (3.5) may be

proved finally. Differences between Eq. (2.10) and Eq. (3.18) can be summarized as follows:

1. Eq. (2.10) is a first order system, while Eq. (3.18) is a controllable second order system with the same unknown parameter relationship. In fact, Eq. (2.10) is equivalent to Eq. (3.18) in a sense that Eq. (3.18) can be written as the first order system with increased dimensions.

2. Because of the property of $M(\boldsymbol{x}_1)$ in Eq. (3.2), we may introduce the attracting manifold described in Lemma 2 although $M(\boldsymbol{x}_1)$ is not a constant matrix such as ϕ^* in Eq. (2.10)

Now, consider the following simple Lyapunov candidate function (without the exponentially decaying term in filter dynamics)

$$V = \frac{k_p}{2}\boldsymbol{e}_{f1}^T\boldsymbol{e}_{f1} + \frac{1}{2}\boldsymbol{e}_{f2}^T\boldsymbol{e}_{f2} + \frac{\zeta}{2\lambda_{\min}}\boldsymbol{z}^T\boldsymbol{z} \tag{3.19}$$

where $\zeta > 1/(2\gamma k_v)$; $\boldsymbol{z}$ is defined by Eq. (2.20) together with $\boldsymbol{\theta}^*$ of Eq. (3.3), $\hat{\boldsymbol{\theta}}$ of Eq. (3.8), and $\boldsymbol{\beta}$ of Eq. (3.9); and $\lambda_{\min}$ is defined in Eq.(3.2). Synthesize $\boldsymbol{u}_f$ same as Eq. (2.18). Then, the time derivative of the given Lyapunov candidate function along the filtered error system in Eq.(3.18) is simplified as follows

$$\begin{aligned}
\dot{V} &= k_p\boldsymbol{e}_{f1}^T\boldsymbol{e}_{f2} + \boldsymbol{e}_{f2}^T\left(-k_v\boldsymbol{e}_{f2} - k_p\boldsymbol{e}_{f1} - M^{-1}(\boldsymbol{x}_1)W_f\boldsymbol{z}\right) + \frac{\zeta}{\lambda_{\min}}\boldsymbol{z}^T\left(\dot{\hat{\boldsymbol{\theta}}} + \dot{\boldsymbol{\beta}}\right) \\
&= -k_v\boldsymbol{e}_{f2}^T\boldsymbol{e}_{f2} - \boldsymbol{e}_{f2}^TM^{-1}W_f\boldsymbol{z} - \frac{\zeta\gamma}{\lambda_{\min}}\boldsymbol{z}^TW_f^TM^{-1}(\boldsymbol{x}_1)W_f\boldsymbol{z} \\
&\leqslant -\frac{k_v}{2}\|\boldsymbol{e}_{f2}\|^2 - \frac{\zeta\gamma}{2}\|M^{-1}(\boldsymbol{x}_1)W_f\boldsymbol{z}\|^2 \\
&\quad - \frac{k_v}{2}\left(\|\boldsymbol{e}_{f2}\|^2 - \frac{2}{k_v}\|\boldsymbol{e}_{f2}\|\|M^{-1}(\boldsymbol{x}_1)W_f\boldsymbol{z}\| + \frac{2\zeta\gamma}{k_v}\|M^{-1}(\boldsymbol{x}_1)W_f\boldsymbol{z}\|^2\right) \\
&\leqslant -\frac{k_v}{2}\|\boldsymbol{e}_{f2}\|^2 - \frac{\zeta\gamma}{2}\|M^{-1}(\boldsymbol{x}_1)W_f\boldsymbol{z}\|^2
\end{aligned} \tag{3.20}$$

Since $k_v, \gamma > 0$, both $V \geqslant 0$ and $\dot{V} \leqslant 0$ mean that $V \in \mathcal{L}_\infty$. This concludes that

every closed loop signal is bounded as long as $\boldsymbol{x}_m$ is bounded, which is true by definition. Thus, $\boldsymbol{e}_{f2}$ and $M^{-1}(\boldsymbol{x}_1)W_f\boldsymbol{z} \in \mathcal{L}_\infty \cap \mathcal{L}_2$. From Eq.(3.11) and the definition of $\boldsymbol{z}$ in Eq.(2.20), we also know $\dot{\boldsymbol{e}}_{f2} \in \mathcal{L}_\infty$ and $\frac{d}{dt}\left[M^{-1}(\boldsymbol{x}_1)W_f\boldsymbol{z}\right] \in \mathcal{L}_\infty$. Using Barbalat's lemma with these facts leads us to the conclusion that $\lim_{t\to\infty} \boldsymbol{e}_{f2} = 0$ and $\lim_{t\to\infty} M^{-1}(\boldsymbol{x}_1)W_f\boldsymbol{z} = 0$. The last thing to prove is the stability of $\boldsymbol{e}_{f1}$. Taking the time derivative of $\dot{\boldsymbol{e}}_{f2}$ in Eq.(3.18) shows that $\ddot{\boldsymbol{e}}_{f2} \in \mathcal{L}_\infty$. This tells us that $\lim_{t\to\infty} \dot{\boldsymbol{e}}_{f2} = 0$ associated with Barbalat's lemma. Finally, from Eq.(3.18), we see that $\lim_{t\to\infty} \boldsymbol{e}_{f1} = 0$ since $\dot{\boldsymbol{e}}_{f2} = -k_v\boldsymbol{e}_{f2} - k_p\boldsymbol{e}_{f1} - M^{-1}(\boldsymbol{x}_1)W_f\boldsymbol{z}$. Therefore, we can guarantee that $\lim_{t\to\infty}[\boldsymbol{e}_{f2}, \boldsymbol{e}_{f1}] = [0, 0]$ globally and asymptotically. Finally, $\boldsymbol{u}$ is obtained by following the same steps as in Eq. (2.23) □

As mentioned in Lemma 2, the error system Eq. (3.5) with the control input $\boldsymbol{u}$ computed by Theorem 2 has the attracting manifold $\mathcal{S}_R$ defined by

$$\mathcal{S}_R = \left\{\boldsymbol{z} \mid M^{-1}(\boldsymbol{x}_1)W_f\boldsymbol{z} = 0\right\} \tag{3.21}$$

whose dynamics is governed by

$$\dot{\boldsymbol{z}} = -\gamma W_f^T M^{-1}(\boldsymbol{x}_1)W_f\boldsymbol{z} \tag{3.22}$$

Properties of $\mathcal{S}_R$ are the same as those of Lemma 2. By virtue of the attracting manifold $\mathcal{S}_R$, Eq. (3.18) recovers its exponential decaying property, which improves the transient response of $\boldsymbol{e}$ in Eq. (3.5). Furthermore, in a perspective of parameter adaptation, we may say that the parameter adaptation error $\boldsymbol{z}$ of Eq. (3.19) remains zero after $\hat{\boldsymbol{\theta}} + \boldsymbol{\beta}$ in Theorem 2 reaches the true parameter vector $\boldsymbol{\theta}^*$ of Eq. (3.3), which is different from conventional certainty equivalent methods.

3.4 Adaptive Control with Parameter Projection

In this section, we extend the proposed control method by combining it with the projection technique. Although it is not listed as one of properties of Eq. (3.1), every inertia-related value is positive. In other words, each element of $\boldsymbol{\theta}^*$ in Eq. (3.3) is positive. Thus, we reparameterize $\boldsymbol{\theta}^*$ using $\boldsymbol{\theta}_p^*$ and introduce the estimate $\hat{\boldsymbol{\theta}}_p$ for $\boldsymbol{\theta}_p^*$ defined as follows:

$$\boldsymbol{\theta}_p^* = \begin{bmatrix} e^{\phi_1^*} \\ e^{\phi_2^*} \\ \vdots \\ e^{\phi_{m-1}^*} \\ e^{\phi_m^*} \end{bmatrix}, \quad \hat{\boldsymbol{\theta}}_p(t) = \begin{bmatrix} e^{\hat{\phi}_1(t)+\beta_1(t)} \\ e^{\hat{\phi}_2(t)+\beta_2(t)} \\ \vdots \\ e^{\hat{\phi}_{m-1}(t)+\beta_{m-1}(t)} \\ e^{\hat{\phi}_m(t)+\beta_m(t)} \end{bmatrix} \tag{3.23}$$

As a result of the reparameterization in Eq. (3.23), each element of $\boldsymbol{\theta}_p^*$ remains positive regardless of ϕ^*. Thus, in the following theorem, we adapt ϕ^* instead of $\boldsymbol{\theta}_p^*$ to keep the estimate $\hat{\boldsymbol{\theta}}_p$ positive to utilize a priori system information.

Theorem 3 (Adaptive Robot Arm Control with Projection)**.** *For the given system in Eq. (3.1) with a nonlinear parameterization defined in Eq. (3.23), the following control* $\boldsymbol{u}$ *guarantees the satisfaction of the tracking problem objective:*

$$\boldsymbol{u} = -W\hat{\boldsymbol{\theta}}_p - \gamma W_f \ \mathrm{Diag}[\hat{\boldsymbol{\theta}}_p] \ W_f^T \left((k_v - \alpha)\boldsymbol{e}_{f2} + k_p \boldsymbol{e}_{f1} + \boldsymbol{e}_2\right) \tag{3.24}$$

where

$$\dot{\hat{\boldsymbol{\phi}}}(t) = \gamma(\alpha W_f - W)^T \boldsymbol{e}_{f2} + \gamma W_f^T (k_v \boldsymbol{e}_{f2} + k_p \boldsymbol{e}_{f1}) \tag{3.25}$$

$$\boldsymbol{\beta} = \gamma W_f^T \boldsymbol{e}_{f2} \tag{3.26}$$

which are identical to Eq. (3.8) and Eq. (3.9) respectively. Other quantities are

defined at Theorem 2. Function $\mathrm{Diag}[\cdot] : \mathbb{R}^m \to \mathbb{R}^{m\times m}$ *is defined as*

$$\mathrm{Diag}\left[\begin{pmatrix} p_1 \\ \vdots \\ p_m \end{pmatrix}\right] = \begin{bmatrix} p_1 & 0 & \cdots & 0 \\ 0 & p_2 & 0 & \vdots \\ \vdots & 0 & \ddots & 0 \\ 0 & \cdots & 0 & p_m \end{bmatrix} \tag{3.27}$$

and k_v, k_p, γ, *and* α *have the same condition in Theorem 2. Each filter definition is identical to Eq. (3.10)-(3.12) with the same regressor matrix* W *in Eq. (3.13).*

Proof. Filtered error dynamics with projection are also derived using Eq. (3.10)-Eq. (3.12) as in the previous section. Thus, the formula of filtered error dynamics are the same as Eq. (3.18) except for the unknown parameter vector representation. Therefore, we only have to consider the adaptation part with projection. Let a new parameter estimation error and adaptation discrepancy be denoted by $\boldsymbol{\eta}$ and $\boldsymbol{z}$ respectively as follows:

$$\boldsymbol{\eta} = \hat{\boldsymbol{\theta}}_p - \boldsymbol{\theta}_p^* \tag{3.28}$$

$$\boldsymbol{z} = \hat{\boldsymbol{\phi}} + \boldsymbol{\beta} - \boldsymbol{\phi}^* \tag{3.29}$$

where $\phi^* = [\phi_1^*, \cdots, \phi_m^*]^T$ and a subscript i denotes the i^{th} element of the given vector. Then, consider the Lyapunov candidate function V_p given by

$$V_p = \frac{k_p}{2}\boldsymbol{e}_{f1}^T\boldsymbol{e}_{f1} + \frac{1}{2}\boldsymbol{e}_{f2}^T\boldsymbol{e}_{f2} + \frac{\zeta}{\lambda_{\min}}\underbrace{\sum_{i=1}^{m}\left(e^{z_i+\phi_i^*} - e^{\phi_i^*}z_i\right)}_{V_{\boldsymbol{z}}} \tag{3.30}$$

Only difference between Eq. (3.19) and Eq. (3.30) is a newly introduced $V_{\boldsymbol{z}}$ which replaces $\boldsymbol{z}^T\boldsymbol{z}$ in Eq. (3.19). $V_{\boldsymbol{z}}$ is lower bounded at $\boldsymbol{z} = 0$ and monotonically increasing as $\|\boldsymbol{z}\|$ increases. This is easily shown by taking derivative of $V_{\boldsymbol{z}}$ with respect to

$\boldsymbol{z}$ as follows:

$$V'_{z_i} = \frac{\partial}{\partial z_i}\left(e^{z_i+\phi_i^*} - e^{\phi_i^*} z_i\right) = e^{z_i+\phi_i^*} - e^{\phi_i^*} \begin{cases} > 0 & \text{if } z_i > 0 \\ < 0 & \text{if } z_i < 0 \\ = 0 & \text{at } z_i = 0 \end{cases} \tag{3.31}$$

$$V''_{z_i} = \frac{\partial}{\partial z_i}\left(e^{z_i+\phi_i^*} - e^{\phi_i^*}\right) = e^{z_i+\phi_i^*} > 0 \quad \text{for all } z_i \tag{3.32}$$

Therefore, we may conclude that V_p is lower bounded and unbounded with respect to $[\boldsymbol{e}_{f1}, \boldsymbol{e}_{f2}, \boldsymbol{z}]$. Furthermore, since we use the same filter states and regressor matrix, the following filtered error dynamics are obtained:

$$\dot{\boldsymbol{e}}_{f1} = \boldsymbol{e}_{f2} \tag{3.33}$$

$$\dot{\boldsymbol{e}}_{f2} = -k_v \boldsymbol{e}_{f2} - k_p \boldsymbol{e}_{f1} - M^{-1}(\boldsymbol{x}_1) W_f \boldsymbol{\eta} \tag{3.34}$$

which is also identical to Eq. (3.18) except that $\boldsymbol{\eta}$ of Eq. (3.28) is used instead of $\boldsymbol{z}$ in Eq. (3.19). This is because we choose $\boldsymbol{u}_f$ as follows

$$\boldsymbol{u}_f = -W_f \hat{\theta}_p \tag{3.35}$$

The time derivative of V_p in Eq. (3.30) along with Eq. (3.33), Eq. (3.34), Eq. (3.25),

and Eq. (3.26) leads to the following inequality

$$\begin{aligned}
\dot{V}_p &= k_p \boldsymbol{e}_{f1}^T \dot{\boldsymbol{e}}_{f1} + \boldsymbol{e}_{f2}^T \dot{\boldsymbol{e}}_{f2} + \frac{\zeta}{\lambda_{\min}} \underbrace{\sum_{i=1}^{m} \left(e^{z_i + \phi_i^*} - e^{\phi_i^*} \right) \dot{z}_i}_{=\boldsymbol{\eta}^T \dot{\boldsymbol{z}}} \\
&= k_p \boldsymbol{e}_{f1}^T \boldsymbol{e}_{f2} + \boldsymbol{e}_{f2}^T \left(-k_v \boldsymbol{e}_{f2} - k_p \boldsymbol{e}_{f1} - M^{-1}(\boldsymbol{x}_1) W_f \boldsymbol{\eta} \right) + \frac{\zeta}{\lambda_{\min}} \boldsymbol{\eta}^T \left(\dot{\hat{\boldsymbol{\theta}}} + \dot{\boldsymbol{\beta}} \right) \\
&= -k_v \boldsymbol{e}_{f2}^T \boldsymbol{e}_{f2} - \boldsymbol{e}_{f2}^T M^{-1}(\boldsymbol{x}_1) W_f \boldsymbol{\eta} - \frac{\zeta\gamma}{\lambda_{\min}} \boldsymbol{\eta}^T W_f^T M^{-1}(\boldsymbol{x}_1) W_f \boldsymbol{\eta} \\
&\leqslant -\frac{k_v}{2} \|\boldsymbol{e}_{f2}\|^2 - \frac{\zeta\gamma}{2} \|M^{-1}(\boldsymbol{x}_1) W_f \boldsymbol{\eta}\|^2 \\
&\quad - \frac{k_v}{2} \left(\|\boldsymbol{e}_{f2}\|^2 - \frac{2}{k_v} \|\boldsymbol{e}_{f2}\| \|M^{-1}(\boldsymbol{x}_1) W_f^T \boldsymbol{z}\| + \frac{2\zeta\gamma}{k_v} \|M^{-1}(\boldsymbol{x}_1) W_f \boldsymbol{\eta}\|^2 \right) \\
&\leqslant -\frac{k_v}{2} \|\boldsymbol{e}_{f2}\|^2 - \frac{\zeta\gamma}{2} \|M^{-1}(\boldsymbol{x}_1) W_f \boldsymbol{\eta}\|^2
\end{aligned} \tag{3.36}$$

This negative semi-definiteness of $\dot{V}_p$ in Eq.(3.36) is exactly same as in Eq.(3.20) except that $\boldsymbol{z}$ is replaced with $\boldsymbol{\eta}$. Therefore, since the same arguments for the stability issue on Eq.(3.19) in the previous section can be applied here, we can also guarantee that $\lim_{t\to\infty}[\boldsymbol{e}_{f2}, \boldsymbol{e}_{f1}] = [0, 0]$ globally and asymptotically. Finally, $\boldsymbol{u}$ is obtained as follows

$$\begin{aligned}
\boldsymbol{u} &= \dot{\boldsymbol{u}}_f + \alpha \boldsymbol{u}_f \\
&= -\dot{W}_f \hat{\boldsymbol{\theta}}_p - W_f \dot{\hat{\boldsymbol{\theta}}}_p - \alpha W_f \hat{\boldsymbol{\theta}}_p \\
&= -W \hat{\boldsymbol{\theta}}_p - W_f \mathrm{Diag}[e^{\hat{\boldsymbol{\phi}} + \boldsymbol{\beta}}] (\dot{\hat{\boldsymbol{\phi}}} + \dot{\boldsymbol{\beta}})
\end{aligned} \tag{3.37}$$

Finally, by substituting Eq. (3.25) and Eq. (3.26) into Eq. (3.37), Eq. (3.24) is obtained and this proves Theorem 3. □

The following attracting manifold $\mathcal{S}_{RP}$ is defined as

$$\mathcal{S}_{RP} = \left\{ \boldsymbol{\eta} \mid M^{-1}(\boldsymbol{x}_1) W_f \boldsymbol{\eta} = 0 \right\} \tag{3.38}$$

It inherits all properties of Eq. (3.21) except for $\boldsymbol{z}$ dynamics of Eq. (3.22). Since $\boldsymbol{\eta}$ is an estimation error, $\boldsymbol{\eta}$ has the same property as $\boldsymbol{z}$ in Eq. (3.22).

3.5 Numerical Simulations

As we pointed out, the proposed control method can recover the performance of the deterministic controller within a filter state space without being affected by the dynamics of the parameter estimator, which enables us to expect the improvement of the transient response in trajectory tracking adaptive control problems. In the following simulation, we compare the proposed control method with the conventional certainty equivalent one to highlight the performance improvement in transient responses. The example robot arm system is taken from [31] and depicted in Fig. 3.1. System equations are given by following definitions:

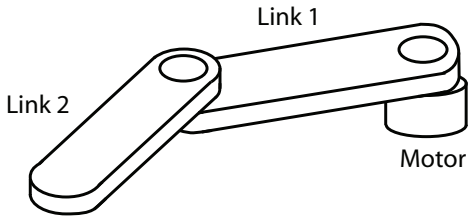

Link 1:
Mass 10.6 kg
Length 380 mm

Link 2:
Mass 4.85 kg
Length 240 mm

Figure 3.1: 2-Link planar robot arm

$$
\begin{aligned}
\boldsymbol{x}_1 &= [x_{11}\ x_{12}]^T \\
\boldsymbol{x}_2 &= [x_{21}\ x_{22}]^T \\
M(\boldsymbol{x}_1) &= \begin{pmatrix} p_1 + 2p_3 \cos x_{12} & p_2 + p_3 \cos x_{12} \\ p_2 + p_3 \cos x_{12} & p_2 \end{pmatrix} \\
C(\boldsymbol{x}_1, \boldsymbol{x}_2) &= \begin{pmatrix} -p_3 x_{22} \sin x_{12} & -p_3(x_{21} + x_{22}) \sin x_{12} \\ p_3 x_{21} \sin x_{12} & 0 \end{pmatrix}
\end{aligned} \tag{3.39}
$$

where $[p_1, p_2, p_3] = [3.6, 0.2, 0.15] = \boldsymbol{\theta}^*$ and x_{ij} represent j^{th} arm angular position ($i = 1$) and angular velocity ($i = 2$) respectively. Since the robot arm is configured on a plane, there is no gravity term and friction term is also negligible.

3.5.1 Proposed Adaptive Control

First, we simulate an adaptive control case without projection mechanism. Certainty equivalent control is chosen as

$$\boldsymbol{u}_{ce} = -\boldsymbol{e}_1 - k_{v\,ce}\boldsymbol{e} - W_1(\boldsymbol{x})\hat{\boldsymbol{\theta}}_{ce} \tag{3.40}$$

$$\dot{\hat{\boldsymbol{\theta}}}_{ce} = \gamma_{ce} W_1^T(\boldsymbol{x})\boldsymbol{e} \tag{3.41}$$

where $\boldsymbol{e} = k_{p_{ce}}\boldsymbol{e}_1 + \boldsymbol{e}_2$ is introduced to avoid the detectability obstacle. This control law is based on [31] and the subscript ce represents a certainty equivalence method. Reference signals and initial values for simulations are set to the followings:

$$\begin{aligned} \boldsymbol{x}_m(t) &= [\cos t + 2 \;\; \sin t + 2]^T \\ \boldsymbol{x}_1(0) &= \boldsymbol{x}_2(0) = [0 \;\; 0]^T \\ \hat{\boldsymbol{\theta}}_{ce}(0) &= \hat{\boldsymbol{\theta}}(0) = [4.6, 1.2, 1.15]^T \end{aligned} \tag{3.42}$$

Filter initial states are decided by Eq. (3.17).

In Fig. 3.2, the Ideal result is from the deterministic controller case where the true parameter values are available to the controller, which means there is no estimator to decrease the transient performance. Since both CE (certainty equivalence) and the proposed method have different error and regressor definitions, the CE method is tuned ($k_{p_{ce}} = 0.6,\ k_{v\,ce} = 0.8$ when $k_p = 1,\ k_v = 1$) to have the same error convergence rate as of the proposed method for the sake of fair comparison in Fig. 3.2. A wriggle in the error trajectories is explained by the fact that our robot system is second order. After tuning the transient performance, only the learning

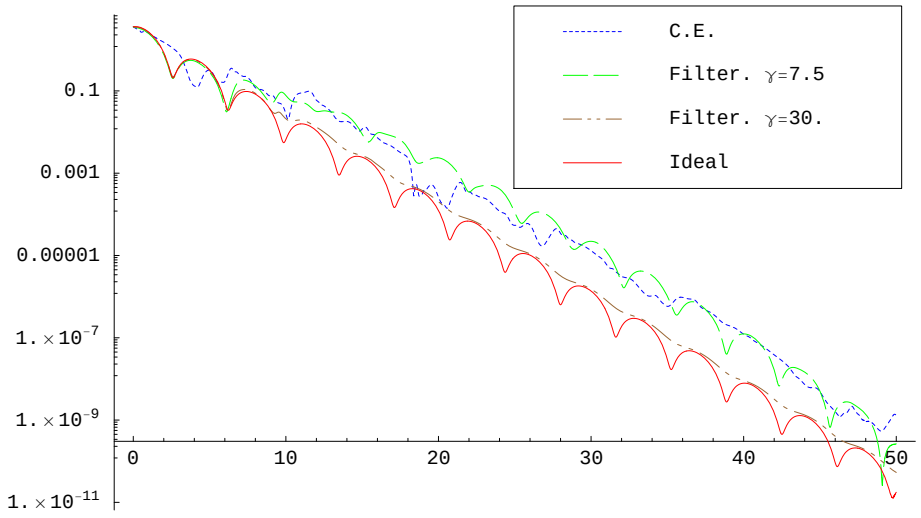

(a) Generalized position error trajectory $\|\boldsymbol{e}_1(t)\|$

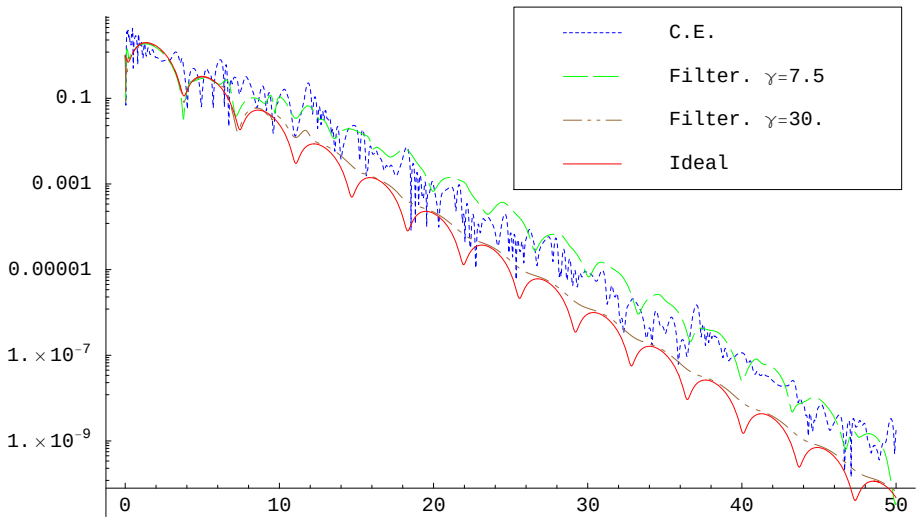

(b) Generalized velocity error trajectory $\|\boldsymbol{e}_2(t)\|$

Figure 3.2: Tracking error norm trajectory along the time t

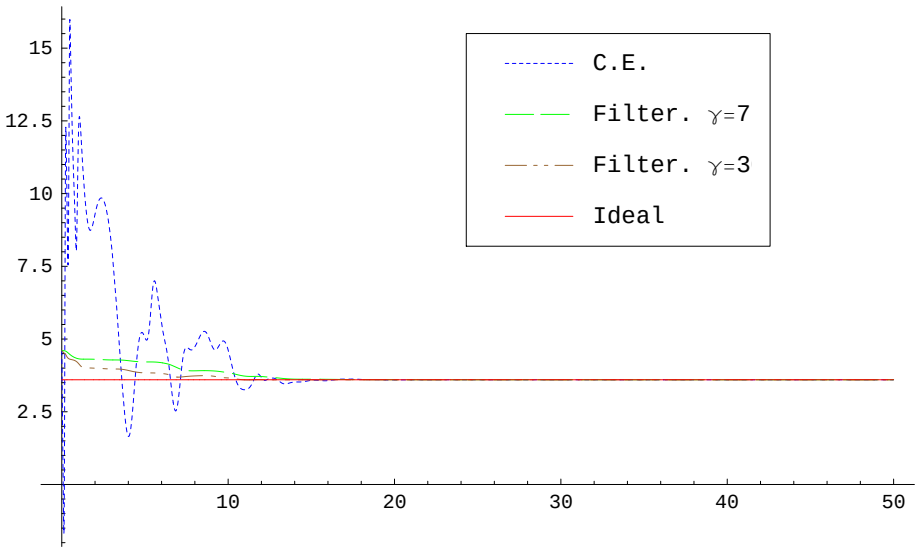

(a) Parameter estimate trajectory for $\boldsymbol{\theta}_1^*$

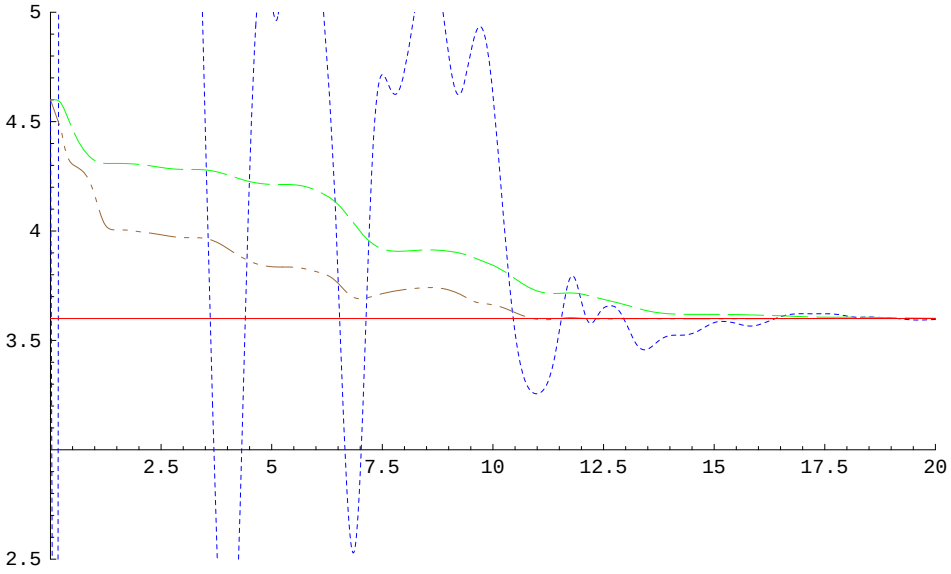

(b) Zoomed-in parameter estimate trajectory for $\boldsymbol{\theta}_1^*$

Figure 3.3: Parameter estimates trajectory of $\hat{\boldsymbol{\theta}}_1(t)$ along the time t

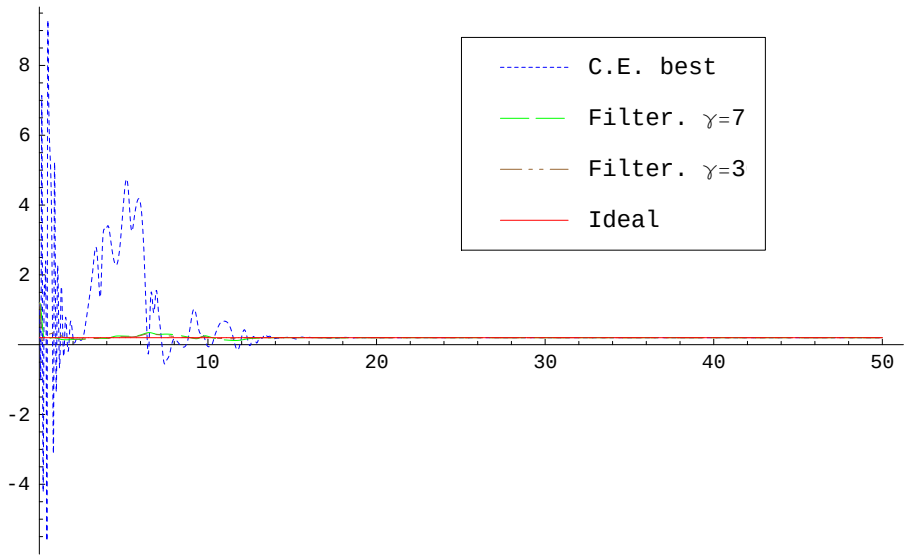

(a) Parameter estimate trajectory for $\boldsymbol{\theta}_2^*$

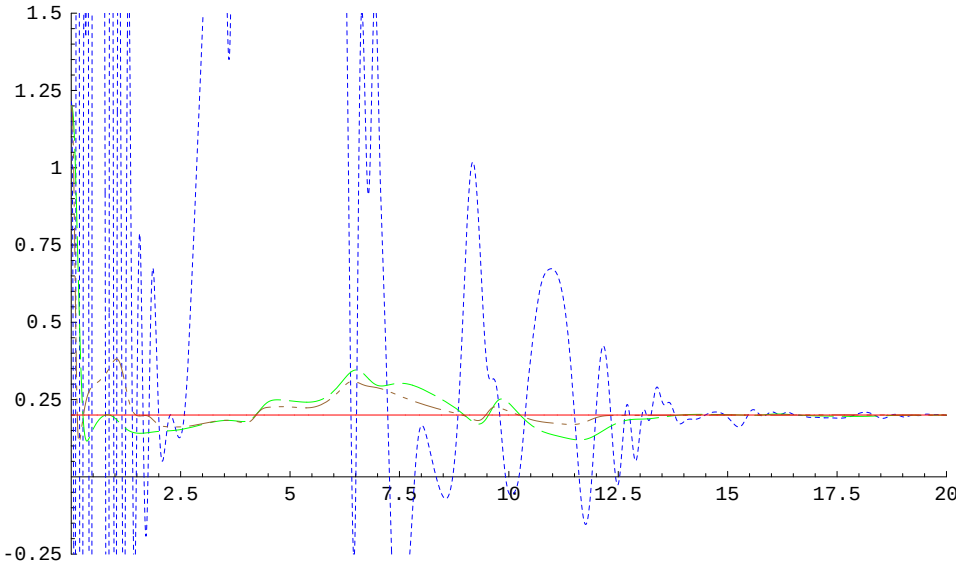

(b) Zoomed-in parameter estimate trajectory for $\boldsymbol{\theta}_2^*$ during the first 20 sec

Figure 3.4: Parameter estimates trajectory of $\hat{\boldsymbol{\theta}}_2(t)$ along the time t

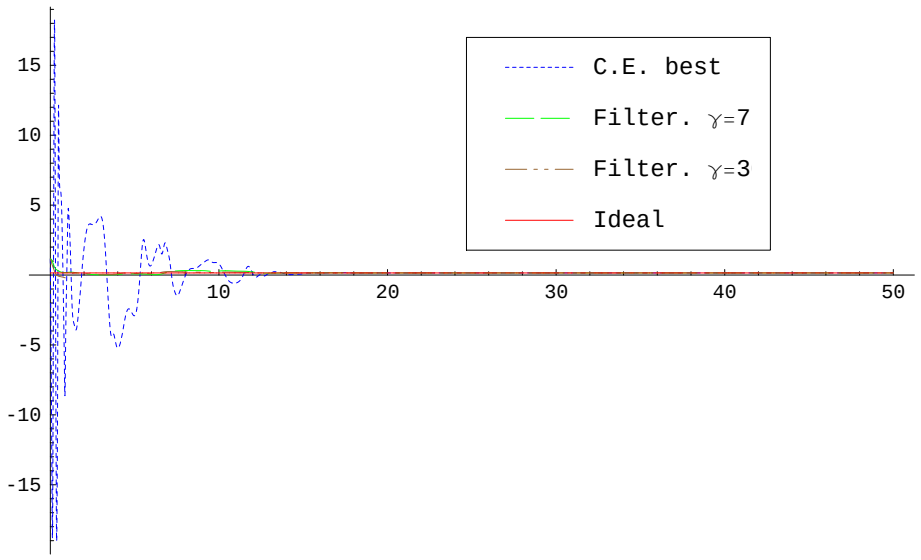

(a) Parameter estimate trajectory for $\boldsymbol{\theta}_3^*$

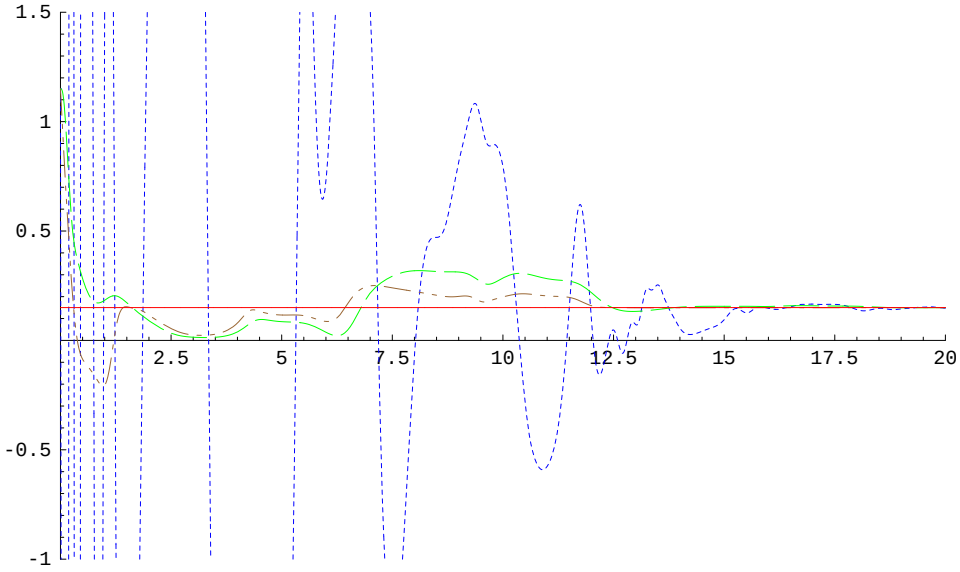

(b) Zoomed-in parameter estimate trajectory for $\boldsymbol{\theta}_3^*$

Figure 3.5: Parameter estimates trajectory of $\hat{\boldsymbol{\theta}}_3(t)$ along the time t

rate γ_{ce} for the CE method and its corresponding γ in $\boldsymbol{\beta}$ of Eq. (3.9) are changed to compare the effect of the estimator structure. In the CE simulation, best performance is achieved when the learning rate is set to $\gamma = 30$. Compared to the best CE result, the proposed method already achieves almost the same performance when the corresponding $\gamma = 7.5$. In our context, "almost the same performance" means the rate of convergence is almost the same as with each other. Furthermore, the proposed method attains the ideal performance at $\gamma = 30$. Since the reference signal is persistently exciting, we can easily expect that the parameter estimates converge to the true values. This behavior is shown in Fig. 3.3-Fig. 3.5. We may also recognize in the same figures that the parameter estimate convergence to the true value in the proposed method is much faster than the CE method because of the attractive property of $\mathcal{S}_R$ represented by Eq. (3.22). The Ideal case means the true parameter value. Because of the high learning rate in the CE method ($\gamma = 30$), we can recognize radical changes in the CE estimates during the updating procedure. However, the proposed method is performing the update with relatively small efforts compared to the CE method. In fact, γ in the proposed method is different from the learning rate in the CE method. The γ in $\boldsymbol{\beta}$ of Eq. (3.9) is used to modify the $\boldsymbol{z}$ dynamics of Eq. (3.22). This benefit is dramatically shown in the Fig. 3.6. The control norm of the CE method reaches 200, while the proposed method reaches only 20. This difference is from the different role of γ/γ_{ce} between the CE and proposed method. In the proposed method, γ effect in $\boldsymbol{\beta}$ is reduced by the attracting manifold for $\boldsymbol{z}$. Since both $\boldsymbol{z}$ and $\boldsymbol{e}$ decay fast, γ related control signal decay fast compared to the CE control method within the transient region (parameter estimation error signal is dominant at this region), while γ_{ce} in $\hat{\theta}_{ce}$ is directly fed up to the error dynamics. Through Fig. 3.2 - Fig. 3.6, it is clear that the proposed control method outperforms in the perspective of transient performance due to the stable manifold designated by $\boldsymbol{z}$.

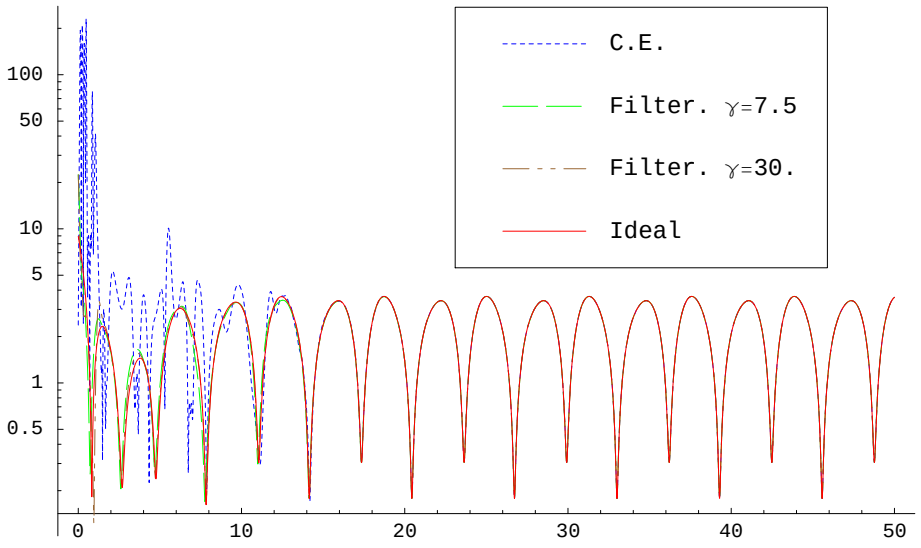

(a) Control efforts $\|\boldsymbol{u}(t)\|$

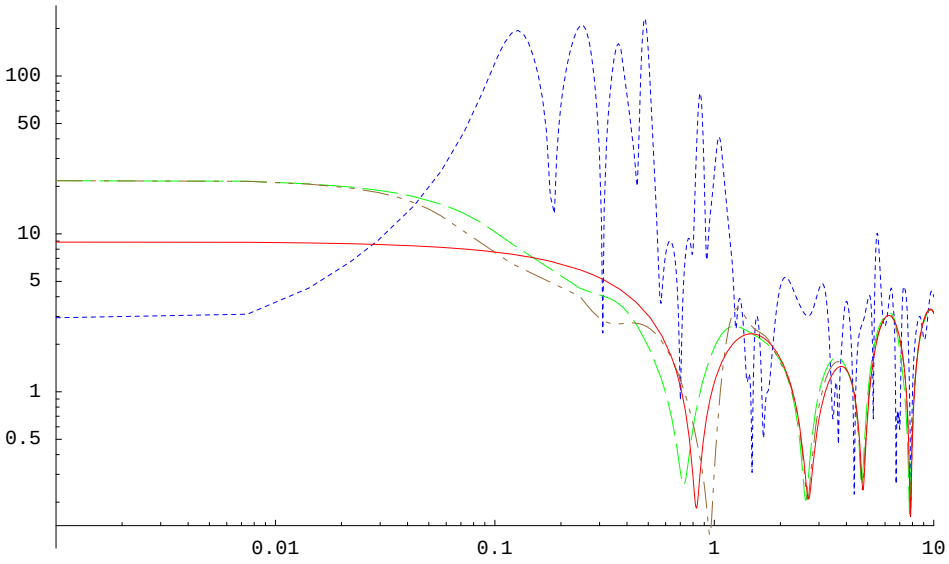

(b) Zoomed picture on the transient region in log-log scale

Figure 3.6: Control norm trajectory along the time t

3.5.2 Proposed Control with Projection Mechanism

The performance of the proposed control scheme may be improved when it is combined with the projection technique. To clearly show the difference dependant upon the existence of a projection mechanism, we simulate the system in Eq. (3.39) based on Theorem 2 and 3 respectively. γ is fixed at 7.5 for both controller. A reference signal is chosen as $\boldsymbol{x}_m(t) = [\cos t, \sin t]^T$. Because $\|\boldsymbol{x}_m(t)\| = 1$ for all $t \geqslant 0$ regardless of the norm of each element, we can think of $\boldsymbol{x}_m(t)$ as a weakly persistently exciting reference signal. The convergence rate of each error norm is compared in Fig. 3.7. By adopting a projection, the error norm with a projection converges to zero faster than one without a projection mechanism. We can observe the actual behavior of adaptation in Fig. 3.8. As we expected, each estimate value of a projection stays at the positive region while estimates go negative in the proposed method without a projection. Although a projection technique decreased control efforts, both of them are still comparable to each other. This can be shown in Fig. 3.9.

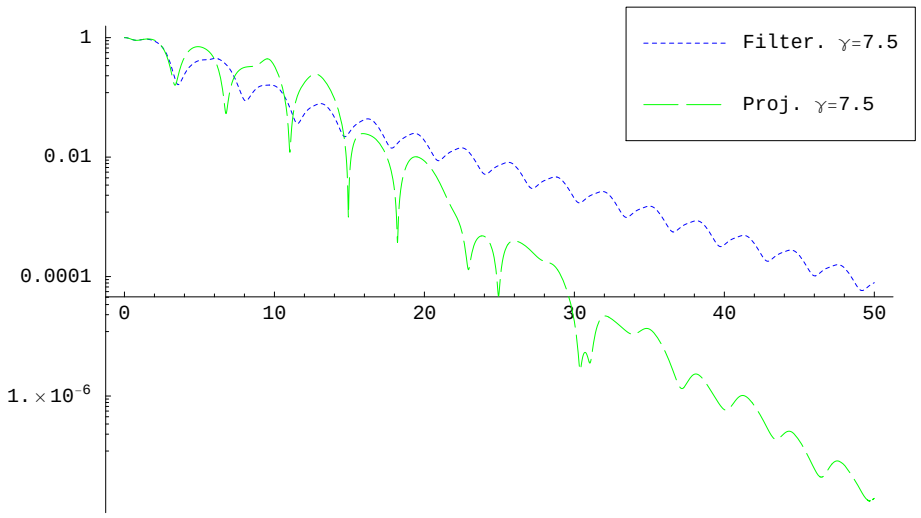

(a) $\|\boldsymbol{e}_1\|$ trajectory

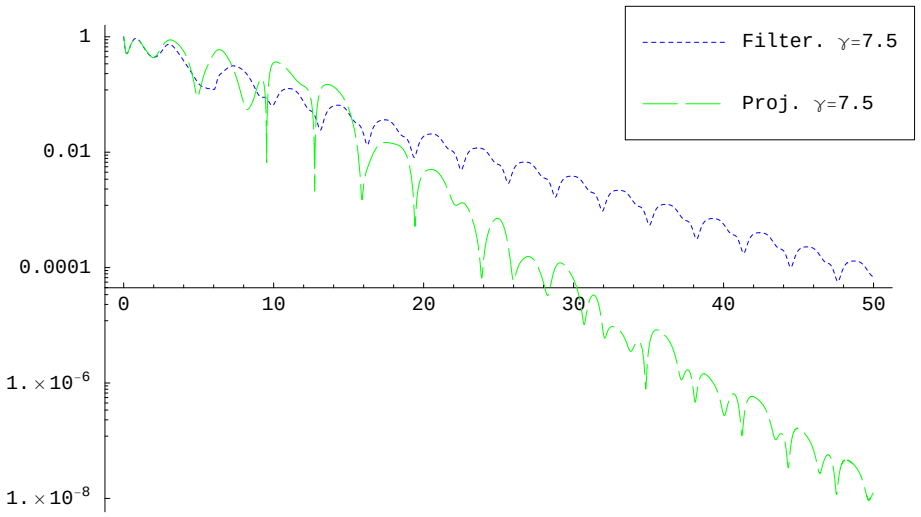

(b) $\|\boldsymbol{e}_2\|$ trajectory

Figure 3.7: Error norm trajectory comparison between the proposed method and the proposed method with a projection

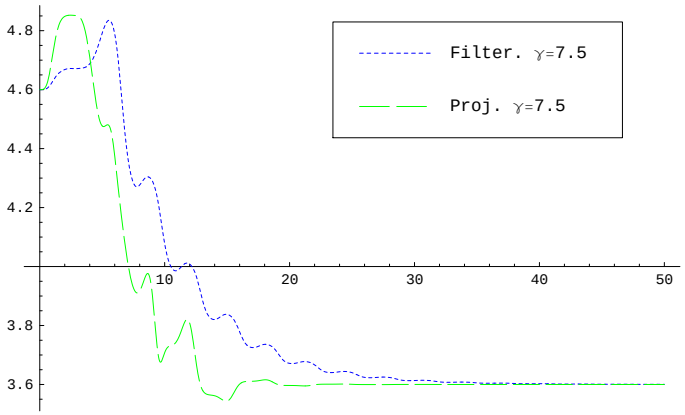

(a) Parameter estimate trajectory for θ_1^*

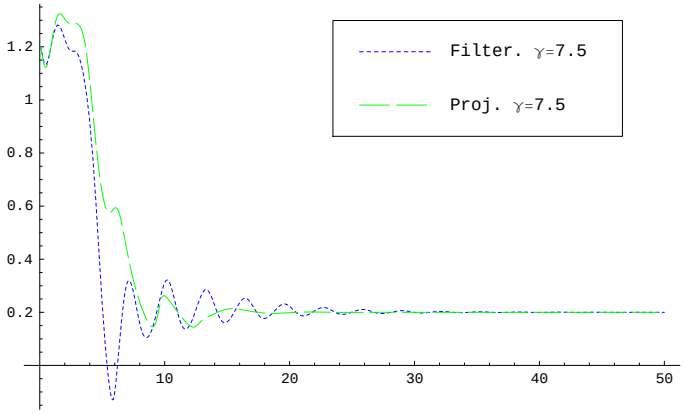

(b) Parameter estimate trajectory for θ_2^*

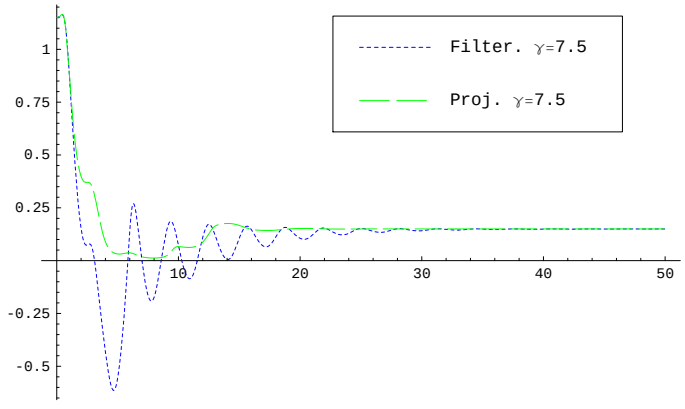

(c) Parameter estimate trajectory for θ_3^*

Figure 3.8: Parameter estimates trajectory comparison according to the existence of a projection mechanism

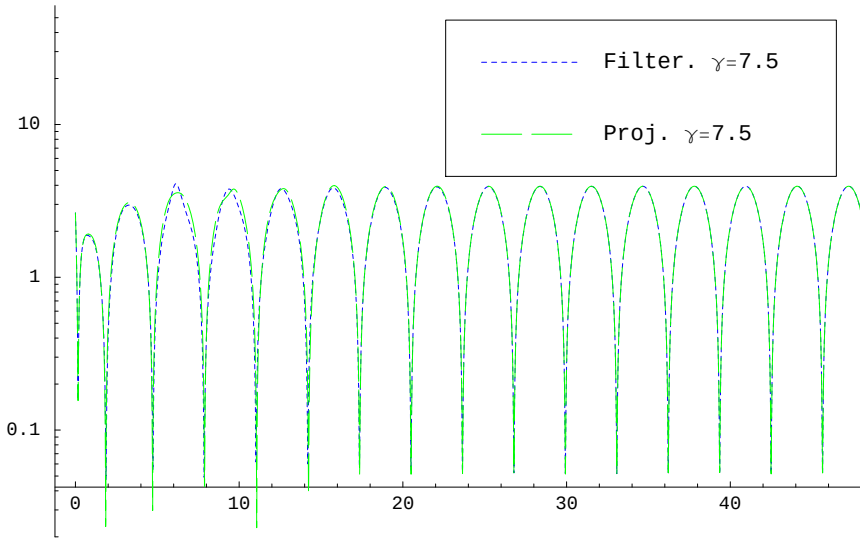

(a) Parameter estimate trajectory for θ_3^*

Figure 3.9: Control trajectory comparison according to the existence of a projection mechanism

Chapter 4

Attitude Tracking Control Problem with Unknown Inertia Parameters

Following the previous chapter, the proposed control method is applied to the adaptive attitude tracking control problem. Since the attitude control system is nonlinear in nature due to the kinematic relationship, it is natural to consider attitude control problems as another application. Further, attitude control problems arise in various fields of industries (e.g., spacecraft, unmanned aerial vehicle, unmanned marine vehicle, etc.) and there have been a strong demand for the high performance control scheme although several solutions exist. Thus, the new adaptive attitude control scheme is designed to improve the overall system performance and demonstrated through numerical simulations.

4.1 Introduction

The nonlinear control problem associated with spacecraft attitude dynamics has been extensively studied and various proportional derivative (PD) type stabilizing feedback solutions are currently available in the literature[32–35]. In particular, the application of model reference adaptive control theory for stabilizing spacecraft attitude tracking dynamics in the presence of arbitrarily large inertia matrix uncertainties has been largely enabled by the crucial fact that the governing dynamics permit affine representation of inertia related terms[36–38]. Nearly every one of these existing adaptive attitude tracking control solutions are based upon the classical certainty equivalence (CE) principle[10, 39] which permits the adaptive controller to retain a structure that is identical to that of the deterministic case controller wherein the inertia parameters are fully available (no uncertainty) except for the introduction of an additional carefully designed parameter update (estimation) mechanism that ensures stability with the adaptive controller and boundedness of all resulting closed-loop signals.

In theoretical terms, the closed-loop error dynamics generated by CE-based adaptive control solutions is exactly equivalent to the deterministic case control error dynamics whenever the estimated parameters coincide with their corresponding unknown true values. Of course, this happens only when the underlying reference trajectory satisfies suitable persistence of excitation (PE) conditions[39]. As a result, typically, the control performance of CE-based adaptive attitude control methods for either set-point regulation or trajectory tracking problems can at best match the performance of the deterministic case controller, that too only when the PE hypothesis ensure sufficiently fast convergence of parameter estimates to their true values. However, in practice, the closed-loop performance obtained from CE-based adaptive controllers is often seen to be arbitrarily poor when compared to the ideal deterministic control case either due to non-satisfaction of PE conditions and/or

slow convergence rates for the parameter estimates. All these factors ultimately reflect in terms of imposing wasteful rotational motion due to the control action and thereby significant increases within the torque requirements and fuel costs.

This aforementioned performance degradation of CE-based adaptive control in attitude tracking/regulating problems is mainly caused by the fact that search/estimation efforts of the parameter update law act like a additive disturbance imposed onto the deterministic case closed-loop dynamics. Another potential cause of performance degradation is the fact that parameter estimation dynamics are driven by the state regulation errors or tracking errors, which results in the undesirable feature of parameter estimates being unable to get locked onto their corresponding true values even if at any given instant during the estimation process the estimates are equal to their true values. Moreover, parameter estimates from CE-based adaptive control methods always deviate (drift) from their corresponding true values even if they are initiated to exactly coincide with their true values whenever there exists nonzero tracking/regulating error. Therefore, one may think of improving the overall closed-loop performance of adaptive control schemes by either eliminating in a stable fashion the disturbance type of terms within closed-loop error dynamics arising due to estimation of uncertain parameters or by forcing the parameter estimates stay locked at their true parameters once they are attained during the estimation process. A technical challenge in this matter is to design such a parameter update rule that would deal with both uncertain parameter effects and estimation drift.

The main contribution is the introduction of a new non-certainty equivalence (non-CE) adaptive attitude tracking control method that has potential to deliver significantly superior closed-loop performance when compared to the classical CE-based adaptive control schemes. Our results are partly motivated by the recently formulated Immersion and Invariance (I&I) adaptive control theory[6, 9, 19]. The

I&I design is essentially a non-CE based adaptive control methodology that overcomes many of the performance limitations arising from CE-based designs but applications of I&I adaptive control have thus far been somewhat limited to either single-input nonlinear systems or linear multivariable systems. In this chapter, we extend the I&I framework to the nonlinear spacecraft adaptive attitude tracking problem endowed with three independent torque actuators. We are able to do so while preserving all the key beneficial features of the I&I adaptive control methodology by introducing a stable linear filter for the regressor matrix so that the parameter adaptation dynamics reside within a stable and attracting manifold. In particular, our novel controller design approach ensures that the additive disturbance type of term arising within the closed-loop dynamics due to the parameter estimation error decays to zero independent of satisfaction of any PE type conditions. Moreover, rate of this decay can be prescribed to be arbitrarily fast while negligible or at worst minimal impact on the overall fuel/control budgets. Yet another interesting and important consequence of our new result that is never possible with existing CE-based solutions is the fact that the proposed adaptive parameter estimation process automatically stops if and when the parameter estimates happen to coincide with their corresponding unknown true values. Our formulation is given in terms of the globally valid (singularity-free) four-dimensional unit quaternion representation for attitude. Assuming the spacecraft inertia matrix to be unknown, we make use of full-state feedback, i.e., perfect measurement of body angular rate and the attitude measurement in terms of the quaternion parameterization to guarantee *globally stable* closed-loop behavior with asymptotic convergence of regulation/tracking errors for all possible initial conditions. It is pertinent here to observe the fact that the set of special group of rotation matrices that describe body orientation in three dimensions $SO(3)$ is not a contractable space and hence quaternion based formulations do not permit globally continuous stabilizing controllers[32, 33]. In this sense, we

adopt the standard terminology/notion of (almost) global stability for this problem to imply stability over an open and dense set in $SO(3)$ as is usually seen in literature dealing with this problem[40]. It should also be emphasized that the basic approach outlined in this chapter can be readily extended to other attitude representations including minimal three-parameter sets[41–43].

This chapter is organized as follows. In section 4.2, the attitude tracking control problem is formulated starting from basic description of quaternion kinematics and the Euler rotational dynamics equations. Then, in section 4.3, the main theoretical results are presented along with detailed stability proofs. In section 4.5, we show numerical simulation results for spacecraft attitude tracking control problems comparing our new non-CE method with a conventional CE-based method to highlight the performance improvement due to presence of an attracting manifold within the proposed parameter adaptation mechanism.

4.2 Problem Formulation

Euler's rotational equations of motion state the rigid body attitude dynamics in terms of its angular velocity $\boldsymbol{\omega}(t) \in \mathbb{R}^3$ prescribed in a body fixed frame, the mass moment of inertia defined through the 3×3 symmetric positive-definite matrix J (assumed to be an unknown constant), and an external control torque $\boldsymbol{u}(t) \in \mathbb{R}^3$, as follows

$$J\dot{\boldsymbol{\omega}}(t) = -S(\boldsymbol{\omega}(t))J\boldsymbol{\omega}(t) + \boldsymbol{u}(t) \tag{4.1}$$

where the skew-symmetric matrix operator $S(\cdot)$ represents the vector cross product operation between any two vectors as defined by

$$S(\boldsymbol{x})\boldsymbol{y} = \boldsymbol{x} \times \boldsymbol{y}; \quad \boldsymbol{x}, \boldsymbol{y} \in \mathbb{R}^3 \tag{4.2}$$

The corresponding kinematic differential equations governing the attitude motion are given by

$$\dot{\boldsymbol{q}}(t) = \frac{1}{2} E(\boldsymbol{q}(t))\boldsymbol{\omega}(t) \tag{4.3}$$

where $\boldsymbol{q}(t)$ is the four-dimensional unit-norm constrained quaternion vector representing the attitude of the body-fixed frame $\mathcal{F}_B$ with respect to the inertial frame $\mathcal{F}_N$. In the following development, for the sake of notational simplicity, the time argument 't' is left out except at places where it is noted for emphasis. We denote q_o and $\boldsymbol{q_v}$ as scalar and vector parts of the unit quaternion respectively, i.e., $\boldsymbol{q} = [q_o, \boldsymbol{q_v}]^T$ along with the unit quaternion constraint $\boldsymbol{q}^T\boldsymbol{q} = 1$. Quaternion operator $E(\boldsymbol{q})$ in Eq. (4.3) is defined by

$$E(\boldsymbol{q}) = \begin{bmatrix} -\boldsymbol{q_v}^T \\ q_o I_{3\times 3} + S(\boldsymbol{q_v}) \end{bmatrix} \tag{4.4}$$

where $I_{3\times 3}$ is the 3×3 identity matrix. The direction cosine matrix can be obtained from the quaternion vector through the following identity[34]

$$C(\boldsymbol{q}) = I_{3\times 3} - 2q_o S(\boldsymbol{q_v}) + 2S^2(\boldsymbol{q_v}) \tag{4.5}$$

and the time rate of change for the direction cosine matrix $C(\boldsymbol{q})$ is given by the well-known Poisson differential equation[34]

$$\frac{d}{dt} C(\boldsymbol{q}) = -S(\boldsymbol{\omega})C(\boldsymbol{q}) \tag{4.6}$$

which is the matrix version of the rotational kinematics stated through Eq. (4.3). Since it is natural for the commanded angular velocity to be specified in its own reference frame $\mathcal{F}_R$, we assume the commanded angular velocity $\boldsymbol{\omega}_r$ to be stated in the reference frame $\mathcal{F}_R$ and we denote $\boldsymbol{q}_r$ to orient the commanded reference frame

$\mathcal{F}_R$ with respect to the inertial frame $\mathcal{F}_N$. Then, the attitude and angular velocity tracking errors are obtained as follows

$$C(\delta\boldsymbol{q}) = C(\boldsymbol{q})C^T(\boldsymbol{q}_r) \tag{4.7}$$

$$\delta\boldsymbol{\omega} = \boldsymbol{\omega} - C(\delta\boldsymbol{q})\boldsymbol{\omega}_r \tag{4.8}$$

where the attitude error quaternion $\delta\boldsymbol{q} = [\delta q_o, \delta\boldsymbol{q_v}]^T$ follows our notational convention. We note here that $\mathcal{F}_B \to \mathcal{F}_R$ means $C(\delta\boldsymbol{q}) \to I_{3\times3}$ (i.e., $\delta\boldsymbol{q} \to [\pm1, 0, 0, 0]^T$). From the attitude error definition in Eq. (4.7), the attitude error dynamics is obtained in a matrix form as follows

$$\begin{aligned}
\frac{d}{dt}C(\delta\boldsymbol{q}) &= -S(\boldsymbol{\omega})C(\boldsymbol{q})C^T(\boldsymbol{q}_r) + C(\boldsymbol{q})C^T(\boldsymbol{q}_r)S(\boldsymbol{\omega}_r) \\
&= -S(\boldsymbol{\omega})C(\delta\boldsymbol{q}) + C(\delta\boldsymbol{q})S(\boldsymbol{\omega}_r) \\
&= -S(\boldsymbol{\omega})C(\delta\boldsymbol{q}) + S(C(\delta\boldsymbol{q})\boldsymbol{\omega}_r)C(\delta\boldsymbol{q}) \\
&= -S(\boldsymbol{\omega} - C(\delta\boldsymbol{q})\boldsymbol{\omega}_r)C(\delta\boldsymbol{q}) \\
\implies \frac{d}{dt}C(\delta\boldsymbol{q}) &= -S(\delta\boldsymbol{\omega})C(\delta\boldsymbol{q}) \quad \iff \quad \delta\dot{\boldsymbol{q}} = \frac{1}{2}E(\delta\boldsymbol{q})\delta\boldsymbol{\omega}
\end{aligned} \tag{4.9}$$

wherein the identity $C(\delta\boldsymbol{q})S(\boldsymbol{\omega}_r) = S(C(\delta\boldsymbol{q})\boldsymbol{\omega}_r)C(\delta\boldsymbol{q})$ has been employed which can be easily proved by using the identity of the vector cross product under three dimensional rigid rotation such that

$$C(\delta\boldsymbol{q})S(\boldsymbol{\omega}_r)\boldsymbol{\nu} = C(\delta\boldsymbol{q})(\boldsymbol{\omega}_r\times\boldsymbol{\nu}) = C(\delta\boldsymbol{q})\boldsymbol{\omega}_r\times C(\delta\boldsymbol{q})\boldsymbol{\nu} = S(C(\delta\boldsymbol{q})\boldsymbol{\omega}_r)C(\delta\boldsymbol{q})\boldsymbol{\nu}, \quad \forall\boldsymbol{\nu}\in\mathbb{R}^3 \tag{4.10}$$

Corresponding angular rate error dynamics for the rigid-body rotational motion is given by differentiating Eq. (4.8) along Eq. (4.1) and Eq. (4.9). Thus, the overall

attitude tracking error dynamics are represented by

$$\delta\dot{\boldsymbol{q}} = \frac{1}{2}E(\delta\boldsymbol{q})\delta\boldsymbol{\omega} \tag{4.11}$$

$$J\delta\dot{\boldsymbol{\omega}} = -S(\boldsymbol{\omega})J\boldsymbol{\omega} + \boldsymbol{u} + J\left[S(\delta\boldsymbol{\omega})C(\delta\boldsymbol{q})\boldsymbol{\omega}_r - C(\delta\boldsymbol{q})\dot{\boldsymbol{\omega}}_r\right] \tag{4.12}$$

wherein the inertia matrix J is unknown and the adaptive control objective is to determine control torque $\boldsymbol{u}(t)$ while employing full-state feedback $[\boldsymbol{\omega}(t),\ \boldsymbol{q}(t)]$ so as to achieve boundedness of all closed-loop signals and convergence of tracking errors $\lim_{t\to\infty}[\delta\boldsymbol{q}_{\boldsymbol{v}}(t), \delta\boldsymbol{\omega}(t)] = 0$ for all possible reference trajectories $[\boldsymbol{\omega}_r(t),\ \boldsymbol{q}_r(t)]$ and initial conditions $[\boldsymbol{\omega}(0),\ \boldsymbol{q}(0)]$. We can summarize frames used in the analysis as follows

$$\begin{aligned}
\mathcal{F}_N &\xrightarrow{\boldsymbol{q}} \mathcal{F}_B \implies \hat{\boldsymbol{b}} = C(\boldsymbol{q})\hat{\boldsymbol{n}} \\
\mathcal{F}_N &\xrightarrow{\boldsymbol{q}_r} \mathcal{F}_R \implies \hat{\boldsymbol{r}} = C(\boldsymbol{q}_r)\hat{\boldsymbol{n}} \\
\mathcal{F}_R &\xrightarrow{\delta\boldsymbol{q}} \mathcal{F}_B \implies \hat{\boldsymbol{b}} = C(\delta\boldsymbol{q})\hat{\boldsymbol{r}}
\end{aligned} \tag{4.13}$$

where $\hat{\boldsymbol{b}},\ \hat{\boldsymbol{n}}$, and $\hat{\boldsymbol{r}}$ are the unit vector triads about $\mathcal{F}_B,\ \mathcal{F}_N$, and $\mathcal{F}_R$ respectively.

4.3 Adaptive Attitude Tracking Control

In this section, we present a novel non-CE adaptive control method for the attitude tracking problem represented by Eq. (4.11) and Eq. (4.12) while we specifically focus on obtaining closed-loop performance improvement. The following theorem represents the main results.

Theorem 4. *Consider the attitude tracking error system Eq. (4.11) and Eq. (4.12) with the inertia matrix J being unknown, and suppose the adaptive control input $\boldsymbol{u}$*

is determined through

$$\boldsymbol{u} = -W(\hat{\boldsymbol{\theta}} + \boldsymbol{\beta}) - \gamma W_f W_f^T \left[k_p(\boldsymbol{\omega}_f - \delta\boldsymbol{q_v}) - \delta\boldsymbol{\omega}\right] \tag{4.14}$$

$$\dot{\hat{\boldsymbol{\theta}}} = \gamma W_f^T \left[(\alpha + k_v)\boldsymbol{\omega}_f + k_p\delta\boldsymbol{q_v}\right] - \gamma W^T\boldsymbol{\omega}_f \tag{4.15}$$

$$\boldsymbol{\beta} = -\gamma W_f^T\boldsymbol{\omega}_f \tag{4.16}$$

wherein $k_p, k_v, \gamma > 0$ *are any scalar constants,* $\alpha = k_p + k_v$ *and the regressor matrix* W *is constructed in the following fashion*

$$W\boldsymbol{\theta}^* = -S(\boldsymbol{\omega})J\boldsymbol{\omega} + J\left[S(\delta\boldsymbol{\omega})C(\delta\boldsymbol{q})\boldsymbol{\omega}_C - C(\delta\boldsymbol{q})\dot{\boldsymbol{\omega}}_C\right] + J\left(k_v\delta\boldsymbol{\omega} + k_p\delta\dot{\boldsymbol{q}}_{\boldsymbol{v}} + \alpha k_p\delta\boldsymbol{q_v}\right) \tag{4.17}$$

where $\boldsymbol{\theta}^* = [J_{11}, J_{12}, J_{13}, J_{22}, J_{23}, J_{33}]^T$ *represents the elements of the unknown symmetric inertia matrix* $J = [J_{ij}]$*. Further, the signals* W_f *and* $\boldsymbol{\omega}_f$ *required in computing the control input* $\boldsymbol{u}$ *in Eq. (4.14) are obtained from stable first-order linear filter dynamics*

$$\dot{\boldsymbol{\omega}}_f = -\alpha\boldsymbol{\omega}_f + \delta\boldsymbol{\omega} \tag{4.18}$$

$$\dot{W}_f = -\alpha W_f + W \tag{4.19}$$

with arbitrary initial conditions $W_f(0) \in \mathbb{R}^{3\times 6}$ *and* $\boldsymbol{\omega}_f(0) \in \mathbb{R}^3$*. Then, for all possible initial conditions* $[\boldsymbol{\omega}(0),\ \boldsymbol{q}(0)]$ *and reference trajectories* $[\boldsymbol{\omega}_C(t),\ \boldsymbol{q}_C(t)]$*, the closed-loop is globally asymptotically stable leading to the convergence condition* $\lim_{t\to}[\delta\boldsymbol{q_v}(t), \delta\boldsymbol{\omega}(t)] = 0$*.*

Proof. First, we re-arrange Eq. (4.12) into parameter affine form consistent with the definition of the regressor matrix W in Eq. (4.17). Starting with the addition and subtraction of terms $J\left(k_v\delta\boldsymbol{\omega} + k_p\delta\dot{\boldsymbol{q}}_{\boldsymbol{v}} + \alpha k_p\delta\boldsymbol{q_v}\right)$ to the right hand side of Eq. (4.12) and following up through the regressor definition in Eq. (4.17) and some minor

algebraic manipulations, it is easy to obtain

$$\delta\dot{\boldsymbol{\omega}} = -k_v\delta\boldsymbol{\omega} - k_p(\delta\dot{\boldsymbol{q}}_{\boldsymbol{v}} + \alpha\delta\boldsymbol{q}_{\boldsymbol{v}}) + J^{-1}(W\boldsymbol{\theta}^* + \boldsymbol{u}) \tag{4.20}$$

where k_v and k_p are any scalar positive gains, and $\alpha = k_v + k_p$ as defined earlier in this section. Obviously, the angular rate tracking error dynamics in Eq. (4.12) is algebraically equivalent to Eq. (4.20) and accordingly, we shall henceforth refer the overall attitude tracking error dynamics to be represented by Eq. (4.11) and Eq. (4.20).

Next, we consider (only for purposes of the ensuing stability analysis) a linear filter involving the control signal defined by

$$\dot{\boldsymbol{u}}_f = -\alpha\boldsymbol{u}_f + \boldsymbol{u} \tag{4.21}$$

so that we are able to work toward introducing a stable and attracting manifold into the adaptation algorithm. Now, we transform the attitude tracking error dynamics into the filtered attitude tracking error dynamics using Eq. (4.18) and Eq. (4.19). Differentiating both sides of the filter dynamics in Eq. (4.18) followed by substitution of the angular velocity error dynamics Eq. (4.20), it is easy to establish the following perfect differential

$$\begin{aligned}\frac{d}{dt}\left[\dot{\boldsymbol{\omega}}_f + k_v\boldsymbol{\omega}_f + k_p\delta\boldsymbol{q}_{\boldsymbol{v}} - J^{-1}(W_f\boldsymbol{\theta}^* + \boldsymbol{u}_f)\right] = \\ -\alpha\left[\dot{\boldsymbol{\omega}}_f + k_v\boldsymbol{\omega}_f + k_p\delta\boldsymbol{q}_{\boldsymbol{v}} - J^{-1}(W_f\boldsymbol{\theta}^* + \boldsymbol{u}_f)\right]\end{aligned} \tag{4.22}$$

whose solution may be immediately established by

$$\dot{\boldsymbol{\omega}}_f = -k_v\boldsymbol{\omega}_f - k_p\delta\boldsymbol{q}_{\boldsymbol{v}} + J^{-1}\left(W_f\boldsymbol{\theta}^* + \boldsymbol{u}_f\right) + \boldsymbol{\varepsilon}e^{-\alpha t} \tag{4.23}$$

where the exponentially decaying term $\boldsymbol{\eta}(t) \doteq \boldsymbol{\varepsilon}e^{-\alpha t}$ on the right hand side of the

preceding equation is characterized by

$$\dot{\boldsymbol{\eta}} = -\alpha\boldsymbol{\eta}; \quad \boldsymbol{\eta}(0) = \boldsymbol{\varepsilon} = \left[\dot{\boldsymbol{\omega}}_f(0) + k_v\boldsymbol{\omega}_f(0) + k_p\delta\boldsymbol{q}_{\boldsymbol{v}}(0) - J^{-1}\left(W_f(0)\boldsymbol{\theta}^* + \boldsymbol{u}_f(0)\right)\right] \tag{4.24}$$

We now suppose the filtered control signal $\boldsymbol{u}_f$ be specified as follows

$$\boldsymbol{u}_f = -W_f\left(\hat{\boldsymbol{\theta}} + \boldsymbol{\beta}\right) \tag{4.25}$$

in such a way that the composite term $(\hat{\boldsymbol{\theta}}+\boldsymbol{\beta})$ indicates an instantaneous estimate for the unknown parameter vector $\boldsymbol{\theta}^*$ which therefore amounts to a significant departure from the classical certainty equivalence adaptive control methodology. Accordingly Eq. (4.23) becomes

$$\dot{\boldsymbol{\omega}}_f = -k_v\boldsymbol{\omega}_f - k_p\delta\boldsymbol{q}_{\boldsymbol{v}} - J^{-1}W_f\boldsymbol{z} + \boldsymbol{\varepsilon}e^{-\alpha t} \tag{4.26}$$

wherein the quantity $\boldsymbol{z} \doteq \hat{\boldsymbol{\theta}} + \boldsymbol{\beta} - \boldsymbol{\theta}^*$ is introduced to indicate the parameter estimation error. The dynamics of the parameter estimation error can be derived by making use of Eq. (4.15), Eq. (4.16) and Eq. (4.26) to yield the following

$$\dot{\boldsymbol{z}} = \dot{\hat{\boldsymbol{\theta}}} + \dot{\boldsymbol{\beta}} = -\gamma W_f^T J^{-1} W_f\boldsymbol{z} + \gamma W_f^T\boldsymbol{\eta} \tag{4.27}$$

Now, consider the lower bounded Lyapunov-like function given by

$$V = \frac{1}{2}\boldsymbol{\omega}_f^T\boldsymbol{\omega}_f + (\delta q_o - 1)^2 + \delta\boldsymbol{q}_{\boldsymbol{v}}^T\delta\boldsymbol{q}_{\boldsymbol{v}} + \frac{\zeta}{2\lambda_{\min}}\boldsymbol{z}^T\boldsymbol{z} + \frac{\mu}{2}\boldsymbol{\eta}^T\boldsymbol{\eta} \tag{4.28}$$

where $\lambda_{\min}$ is the minimum eigenvalue of the unknown symmetric positive definite inertia matrix J, $\zeta > 9/(4\gamma)\max\left[1/k_v, 1/k_p\right]$ and $\mu > 9/(4\alpha)\max\left[1/k_v, 1/k_p\right]$. By taking the time derivative of V along trajectories generated from Eq. (4.11),

Eq. (4.15), Eq. (4.16), Eq. (4.24) and Eq. (4.26), we have the following

$$
\begin{aligned}
\dot{V} &= \boldsymbol{\omega}_f^T \left(-k_v\boldsymbol{\omega}_f - k_p\delta\boldsymbol{q_v} - J^{-1}W_f\boldsymbol{z} + \boldsymbol{\eta}\right) + \delta\boldsymbol{q}_{\boldsymbol{v}}^T\delta\boldsymbol{\omega} + \frac{\zeta}{\lambda_{\min}}\boldsymbol{z}^T(\dot{\hat{\boldsymbol{\theta}}} + \dot{\boldsymbol{\beta}}) - \mu\alpha\boldsymbol{\eta}^T\boldsymbol{\eta} \\
&= -k_v\|\boldsymbol{\omega}_f\|^2 - k_p\boldsymbol{\omega}_f^T\delta\boldsymbol{q_v} - \boldsymbol{\omega}_f^T J^{-1}W_f\boldsymbol{z} + \boldsymbol{\omega}_f^T\boldsymbol{\eta} + \delta\boldsymbol{q}_{\boldsymbol{v}}^T(\dot{\boldsymbol{\omega}}_f + \alpha\boldsymbol{\omega}_f) - \\
&\quad \frac{\zeta\gamma}{\lambda_{\min}}\boldsymbol{z}^T W_f^T J^{-1}W_f\boldsymbol{z} - \mu\alpha\boldsymbol{\eta}^T\boldsymbol{\eta} \\
&= -k_v\|\boldsymbol{\omega}_f\|^2 - k_p\boldsymbol{\omega}_f^T\delta\boldsymbol{q_v} - \boldsymbol{\omega}_f^T J^{-1}W_f\boldsymbol{z} + \boldsymbol{\omega}_f^T\boldsymbol{\eta} + \\
&\quad \delta\boldsymbol{q}_{\boldsymbol{v}}^T\left(-k_v\boldsymbol{\omega}_f - k_p\delta\boldsymbol{q_v} - J^{-1}W_f\boldsymbol{z} + \boldsymbol{\eta} + \alpha\boldsymbol{\omega}_f\right) - \frac{\zeta\gamma}{\lambda_{\min}}\boldsymbol{z}^T W_f^T J^{-1}W_f\boldsymbol{z} - \mu\alpha\boldsymbol{\eta}^T\boldsymbol{\eta} \\
&= -k_v\|\boldsymbol{\omega}_f\|^2 - k_p\|\delta\boldsymbol{q_v}\|^2 - \boldsymbol{\omega}_f^T J^{-1}W_f\boldsymbol{z} + \boldsymbol{\omega}_f^T\boldsymbol{\eta} - \delta\boldsymbol{q}_{\boldsymbol{v}}^T J^{-1}W_f\boldsymbol{z} + \delta\boldsymbol{q}_{\boldsymbol{v}}^T\boldsymbol{\eta} - \\
&\quad \frac{\zeta\gamma}{\lambda_{\min}}\boldsymbol{z}^T W_f^T J^{-1}W_f\boldsymbol{z} - \mu\alpha\boldsymbol{\eta}^T\boldsymbol{\eta} \\
&\leq -\frac{k_v}{3}\|\boldsymbol{\omega}_f\|^2 - \frac{k_p}{3}\|\delta\boldsymbol{q_v}\|^2 - \frac{\zeta\gamma}{3}\|J^{-1}W_f\boldsymbol{z}\|^2 - \frac{\mu\alpha}{3}\|\boldsymbol{\eta}\|^2 - \\
&\quad \frac{k_v}{3}\left(\|\boldsymbol{\omega}_f\|^2 + \frac{3}{k_v}\boldsymbol{\omega}_f^T J^{-1}W_f\boldsymbol{z} + \frac{\zeta\gamma}{k_v}\|J^{-1}W_f\boldsymbol{z}\|^2\right) - \frac{k_v}{3}\left(\|\boldsymbol{\omega}_f\|^2 - \frac{3}{k_v}\boldsymbol{\omega}_f^T\boldsymbol{\eta} + \frac{\mu\alpha}{k_v}\|\boldsymbol{\eta}\|^2\right) - \\
&\quad \frac{k_p}{3}\left(\|\delta\boldsymbol{q_v}\|^2 + \frac{3}{k_p}\delta\boldsymbol{q}_{\boldsymbol{v}}^T J^{-1}W_f\boldsymbol{z} + \frac{\zeta\gamma}{k_p}\|J^{-1}W_f\boldsymbol{z}\|^2\right) - \frac{k_p}{3}\left(\|\delta\boldsymbol{q_v}\|^2 - \frac{3}{k_p}\delta\boldsymbol{q}_{\boldsymbol{v}}^T\boldsymbol{\eta} + \frac{\mu\alpha}{k_p}\|\boldsymbol{\eta}\|^2\right) \\
&\leq -\frac{k_v}{3}\|\boldsymbol{\omega}_f\|^2 - \frac{k_p}{3}\|\delta\boldsymbol{q_v}\|^2 - \frac{\zeta\gamma}{3}\|J^{-1}W_f\boldsymbol{z}\|^2 - \frac{\mu\alpha}{3}\|\boldsymbol{\eta}\|^2 \qquad (4.29)
\end{aligned}
$$

which is negative semidefinite indicating boundedness for all closed-loop signals. Further, since V is lower bounded and monotonic by the negative semidefiniteness of $\dot{V}$, we know that $\int_0^\infty \dot{V}(t)dt$ exists and is finite, which, in turn, implies $\boldsymbol{\omega}_f, \delta\boldsymbol{q_v}, J^{-1}W_f\boldsymbol{z}, \boldsymbol{\eta} \in \mathcal{L}_2 \cap \mathcal{L}_\infty$. This also implies boundedness of $\dot{\boldsymbol{\omega}}_f$, $\delta\dot{\boldsymbol{q}}_{\boldsymbol{v}}$, $\dot{W}_f$, and $\dot{\boldsymbol{z}}$ from Eq. (4.11), Eq. (4.15), Eq. (4.16), Eq. (4.19), and Eq. (4.26). By using Barbalat's lemma, we can now guarantee $\lim_{t\to\infty}[\boldsymbol{\omega}_f(t), \delta\boldsymbol{q_v}(t), J^{-1}W_f(t)\boldsymbol{z}(t)] = 0$. Based on the last result, we may also show that $\lim_{t\to\infty}\dot{\boldsymbol{\omega}}_f(t) = 0$ from Eq. (4.26). Finally, from Eq. (4.18), it follows that $\lim_{t\to\infty}\delta\boldsymbol{\omega}(t) = 0$.

One last step remains now which is to recover the actual control input $\boldsymbol{u}$ from the filtered control signal $\boldsymbol{u}_f$ defined through Eq. (4.21) and Eq. (4.25). This

can be accomplished through

$$\boldsymbol{u} = \dot{\boldsymbol{u}}_f + \alpha \boldsymbol{u}_f = -\dot{W}_f(\hat{\boldsymbol{\theta}} + \boldsymbol{\beta}) - W_f\left(\dot{\hat{\boldsymbol{\theta}}} + \dot{\boldsymbol{\beta}}\right) + \alpha \boldsymbol{u}_f \tag{4.30}$$

By substituting Eq. (4.15), Eq. (4.16), and Eq. (4.19) in the preceding expression, the adaptive control torque $\boldsymbol{u}$ can be recovered to be the expression given in Eq. (4.14), thereby completing the proof of Theorem 4. □

The following observations are now in order.

1. From positive definiteness of matrix J and the fact that we are able to prove convergence condition $\lim_{t\to\infty} J^{-1}W_f(t)\boldsymbol{z}(t) = 0$, it follows that the proposed adaptive controller provides for the establishment of an attracting manifold $\mathcal{S}$ defined by

$$\mathcal{S} = \left\{\boldsymbol{z} \in \mathbb{R}^6 \mid W_f \boldsymbol{z} = 0\right\} \tag{4.31}$$

in such a way that all closed-loop trajectories ultimately end up inside $\mathcal{S}$. Moreover, convergence to this attracting manifold can be made arbitrarily fast by tuning the learning rate parameter γ present within the control law in Eq. 4.14. This is a most significant feature of the non-CE adaptive controller derived here given the fact that the term $J^{-1}W_f(t)\boldsymbol{z}(t)$ essentially arises in Eq. (4.26) due to the mismatch between current estimate of the parameter ($\hat{\boldsymbol{\theta}}+\boldsymbol{\beta}$) and its corresponding true value $\boldsymbol{\theta}^*$ and therefore plays the role of being an additive disturbance imposed onto the ideal case (no parameter uncertainty) closed-loop system having dynamics given by

$$\dot{\boldsymbol{\omega}}_f = -k_v\boldsymbol{\omega}_f - k_p\delta\boldsymbol{q}_{\boldsymbol{v}} + \boldsymbol{\varepsilon}e^{-\alpha t} \tag{4.32}$$

A primary implication of this assertion is that the closed-loop performance obtained in the ideal case is recovered through the presence of the attracting

manifold in the adaptive case; a feature that is seldom available with existing CE-based adaptive control schemes. This statement can be further elaborated based on the fact that conventional CE-based adaptive controllers rely upon the cancelation of the uncertain parameter effects (within the time derivatives of suitable Lyapunov-like candidate functions to render them negative semi-definite), and accordingly the recovery of the ideal case (no uncertainty; deterministic control) closed-loop performance happens only after either the parameter estimates converge to their corresponding true values and/or the tracking/regulating errors converge to zero. The role played by the learning rate parameter γ will be further illuminated in the numerical simulations section.

2. The key steps that permit extension of the non-CE based I&I adaptive control framework[6, 9] to the spacecraft adaptive attitude tracking control problem are represented through our introduction of the regressor filter in Eq. (4.19) and the algebraic developments leading to establishment of Eq. (4.20) which were made possible by judiciously adding and subtracting the following term

$$J\left(k_v\delta\boldsymbol{\omega} + k_p\delta\dot{\boldsymbol{q}}_{\boldsymbol{v}} + \alpha k_p\delta\boldsymbol{q}_{\boldsymbol{v}}\right)$$

to the right hand side of Eq. (4.12). Also important to note is the fact that only the angular rate error signal $\delta\boldsymbol{\omega}$ needs to be filtered through Eq. (4.18) to obtain the signal $\boldsymbol{\omega}_f$ which is required for the controller implementation whereas no filtering is needed on the attitude error signal represented by the unit-norm constrained error quaternion $\delta\boldsymbol{q}$. Moreover, in the non-adaptive ideal case, if the parameter $\boldsymbol{\theta}^*$ is exactly known (no uncertainty), then the filtered control signal specified in Eq. (4.25) can be replaced by simply using $\boldsymbol{u}_f = -W_f\boldsymbol{\theta}^*$ ultimately leading to $\boldsymbol{u} = \alpha\boldsymbol{u}_f + \dot{\boldsymbol{u}}_f = -W\boldsymbol{\theta}^*$ thereby obviating

any need for the regressor filter of Eq. (4.19) during controller implementation.

3. It is always possible to introduce the filter states such that $\boldsymbol{\eta}(t) = 0$ for all $t \geq 0$ by letting $\boldsymbol{\eta}(0) = 0$ based on the suitable selection of initial filter states such as $\boldsymbol{\omega}_f(0) = (\delta\boldsymbol{\omega}(0) + k_p\delta\boldsymbol{q_v}(0))/k_p$ and $W_f(0) = 0$ in Eq. (4.26). This will further improve the transient performance of the closed-loop adaptive attitude control system because $\boldsymbol{\eta}(t) = 0$ eliminates the time and control effort needed toward enabling the filter state convergence. Of course, as seen from the preceding proof, even in the case that $\boldsymbol{\eta}(0) \neq 0$, closed-loop stability and overall convergence of the trajectories to the attracting manifold $\mathcal{S}$ remains true and the signal $\boldsymbol{\eta}(t)$ still converges to zero exponentially fast. However, having $\boldsymbol{\eta}(0) = 0$ permits us rewrite the dynamics governing the parameter estimation error signal $\boldsymbol{z}$ given in Eq. (4.27) as follows

$$\dot{\boldsymbol{z}} = -\gamma W_f^T J^{-1} W_f \boldsymbol{z} \tag{4.33}$$

which is rigorously linear with respect to the parameter estimation error $\boldsymbol{z}$. Thus, if at any instant of time t, the parameter estimation error $\boldsymbol{z}$ is equal to zero, then adaptation stops henceforth and thereby parameter estimates stay locked at their true values (i.e., if $\boldsymbol{z}(t^*) = 0$ for some $t^* > 0$, then $\boldsymbol{z}(t) = 0$ for all $t \geq t^*$). We emphasize here that this nice feature is available only if the filter initial conditions are chosen such that $\boldsymbol{\eta}(0) = 0$ and such a possibility is never available with existing CE-based formulations.

4. Finally, one needs to be extra careful while interpreting the properties of the attracting manifold definition $\mathcal{S}$ defined in Eq. (4.31) to the extent that $\lim_{t\to\infty} \boldsymbol{z}(t) = 0$ obviously implies $\lim_{t\to\infty} W_f(t)\boldsymbol{z}(t) = 0$ but the converse is not necessarily true. Therefore, just as with CE-based controllers, even under the proposed non-CE adaptive control scheme, there is no recourse from en-

suring satisfaction of suitable PE conditions on the reference trajectory if one were interested in ensuring convergence of all the parameter estimates to their respective unknown true values.

4.4 Adaptive Control with Parameter Projection

In Chapter 3, we use a projection technique wherein the unknown parameters are positive real. Here, we assume that the bounds for each element of the inertia matrix are given as a priori (i.e., $\theta_k \in (\theta_{\min}, \theta_{\max})$ for $k = 1, \ldots, 6$). Then, from the definition of $\boldsymbol{\theta}^*$ in Eq. (4.17), the necessary reparameterization $\boldsymbol{\theta}_p^*$ is given as follows:

$$\boldsymbol{\theta}_p^* = \begin{bmatrix} \delta_1(\tanh\phi_1^* + 1) + \theta_{1_{\min}}^* \\ \delta_2(\tanh\phi_2^* + 1) + \theta_{2_{\min}}^* \\ \vdots \\ \delta_6(\tanh\phi_6^* + 1) + \theta_{6_{\min}}^* \end{bmatrix} \tag{4.34}$$

$$\hat{\boldsymbol{\theta}}_p(t) = \begin{bmatrix} \delta_1(\tanh(\hat{\phi}_1(t) + \beta_1(t)) + 1) + \theta_{1_{\min}}^* \\ \delta_2(\tanh(\hat{\phi}_2(t) + \beta_2(t)) + 1) + \theta_{2_{\min}}^* \\ \vdots \\ \delta_6(\tanh(\hat{\phi}_6(t) + \beta_6(t)) + 1) + \theta_{6_{\min}}^* \end{bmatrix} \tag{4.35}$$

where $\delta_k = (\theta_{k_{\max}}^* - \theta_{k_{\min}}^*)/2$ for $k = 1, \ldots, 6$. We see in Eq. (4.35) that each element of $\hat{\boldsymbol{\theta}}_p$ remains within the a priori bounds of θ_p^* by definition. Based on the reparameterization in Eq. (4.34) and Eq. (4.35), the stability of the proposed attitude control method combined with the smooth projection technique is presented in the followings.

Theorem 5 (Adaptive Attitude Tracking Control with Projection)**.** *For the attitude tracking system represented by the error dynamics Eq. (4.11) and Eq. (4.12), let the*

control torque $\boldsymbol{u}$ *computed by*

$$\boldsymbol{u} = -W\hat{\boldsymbol{\theta}}_p - \gamma W_f \text{Diag}[\kappa] W_f^T \left((k_v - \alpha)\boldsymbol{\omega}_f + k_p \delta \boldsymbol{q}_v + \delta\omega\right) \tag{4.36}$$

wherein $\hat{\boldsymbol{\phi}}$ *and* $\boldsymbol{\beta}$ *is computed by*

$$\dot{\hat{\boldsymbol{\phi}}}(t) = \gamma(\alpha W_f - W)^T \boldsymbol{\omega}_f + \gamma W_f^T (k_v \boldsymbol{\omega}_f + k_p \delta \boldsymbol{q}_v) \tag{4.37}$$

$$\boldsymbol{\beta} = \gamma W_f^T \boldsymbol{\omega}_f \tag{4.38}$$

In addition, Diag[$\cdot$] *is defined in Eq. (3.27) and*

$$\kappa = \begin{pmatrix} \delta_1 \text{sech}^2(\hat{\phi}_1 + \beta_1) \\ \delta_2 \text{sech}^2(\hat{\phi}_2 + \beta_2) \\ \vdots \\ \delta_6 \text{sech}^2(\hat{\phi}_6 + \beta_6) \end{pmatrix} \tag{4.39}$$

k_p, k_v, γ, *and* α *are defined in Theorem 4. Filters and regressor matrix* W *are identical to Eq. (4.18), Eq. (4.19), and Eq. (4.17) respectively. Then, the attitude tracking control objective is satisfied, i.e.,* $\lim_{t\to\infty}[\delta\boldsymbol{q}_v(t), \delta\boldsymbol{\omega}(t)] = 0$ *for all* $[\delta\boldsymbol{q}_v(0), \delta\boldsymbol{\omega}(0)] \in \mathbb{R}^6$.

Proof. Starting from Eq. (4.20), filtered error dynamics for $\boldsymbol{\omega}_f$ are obtained by substituting filter states Eq. (4.18), Eq. (4.19), and Eq. (2.8) along with $\boldsymbol{u}_f = -W_f\hat{\boldsymbol{\theta}}_p$ as follows

$$\dot{\boldsymbol{\omega}}_f = -k_v \boldsymbol{\omega}_f - k_p \delta \boldsymbol{q}_v - J^{-1} W_f \boldsymbol{\chi} \tag{4.40}$$

where we use the same definitions for a parameter estimation error $\boldsymbol{\chi}$ and adaptation discrepancy $\boldsymbol{z}$ as in Eq. (3.28) and Eq. (3.29). More specifically, $\boldsymbol{\chi}$ is expressed as follows

$$\boldsymbol{\chi}_k = \delta_k \left[\tanh(\hat{\phi}_k + \beta_k) - \tanh \phi_k^*\right] \tag{4.41}$$

Then, consider the following Lyapunov candidate function V_p given by

$$V_p = \frac{1}{2}\boldsymbol{\omega}_f^T \boldsymbol{\omega}_f + (\delta q_0 - 1)^2 + \delta \boldsymbol{q}_v^T \delta \boldsymbol{q}_v + \underbrace{\frac{\zeta}{2\lambda_{\min}} \sum_{k=1}^{6} \delta_k \left[\log\cosh(z_k + \phi_k^*) - z_k \tanh \phi_k^*\right]}_{P} \tag{4.42}$$

which is an identical definition of Eq. (4.28) except for P function and missing $\boldsymbol{\eta}$ term (we ignored $\boldsymbol{\eta}$ because it plays no role on the stability proof as already shown in the previous section). In a similar way in the projection section in Chap. 3, we can prove that P is a lower bounded and monotonically increasing function with respect to $\|\boldsymbol{z}\|$ by the followings:

$$\begin{aligned} P'_{z_k} &= \delta_k \frac{\partial}{\partial z_k} \left(\log\cosh(z_k + \phi_k^*) - z_k \tanh \phi_k^*\right) \\ &= \delta_k \left(\tanh(z_k + \phi_k^*) - \tanh \phi_k^*\right) \begin{cases} > 0 & \text{if } z_k > 0 \\ < 0 & \text{if } z_k < 0 \\ = 0 & \text{at } z_k = 0 \end{cases} \end{aligned} \tag{4.43}$$

$$P''_{z_k} = \delta_k \frac{\partial}{\partial z_k} \left(\tanh(z_k + \phi_k^*) - \tanh \phi_k^*\right) = \delta_k \mathrm{sech}^2(z_k + \phi_k^*) > 0 \quad \text{for all } z_k \tag{4.44}$$

Thus, V_p is lower bounded and positive with respect to $[\boldsymbol{\omega}_f, \delta \boldsymbol{q}_v, \boldsymbol{z}]$. Next, by taking time derivative of V_p in Eq. (4.42) and substituting Eq. (4.40), Eq. (4.11), Eq. (4.37),

and Eq. (4.38), we obtain the result

$$
\begin{aligned}
\dot{V}_p =& \boldsymbol{\omega}_f^T \left(-k_v \boldsymbol{\omega}_f - k_p \delta \boldsymbol{q}_v - J^{-1} W_f \boldsymbol{\chi}\right) + \delta \boldsymbol{q}_v^T \left(\dot{\boldsymbol{\omega}}_f + \alpha \boldsymbol{\omega}_f\right) + \\
& \frac{\zeta}{\lambda_{\min}} \underbrace{\sum_{k=1}^{6} \delta_k \left[\tanh(z_k + \phi_k^*) - z_k \tanh \phi_k^*\right] \left(\dot{\hat{\phi}}_k + \dot{\beta}_k\right)}_{\boldsymbol{\chi}^T \dot{\boldsymbol{z}}} \\
=& - k_v \boldsymbol{\omega}_f^T \boldsymbol{\omega}_f - k_p \delta \boldsymbol{q}_v^T \delta \boldsymbol{q}_v - \boldsymbol{\omega}_f^T J^{-1} W_f \boldsymbol{\chi} - \delta \boldsymbol{q}_v^T J^{-1} W_f \boldsymbol{\chi} - \frac{\zeta \gamma}{\lambda_{\min}} \boldsymbol{\chi}^T W_f^T J^{-1} W_f \boldsymbol{\chi} \\
\leqslant& - \frac{k_v}{2} \|\boldsymbol{\omega}_f\|^2 - \frac{k_p}{2} \|\delta \boldsymbol{q}_v\|^2 - \frac{\zeta \gamma}{3} \|J^{-1} W_f \boldsymbol{\chi}\|^2 \\
& - \frac{k_v}{2} \left(\|\boldsymbol{\omega}_f\|^2 - \frac{2}{k_v} \|\boldsymbol{\omega}_f\| \|J^{-1} W_f \boldsymbol{\chi}\| + \frac{2\zeta\gamma}{3k_v} \|J^{-1} W_f \boldsymbol{\chi}\|^2 \right) \\
& - \frac{k_p}{2} \left(\|\delta \boldsymbol{q}_v\|^2 - \frac{2}{k_p} \|\delta \boldsymbol{q}_v\| \|J^{-1} W_f \boldsymbol{\chi}\| + \frac{2\zeta\gamma}{3k_p} \|J^{-1} W_f \boldsymbol{\chi}\|^2 \right) \\
\leqslant& - \frac{k_v}{2} \|\boldsymbol{\omega}_f\|^2 - \frac{k_p}{2} \|\delta \boldsymbol{q}_v\|^2 - \frac{\zeta \gamma}{3} \|J^{-1} W_f \boldsymbol{\chi}\|^2
\end{aligned} \tag{4.45}
$$

Because the foregoing inequality result is the same as Eq. (4.29) except that $\boldsymbol{z}$ is replaced by $\boldsymbol{\chi}$ and $\boldsymbol{\eta}$ is ignored, we can argue the similar signal chasing process and thereby it is guaranteed that $\lim_{t\to\infty}[\delta \boldsymbol{q}_v, \delta \boldsymbol{\omega}] = 0$. $\boldsymbol{u}$ is obtained from $\boldsymbol{u} = \dot{\boldsymbol{u}}_f + \alpha \boldsymbol{u}_f$ following the same steps described in Eq. (3.37). □

Attracting manifold is defined by S_{AP} as follows

$$
S_{AP} = \{\boldsymbol{\chi} \mid W_f \boldsymbol{\chi} = 0\} \tag{4.46}
$$

As in the robot application with projection algorithm, $\boldsymbol{\chi}$ has the estimation error property of $\boldsymbol{z}$ in Eq. (4.31).

4.5 Numerical Simulations

4.5.1 Proposed Control without Projection Mechanism

In order to demonstrate the various features of the proposed adaptive attitude control method, we perform numerical simulations and compare the closed-loop trajectory tracking simulation results with the quaternion CE-based adaptive control results from Ref. [38]. Two sets of simulations are performed. In the first case, the reference trajectory does not satisfy the underlying persistence of excitation conditions to ensure convergence of parameter estimates to their corresponding true unknown values. The second set of simulations consider a persistently exciting reference trajectory.

The numerical model for the attitude tracking control system has the following system parameters. The unknown inertia matrix is described by

$$J = \begin{bmatrix} 20 & 1.2 & 0.9 \\ 1.2 & 17 & 1.4 \\ 0.9 & 1.4 & 15 \end{bmatrix} \tag{4.47}$$

which can be rewritten as in vector form as $\boldsymbol{\theta}^* = [20, 1.2, 0.9, 17, 1.4, 15]^T$. The corresponding CE-based adaptive control law taken from Ref. [38] is listed below

$$\boldsymbol{u}_{ce} = 2(P^{-1})^T \left[-Y\hat{\boldsymbol{\theta}}_{ce} - K\boldsymbol{r} - \frac{\delta\boldsymbol{q}_{\boldsymbol{v}}}{1 - \delta\boldsymbol{q}_{\boldsymbol{v}}^T \delta\boldsymbol{q}_{\boldsymbol{v}}} \right] \tag{4.48}$$

$$\dot{\hat{\boldsymbol{\theta}}}_{ce} = \Gamma Y^T \boldsymbol{r} \tag{4.49}$$

where $\boldsymbol{r} \doteq \delta\boldsymbol{q}_{\boldsymbol{v}} + \alpha_{ce}\delta\dot{\boldsymbol{q}}_{\boldsymbol{v}}$; $P \doteq \delta q_o I_{3\times 3} + S(\delta\boldsymbol{q}_{\boldsymbol{v}})$ corresponds to the vector part operator of $E(\boldsymbol{q})$ in Eq. (4.4); $Y \in \mathbb{R}^{3\times 6}$ is a regressor matrix corresponding our W in Eq. (4.17); $\alpha_{ce}, K \in \mathbb{R}^{3\times 3}$ are constant, positive definite, diagonal gain matrices; and $\Gamma \in \mathbb{R}^{6\times 6}$ is any learning rate matrix that is also constant, positive definite, and

diagonal. In the following simulations, the initial value of the parameter estimate for both $\boldsymbol{u}$ and $\boldsymbol{u}_{ce}$ is chosen to be $\hat{\boldsymbol{\theta}}(0) + \boldsymbol{\beta}(0) = \hat{\boldsymbol{\theta}}_{ce} = [21, 2.2, 1.9, 18, 24, 16]^T$, the initial body quaternion $\boldsymbol{q}(0) = [\sqrt{1 - 3 * 0.1826^2}, 0.1826, 0.1826, 0.1826]^T$, and the reference quaternion $\boldsymbol{q}_C(0) = [1, 0, 0, 0]^T$. The body is initially at rest and the corresponding reference angular velocity profile is given at each simulation.

Non-PE Reference Trajectory

For the first set of simulations, we consider a non-PE reference trajectory described by

$$\boldsymbol{\omega}_r(t) = [0.3(1 - e^{-0.01t^2}) \cos t + te^{-0.01t^2}(0.08\pi + 0.006 \sin t)] \cdot [1, 1, 1]^T \qquad (4.50)$$

which has the following principal angle characteristics based on $\boldsymbol{\omega}_r$ as shown in Fig. 4.1.

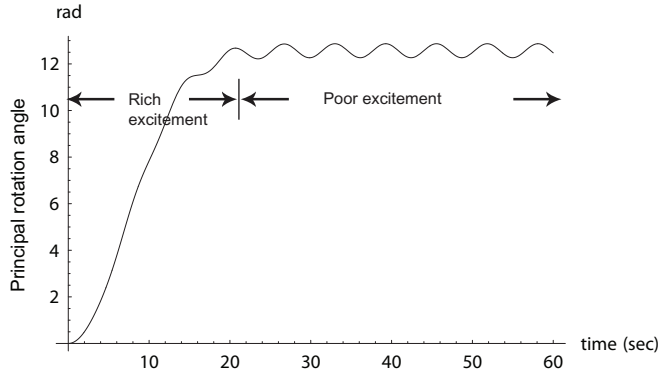

Figure 4.1: Reference signal trajectory in terms of the angular position along the time t. During the first 20 seconds, its excitement to the error dynamics is rich. After that period, the amount of change in the reference signal is no longer enough to excite the error dynamics (i.e. not sufficient to drive the estimation error to zero).

To permit a fair and meaningful comparison between the CE-based controller and proposed non-CE adaptive controller, we have tuned the various controller

parameters to obtain similar error convergence rates as shown in Fig. 4.2 assuming that the inertia matrix J is known (ideal case performance).

The corresponding control gains are determined as follows: $\alpha_{ce} = \text{diag}\{10, 10, 10\}$, $K = \text{diag}\{10, 10, 10\}$, $\Gamma = \text{diag}\{0.1, 0.1, 0.1, 0.1, 0.1, 0.1\}$ for the CE-based method; and $k_v = 0.5, k_p = 0.5, \gamma = 100$ for the proposed method. The wriggle seen in Fig. 4.2 for the proposed method is from the fact that the deterministic/ideal case error dynamics (described by Eq. (4.26) with $W_f z = 0$) correspond to a second-order system whereas the ideal case closed-loop dynamics under the CE-based method result in a stable first-order system in terms of the composite error signal $\boldsymbol{r}$ (for further details, refer [38]).

Next, we assume the inertia matrix J to be unknown and simulate both the CE and non-CE adaptive controllers. The resulting closed-loop simulations are documented in Fig. 4.3. Initial filter state values for the proposed method are chosen as follows: $W_f(0) = 0$ and $\boldsymbol{\omega}_f(0) = (\delta\boldsymbol{\omega}(0) + k_p\delta\boldsymbol{q_v}(0))/k_p$, thereby satisfying $\boldsymbol{\eta}(t) = 0$ for all $t \geq 0$. The learning rate Γ of the CE-based adaptive control method in Eq. (4.49) and its counterpart γ for the proposed adaptive controller are systematically tuned to achieve performance that is as close as possible as the ideal case performance obtained for both methods in Fig. 4.2. The attitude and angular rate errors converge to zero with both adaptive controllers. However, as seen in Fig. 4.3(a) and Fig. 4.3(b), the closed-loop performance from the proposed method remains more or less the same when compared to the corresponding ideal case performance in Fig. 4.2. This is clearly not the case with the CE-based controller because the attitude and angular rate errors exhibit a very slow convergence trend in Fig. 4.3. The norms of the control torques commanded by the CE-based controller and the non-CE controller are both plotted in Fig. 4.3(c) where it can be clearly seen that the torque demands due to the CE-based adaptive controller are severe during the initial transient. Given that we are simulating a trajectory

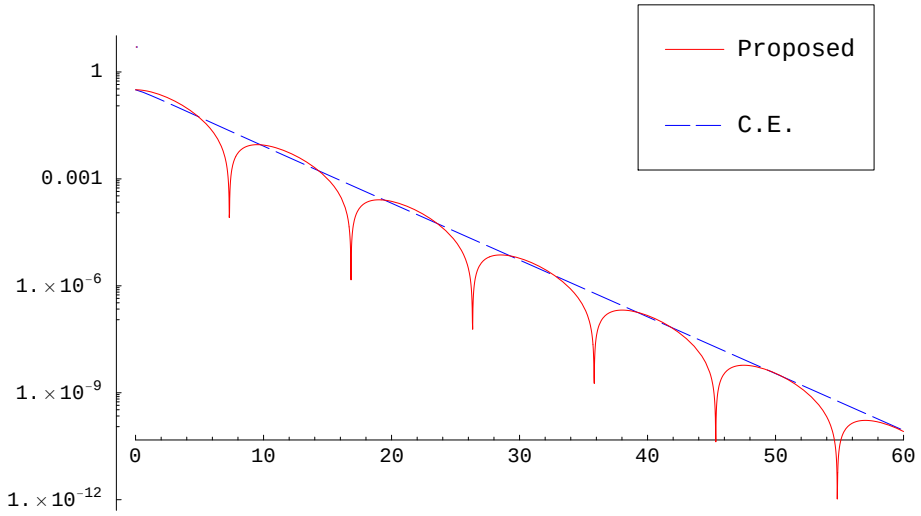

(a) quaternion error $\delta \boldsymbol{q}_v$

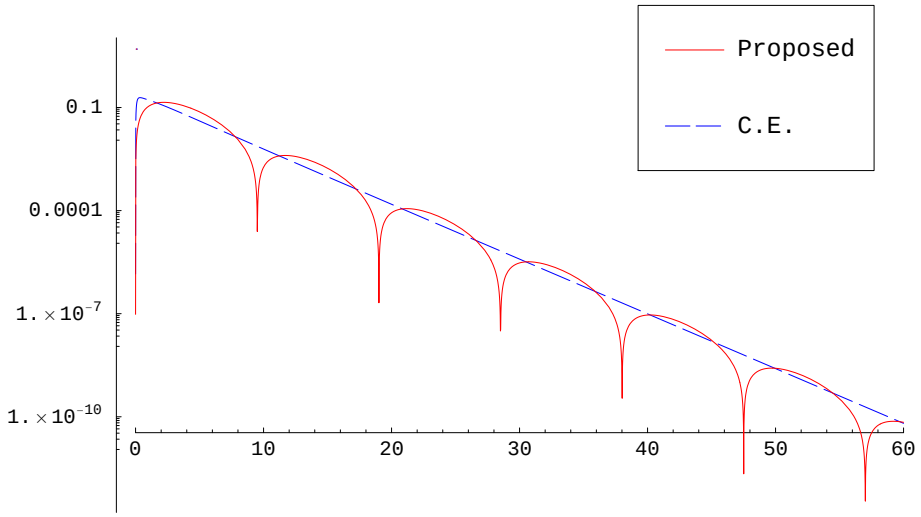

(b) angular velocity error $\delta \boldsymbol{\omega}$

Figure 4.2: Ideal case closed-loop performance obtained with the CE-based and the proposed non-CE controller assuming the inertia matrix J to be known

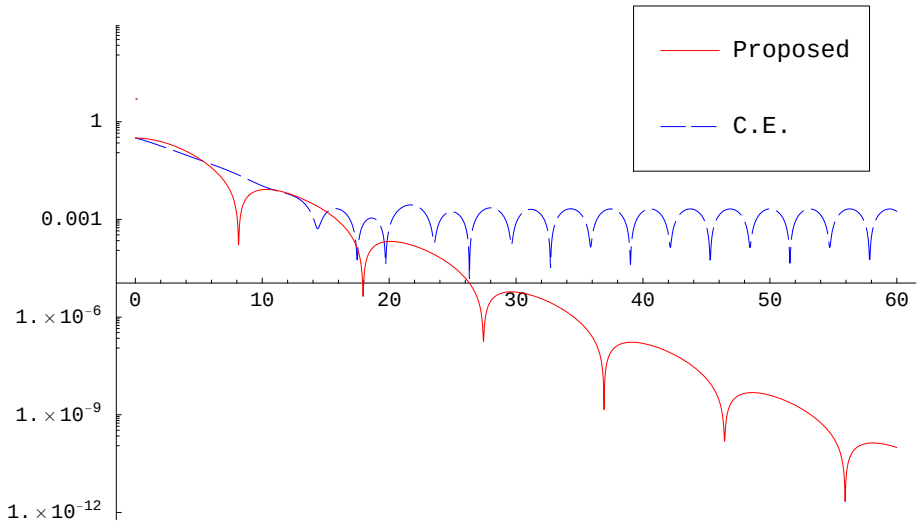

(a) quaternion error $\delta \boldsymbol{q}_v$

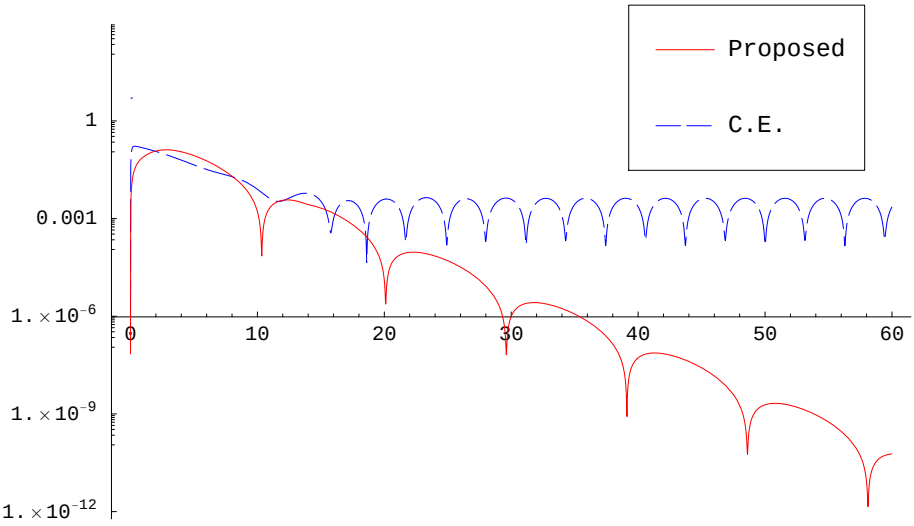

(b) angular velocity error $\delta \boldsymbol{\omega}$

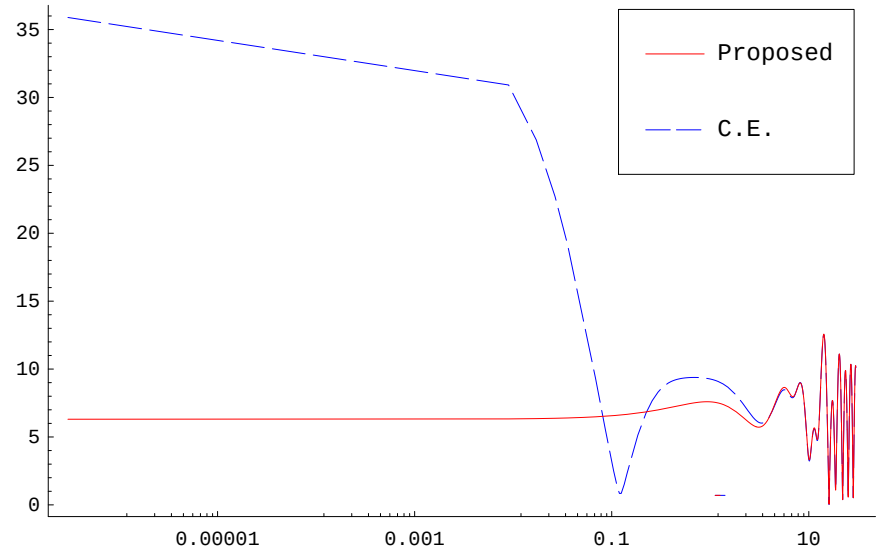

(c) initial transient of control norm highlighting the difference between CE-based and the proposed adaptive control methods

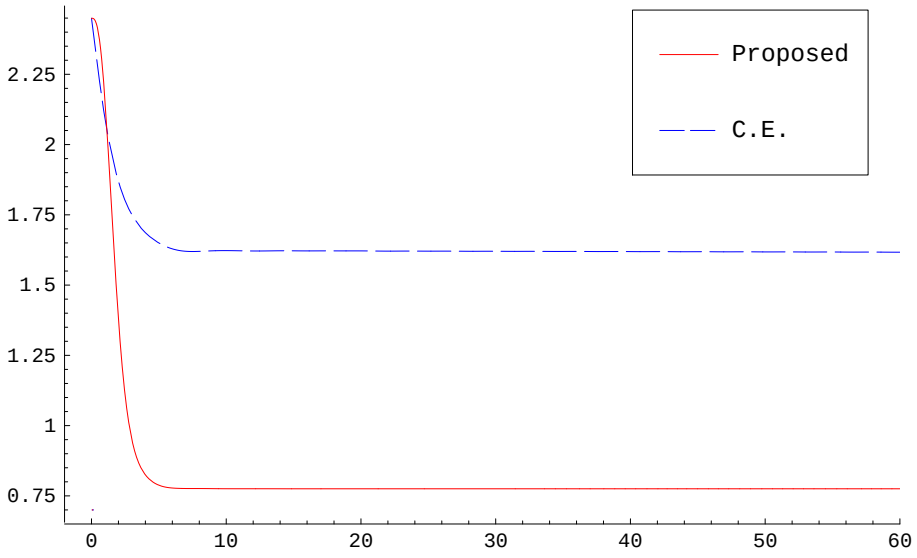

(d) parameter estimation error norm

Figure 4.3: Adaptive attitude tracking closed-loop performance comparison between the classical CE-based controller and the proposed non-CE controller for a non-PE reference trajectory

tracking problem, the steady state torques obviously remain time-varying to ensure tracking along the prescribed reference trajectory. The parameter estimation error norms are compared in Fig. 4.3(d). We recognize that parameter estimation error fails to converge to zero for both methods due to the non-PE nature of the underlying reference trajectory.

The role played by the parameter γ in the proposed adaptive controller is studied next. It is clear from Eq. (4.27) that whenever $\boldsymbol{\eta}(0) = 0$, the attractiveness of manifold $\mathcal{S}$ can be accelerated by increasing the value of γ parameter. This implies the ideal case (no uncertainty) closed-loop performance can be closely recovered with increasing γ values. We consider two different γ values: $\gamma = 10$ and $\gamma = 100$ and report the simulation results in Fig. 4.4. For the larger γ case, the attitude tracking performance is improved as seen from the faster attitude and angular rate error convergence in Fig. 4.4(a) and Fig. 4.4(b). Parameter estimation error with large γ also converges faster than one with small γ in Fig. 4.4(d) since the manifold attractivity of Eq. (6.27) is increased. In Fig. 4.4(c), we recognize that the peak control norm is mostly unchanged in spite of the increased γ value since the reduction in the parameter estimation error due to the larger γ value contributes to a decrease in the control norm during the transient part of the simulation.

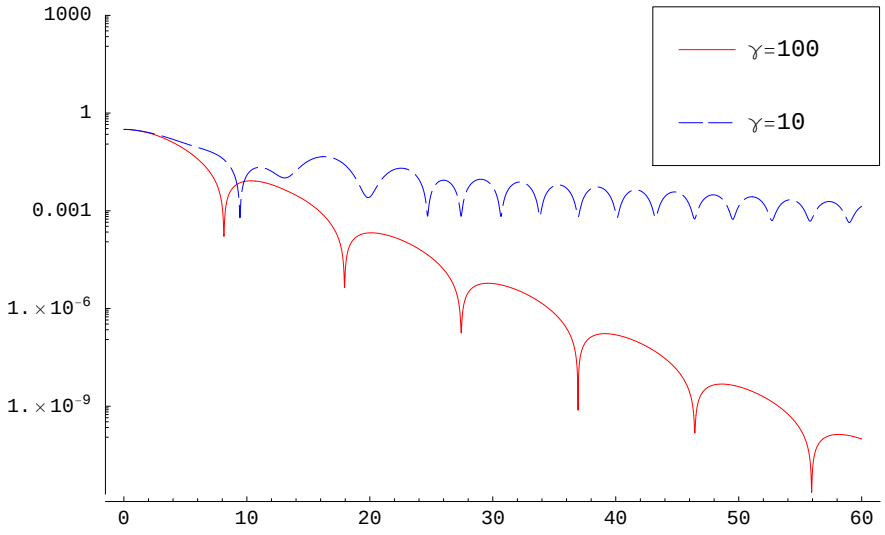

(a) quaternion error $\delta \boldsymbol{q}_v$

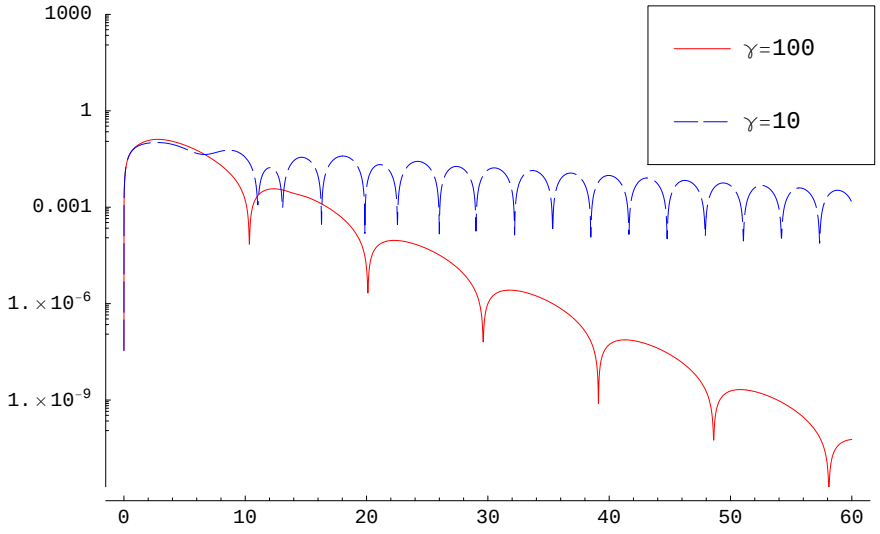

(b) angular velocity error $\delta \boldsymbol{\omega}$

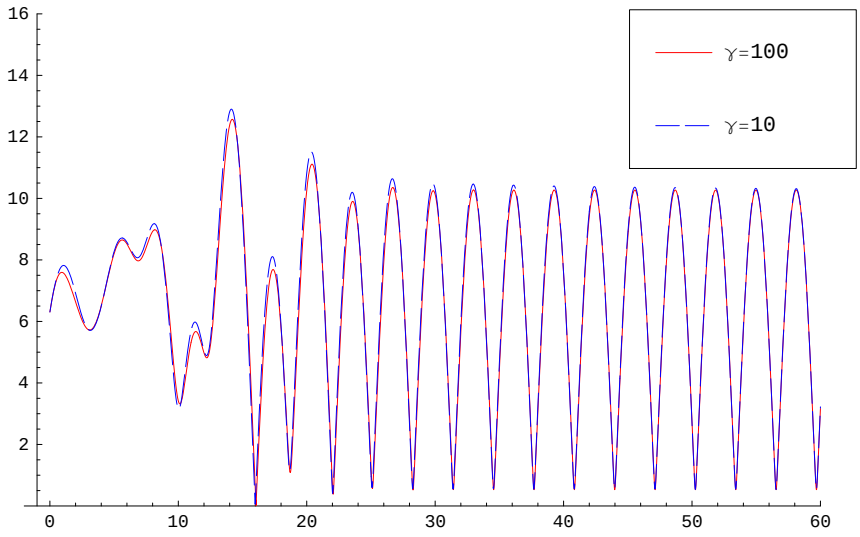

(c) Control norm

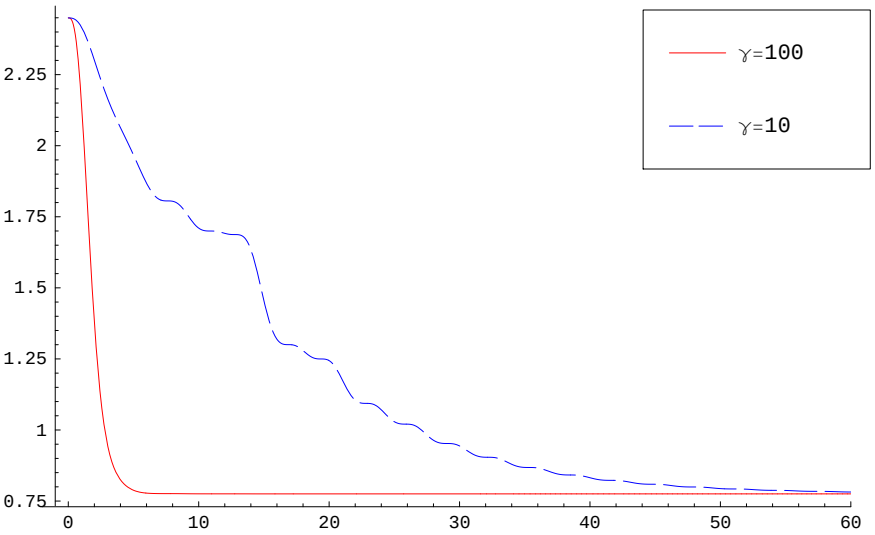

(d) parameter estimation error norm

Figure 4.4: Performance study of the proposed non-CE adaptive attitude tracking controller for two different different γ values

PE Reference Trajectory

We now consider the case wherein the reference trajectory is persistently exciting so that parameter estimates from the CE-based controller and the proposed non-CE controller may converge to their corresponding true values. The reference angular velocity for this simulation is taken to be $\boldsymbol{\omega}_{rp}(t) = [\cos t + 2, 5\cos t, \sin t + 2]^T$. Before comparing the closed-loop performance of each method, we first tune the deterministic (ideal case non-adaptive) control performance as done before in Fig. 4.5, which leads to $\alpha_{ce} = 8$ (the rest of control gains are same as before). The inertia matrix is once again assumed unknown and the adaptive control simulations for the PE reference trajectory case are shown in Fig. 4.6. First, we note that the attitude and angular rate error convergence remains slow with the CE-based method. Since the reference trajectory is persistently exciting, the parameter estimates converge to their true values and this convergence rate is significantly faster for the proposed method compared to the CE-based approach as seen in Fig. 4.6(d).

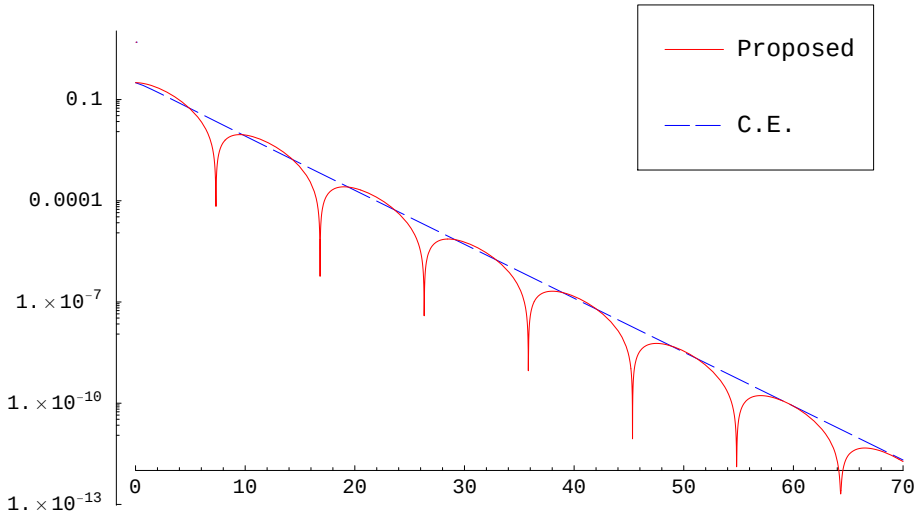

(a) quaternion tracking error $\delta \boldsymbol{q}_v$

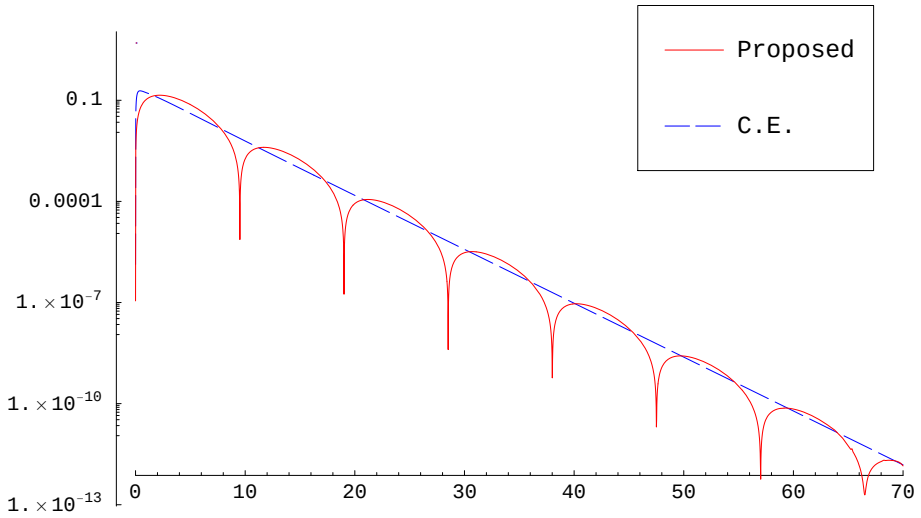

(b) angular velocity error $\delta \boldsymbol{\omega}$

Figure 4.5: Ideal case closed-loop performance for the PE reference trajectory obtained with the CE-based and the proposed non-CE controller assuming the inertia matrix J to be known

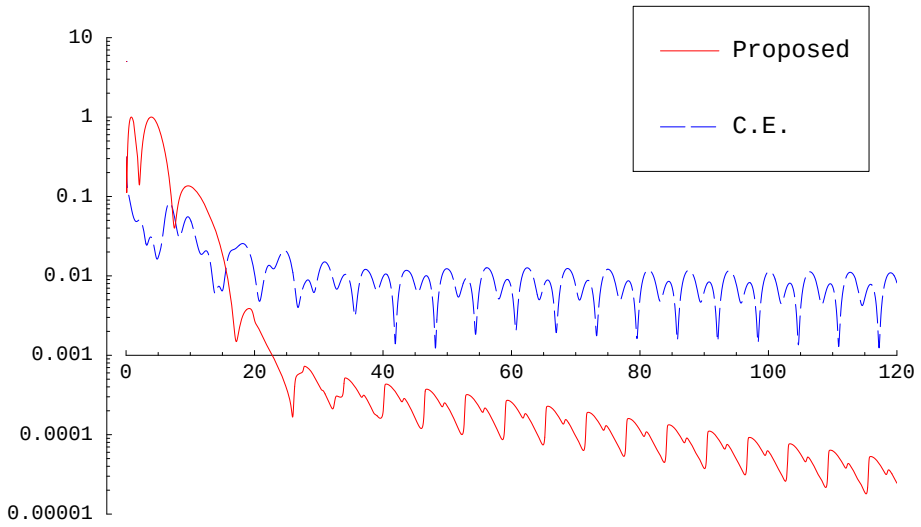

(a) quaternion tracking error $\delta \boldsymbol{q}_v$

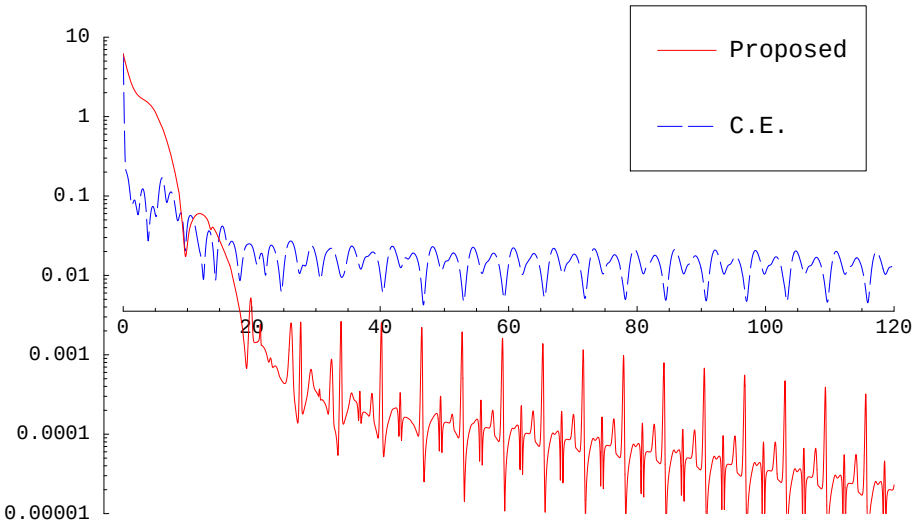

(b) angular velocity error $\delta \boldsymbol{\omega}$

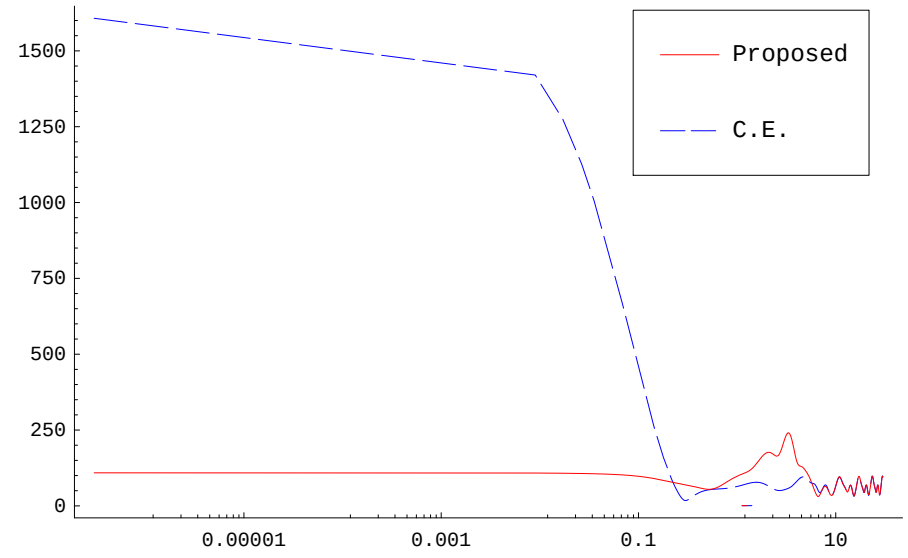

(c) control norm

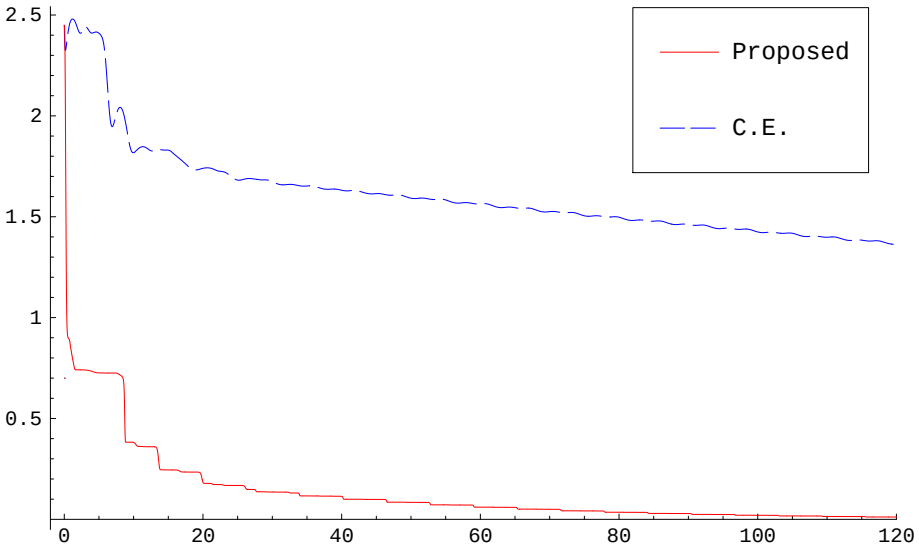

(d) parameter estimation error norm

Figure 4.6: Adaptive attitude tracking closed-loop performance comparison between the classical CE-based controller and the proposed non-CE controller for a PE reference trajectory

4.5.2 Proposed Control with Projection Mechanism

In the following simulation where the proposed control scheme is combined with the projection algorithm, system response trajectories are compared with those of the foregoing adaptive controller. γ is set to 20 during the simulation and the reference attitude trajectory is generated by $\boldsymbol{\omega}_r(t)$ in the previous section. In addition, system parameters of Eq. (4.47) are used. The performance of the proposed controller with projection is better than that of the proposed controller only. Although the transient response of both control methods are comparable during first 20 seconds, we notice in Fig. 4.7 that the proposed controller with projection shows a smaller error-norm trajectory in the long run. One thing needs to be mentioned here is that this simulation is performed with a relatively small γ value. If we increase γ value, then the trajectories of both closed-loop systems converge to the ideal trajectory (deterministic case of the proposed controller) shown in Fig. 4.2. Differences are highlighted in Fig. 4.8. The estimation trajectories of the proposed control method with projection do not leave known parameter bounds (denoted by brown lines) while some of the proposed control method without projection cross the parameter bound line. Lastly, we see that parameter estimates of both methods fail to identify true parameter values because of the non-persistence excitation of the reference signal $\boldsymbol{\omega}_r$.

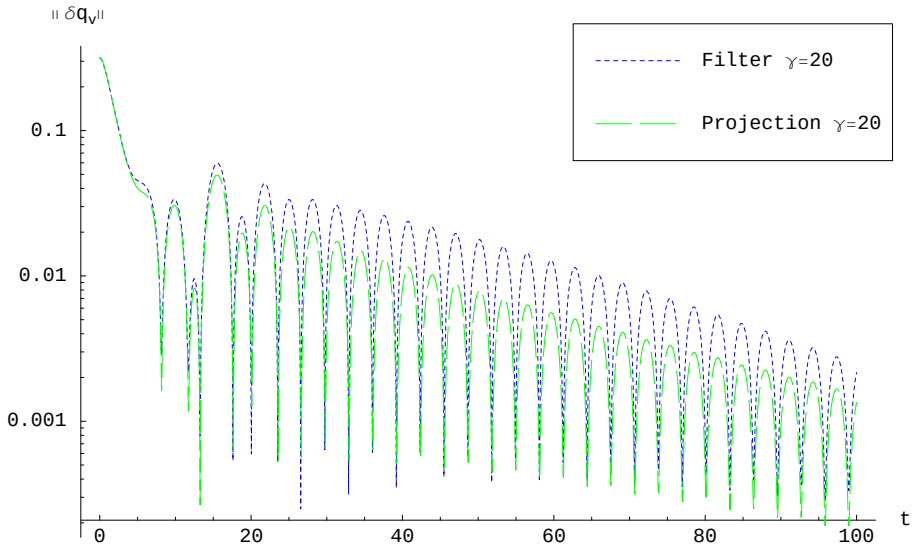

(a) Quaternion error norm trajectory

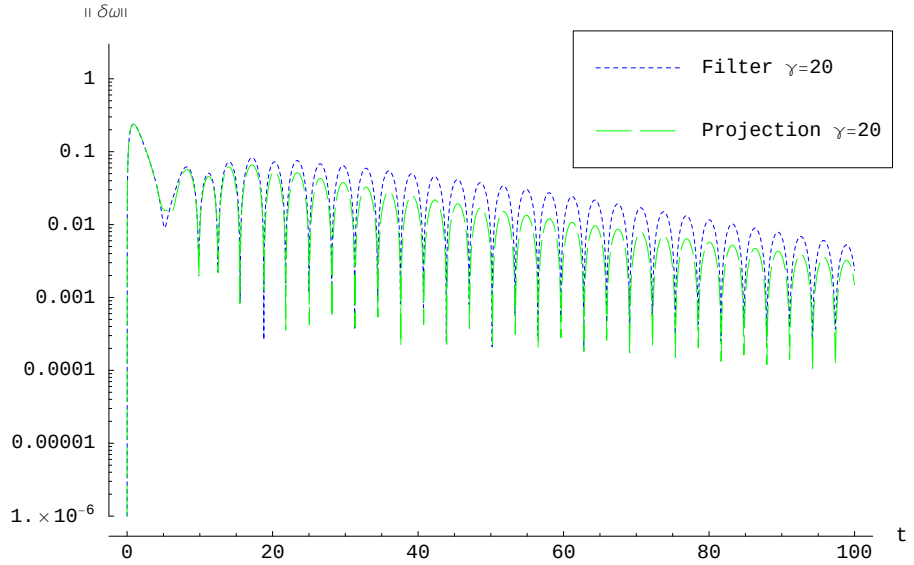

(b) Angular velocity error norm trajectory

Figure 4.7: Error norm trajectory comparison between the proposed method and the proposed method with a projection

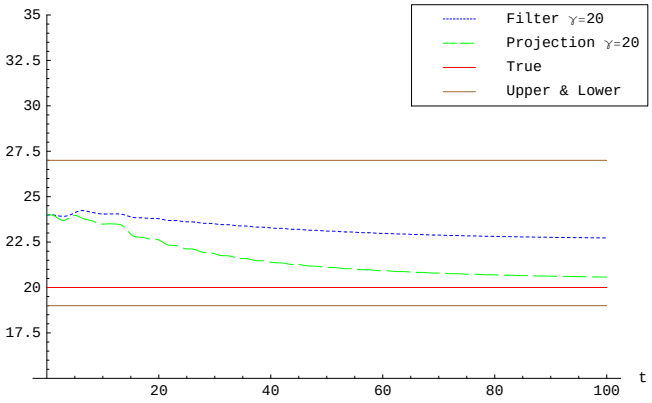

(a) Parameter estimate trajectory for θ_1^*

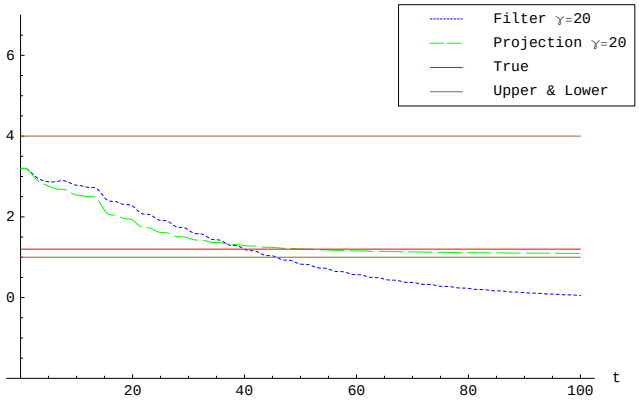

(b) Parameter estimate trajectory for θ_2^*

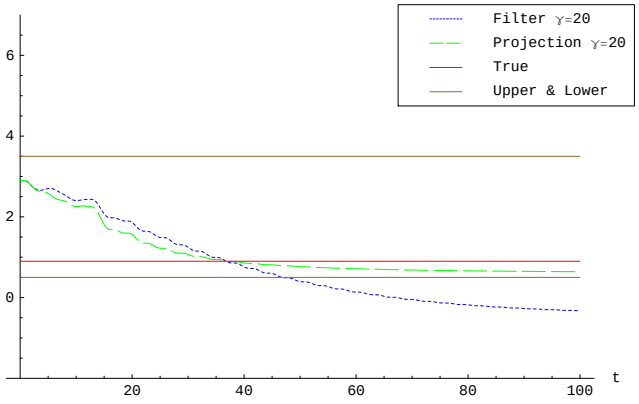

(c) Parameter estimate trajectory for θ_3^*

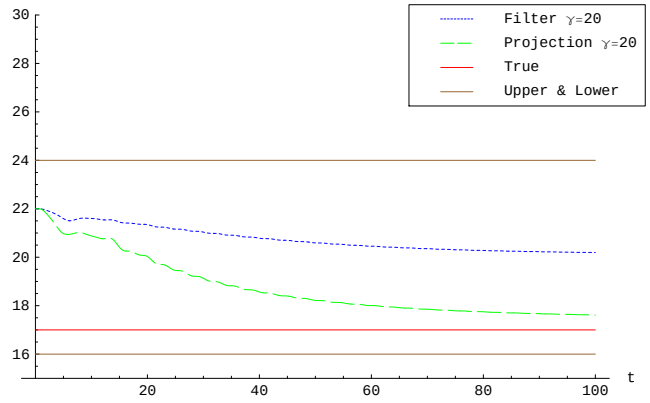

(d) Parameter estimate trajectory for θ_1^*

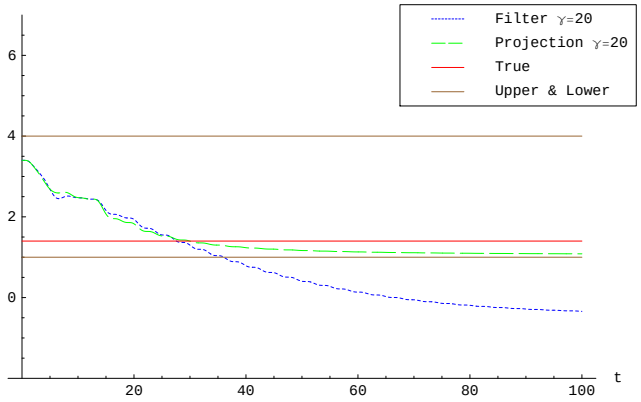

(e) Parameter estimate trajectory for θ_2^*

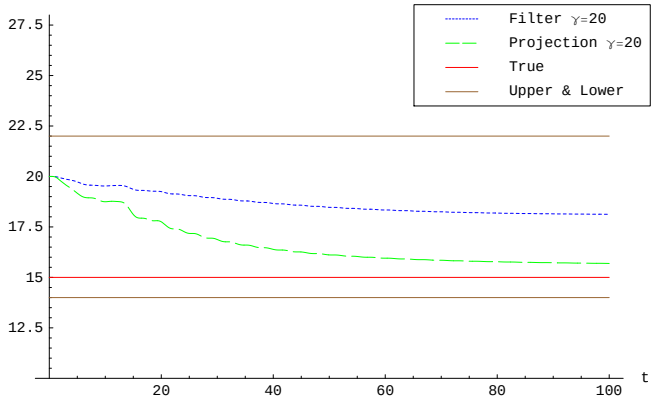

(f) Parameter estimate trajectory for θ_3^*

Figure 4.8: Parameter estimates trajectory comparison according to the existence of a projection mechanism

Chapter 5

Attitude Estimator with Known Angular Velocity

This chapter includes an overview of the attitude estimation problem and presents an novel approach to it by designing an attracting manifold. The designed attracting manifold through an adaptive estimation update preserves the orthogonal structure of attitude matrices on all n-dimensional spaces. In Chapter 6, the developed attitude estimator is combined with the proposed adaptive attitude tracking controller to be implemented in real systems.

5.1 Introduction

Attitude estimation problems arising in numerous aerospace and robotics applications are about how to find a 3-dimensional attitude matrix from an input-output relationship. The attitude matrix is represented by a proper orthogonal matrix in $SO(3)$ topologically. Thus, the actual unknown element number is 6 although the total number of elements in the attitude matrix is 9. Based on this property, numerous attitude estimation/determination algorithms are available in the liter-

ature presented by both control and estimation communities. The important fact is that conventional estimation methods rely on linear over-parameterization of 6 elements[44] although 6 elements are nonlinear parameterization of fewer number of coordinates[42, 45]. In addition to grouping conventional estimation methods based on attitude parameterization, depending on how the underlying attitude estimation algorithm is implemented, we may also categorize them broadly into two classes: batch type and sequential type estimators.

Batch type estimators utilize more than two observations at each observation instant to determine the attitude matrix, thereby necessitating the use of two or more independent sensors. QUEST[46] and FOAM[47] belong to the class of batch type estimators. Estimates of attitude matrix are computed by minimizing a quadratic cost function originally proposed by Wahba[48] in a statistical way. Another variant of batch estimator in use is TRIAD[49], which requires at most $n-1$ linearly independent observation vectors for n-dimensional attitude matrices to solve a matrix equation deterministically[50].

Sequential type estimators, in contrast with batch type estimators, need only one observation at each observation instant. An extended Kalman filter[51] is one of most commonly used sequential type estimators. Instead of fusing measurements from multiple sensors at each instant, sequential type estimators utilize an analytic model of the system to forward propagate the observation data. Attitude estimates are then generated by comparing predicted observations with actual measurements while updating the underlying analytic model through minimization of a suitable optimality criterion. The standardly adopted optimality criterion for Kalman filtering is the minimization of variances between estimates from sensor measurement and predicted values derived from the system analytic model. Applications of extended Kalman filter type sequential estimators are documented for missions such as the Earth Radiation Budget Satellite (ERBS)[52, 53] and the Solar Anomalous

Magnetospheric Particle Explorer (SAMPEX)[54, 55].

Both batch and sequential type estimators have successfully found their application in a wide array of spacecraft missions. However, they usually have a crucial limitation due to the over-parameterization and resulting non-orthogonal attitude estimates. In order to eliminate problems associated with over-parameterization, recently, an adaptive algorithm for orthogonal matrix estimation was developed by Kinsey and Whitcomb[56]. The convergence proof for their algorithm utilizes a matrix logarithmic map defined over the attitude estimation in the 3-dimensional space, which means the extension to n-dimensional space requires a n-dimensional matrix logarithmic map. Further, the matrix logarithmic map is not injective for certain class of orthogonal matrices. Precisely stated, $SO(3)$ group, where attitude matrices belong, does not include the orthogonal matrix whose trace is -1 (the corresponding Euler principal rotation angle $\phi = \pm\pi$).

In this chapter, we present new classes of adaptive estimation algorithms for uncertain $n \times n$ proper orthogonal matrices. The proposed estimation methodology introduces an attracting manifold about the "true" but "unknown" attitude matrix where estimate and true attitude matrices become identical under a standard observation condition. Simultaneously, the attracting manifold helps enforcing the attitude matrix estimate to be proper and orthogonal at every time step. Design of the attracting manifold results in significant reduction of computational burden associated with: (a) being able to fully utilize the available prior information on orthogonality of the unknown attitude and thereby avoiding over-parameterization; and (b) not having to perform the re-orthogonalization process at each time step. The standard observation assumption refer to the availability of persistence in excitation (PE) and we are able to show that the attitude estimate is guaranteed to converge to the corresponding true value with PE condition. Convergence proof for the proposed estimation algorithm is accomplished in such a way that not only are

the restrictions associated with the logarithmic map of Kinsey and Whitcomb[56] are completely eliminated but our results also generalize nicely for attitude matrices on all n-dimensional spaces.

This chapter is organized as follows. In the following section, adaptive attitude estimation problems are formulated under standard assumptions such as known reference signal, bounded noise, and persistent excitation. Then, we present main results that establish a new orthogonality preserving attitude matrix estimation algorithm valid for the general n-dimensional case. In section 5.3.2, robustness analysis for the proposed estimation algorithm subject to the measurement noise is presented. Implications of the developed estimation algorithm for 2-dimensions followed by 3 dimensions are discussed in section 5.4 and 5.5 respectively. Numerical simulation results are presented in section 5.6 to demonstrate and validate the proposed algorithm.

5.2 Problem Formulation

As mentioned before, adaptive attitude estimation method depends on the continuous time input-output attitude equation represented as follows

$$\boldsymbol{y}(t) = C(t)\boldsymbol{r}(t) \tag{5.1}$$

where $C(t)$ is an unknown time-varying proper orthogonal matrix; i.e., a time-varying direction cosine matrix satisfying $C(t)C^T(t) = C^T(t)C(t) = I_{n\times n}$ and $\det(C(t)) = 1$ for all t. Unit vectors $\boldsymbol{r}(t) \in \mathbb{R}^n$ and $\boldsymbol{y}(t) \in \mathbb{R}^n$ respectively correspond to the input and output signals, both of which are assumed accessible for all time t. In addition, $\boldsymbol{r}(t)$ is assumed to be a differentiable function of time with a bounded derivative. The measurement model Eq. (5.1) is from a model of measurement sensors such as star trackers, sun sensors and magnetometers[57]. More

specific examples of star sensor modeling in attitude determination problems can be found in [58, 59]. For the magnetometer and its modeling, refer to [60]. In general, a few sensors are equipped together to achieve high accurate attitude information[61]. $C(t)$ evolves along the time t by the following Poisson differential equation

$$\dot{C}(t) = -S(\boldsymbol{\omega}(t))C(t) \tag{5.2}$$

where $\boldsymbol{\omega}(t) \in \mathbb{R}^m$ is any prescribed/measured bounded signal for $m = n(n-1)/2$, and $S(\cdot) : \mathbb{R}^m \to \mathbb{R}^{n\times n}$ is a skew-symmetric matrix function such that $S^T = -S$. The fact is that if $C(0)$ is a proper orthogonal matrix, then $C(t)$ is always a proper and orthogonal matrix for all t whenever it evolves along Eq. (5.2)[62]. The estimation objective is to find an adaptive algorithm computing the proper orthogonal matrix $\hat{C}(t) \in \mathcal{R}^{n\times n}$ as an estimate for the "true" but unknown matrix $C(t)$ at each instant t. Since $\hat{C}(t)$ is orthogonal, the estimator structure is the same as Eq. (5.1) and represented as

$$\hat{\boldsymbol{y}}(t) = \hat{C}(t)\boldsymbol{r}(t). \tag{5.3}$$

Analogous discrete-time estimator structure with different update laws for $\hat{C}(t)$ can be found in the spacecraft attitude determination problems. In such cases, $\boldsymbol{r}(t)$ and $\boldsymbol{y}(t)$ are respectively interpreted as the star catalog values (inertial) and the corresponding star tracker measurements. Spacecraft rendezvous and proximity operations computing relative navigation solutions are other examples for the proposed adaptive attitude estimation framework. To quantify the error between the true attitude matrix and its estimate, the attitude estimation error matrix $\tilde{C}(t)$ is defined by matrix subtraction as follows

$$\tilde{C}(t) = \hat{C}(t) - C(t) \tag{5.4}$$

Obvious from the definitions in Eq. (5.1) and Eq. (5.3) is the fact that the attitude error convergence, $\lim_{t\to\infty}\tilde{C}(t) = 0$, implies the output estimation error, $\boldsymbol{e}(t) \doteq \hat{\boldsymbol{y}}(t) - \boldsymbol{y}(t) \to 0$ as $t \to \infty$. In the following developments, unless considered necessary, the time argument t is omitted from various signals for the sake of notational simplicity.

5.3 Adaptive Attitude Estimation with Attracting Manifold

In this section, we present an adaptive estimate update law for $\hat{C}(t)$, its robustness analysis subject to bounded measurement noise, and comparison with certainty equivalence principle.

5.3.1 Main Result

Theorem 6. *If the attitude estimate $\hat{C}(t)$ is generated by*

$$\dot{\hat{C}}(t) = -\left[S(\boldsymbol{\omega}) - \gamma(\boldsymbol{y}\hat{\boldsymbol{y}}^T - \hat{\boldsymbol{y}}\boldsymbol{y}^T)\right]\hat{C}(t);$$
$$\text{any real } \gamma > 0, \text{ any proper orthogonal } \hat{C}(0) \in \mathbb{R}^{n\times n} \tag{5.5}$$

then, $\hat{C}(t)$ remains a proper orthogonal matrix for all $t > 0$ implying that attitude matrix estimation error $\tilde{C}(t)$ and the output estimation error $\boldsymbol{e}(t)$ remain bounded for all $t \geq 0$. In addition, the estimation process for $\hat{C}(t)$ is driven along an "attracting manifold" according to the following convergence condition

$$\lim_{t\to\infty}\left(I_{n\times n} - C^T\hat{C}C^T\hat{C}\right)\boldsymbol{r}(t) = 0. \tag{5.6}$$

Proof. Like the Poisson differential equation Eq. (5.2) preserving orthogonality of $C(t)$ for all t, Eq. (5.5) enforces orthogonality of $\hat{C}(t)$ for all t. This is simply because

$(\boldsymbol{y}\hat{\boldsymbol{y}}^T - \hat{\boldsymbol{y}}\boldsymbol{y}^T)$ is also a skew-symmetric matrix. Thus, $\hat{C}(t)$ and $\tilde{C}(t)$ remain bounded for all t, which means $\boldsymbol{e}(t)$ is also bounded for all t. The convergence property along the attracting manifold of Eq. (5.6) is proved by considering the following Lyapunov candidate function

$$V(t) = \frac{1}{2}\text{tr}(\tilde{C}^T(t)\tilde{C}(t)) \tag{5.7}$$

where $\text{tr}(\cdot)$ is the matrix trace operator. Taking the time derivative of $V(t)$ in Eq. (5.7) along the update dynamics Eq. (5.5) leads to the following equality

$$\begin{aligned}
\dot{V}(t) &= \text{tr}\left(-\tilde{C}^T S(\boldsymbol{\omega})\tilde{C} + \gamma\tilde{C}^T(\boldsymbol{y}\hat{\boldsymbol{y}}^T - \hat{\boldsymbol{y}}\boldsymbol{y}^T)\hat{C}\right) \\
&= \gamma\text{tr}\left(\tilde{C}^T(\boldsymbol{y}\hat{\boldsymbol{y}}^T - \hat{\boldsymbol{y}}\boldsymbol{y}^T)\hat{C}\right) \\
&= \gamma\text{tr}\left((\hat{C}^T - C^T)(C\boldsymbol{r}\boldsymbol{r}^T - \hat{C}\boldsymbol{r}\boldsymbol{r}^T C^T\hat{C})\right) \\
&= \gamma\text{tr}\left(-\boldsymbol{r}\boldsymbol{r}^T + C^T\hat{C}C^T\hat{C}\boldsymbol{r}\boldsymbol{r}^T\right) \\
&= -\gamma\boldsymbol{r}^T(I_{n\times n} - C^T\hat{C}C^T\hat{C})\boldsymbol{r} \\
&= -\frac{\gamma}{2}\boldsymbol{r}^T(I_{n\times n} - C^T\hat{C}C^T\hat{C} - \hat{C}^T C\hat{C}^T C + I_{n\times n})\boldsymbol{r} \\
&= -\frac{\gamma}{2}\boldsymbol{r}^T(I_{n\times n} - C^T\hat{C}C^T\hat{C} - \hat{C}^T C\hat{C}^T C + (C^T\hat{C}C^T\hat{C})^T(C^T\hat{C}C^T\hat{C}))\boldsymbol{r} \\
&= -\frac{\gamma}{2}\boldsymbol{r}^T(I_{n\times n} - C^T\hat{C}C^T\hat{C})^T(I_{n\times n} - C^T\hat{C}C^T\hat{C})\boldsymbol{r} \\
&= -\frac{\gamma}{2}\|(I_{n\times n} - C^T\hat{C}C^T\hat{C})\boldsymbol{r}\|^2
\end{aligned} \tag{5.8}$$

Since $V(t) \geq 0$ from Eq. (5.7) and $\dot{V}(t) \leq 0$ from Eq. (5.8), we have existence of $V_\infty \doteq \lim_{t\to\infty} V(t)$. Moreover, from the fact that $\ddot{V}(t)$ is bounded (seen by differentiating both sides of Eq. (5.8)), using Barbalat's lemma, we conclude $\lim_{t\to\infty}(I_{n\times n} - C^T\hat{C}C^T\hat{C})\boldsymbol{r}(t) = 0$. □

Remark 5. From the definition of $\tilde{C}(t)$ in Eq. (5.4), we see that the convergence of $\hat{C}(t)$ to $C(t)$ leads to $\lim_{t\to\infty}\tilde{C}(t) = 0$, which is equivalent to $C^T(t)\hat{C}(t) \to I_{n\times n}$ as $t \to \infty$ by the matrix orthogonality property. This means the satisfaction of

the convergence condition of Theorem 6 in Eq. (5.6). However, the inverse of the pervious statement is not true. In general, the satisfaction of Eq. (5.6) does not guarantee the convergence of $\hat{C}(t)$ to $C(t)$ without certain persistence of excitation (PE) conditions for $\boldsymbol{r}(t)$. These PE conditions will be further elaborated upon in the later sections.

5.3.2 Robustness Analysis

In order to account for the effect of measurement noise, the input-output attitude equation is modified as follows

$$\boldsymbol{y}(t) = C(t)\boldsymbol{r}(t) + \boldsymbol{v}(t) \tag{5.9}$$

where measurement noise $\boldsymbol{v}(t)$ is assumed to be bounded and its bound is $v_{\max} \doteq \sup_t \|v(t)\|$. In addition, from a practical standpoint, we may assume that $v_{\max} \ll 1$ without loss of generality though this assumption is not required for our analysis. With the same estimation update rule for $\hat{C}(t)$ as in Eq. (5.5), consider the following Lyapunov candidate function

$$V_r(t) = \frac{1}{2}\mathrm{tr}\left[\tilde{C}^T\tilde{C}\right]. \tag{5.10}$$

Because of the same estimation update law for $\hat{C}(t)$, proper orthogonality of $\hat{C}(t)$ is preserved regardless of measurement noise $\boldsymbol{v}(t)$. Thus, $V_r(t)$ is uniformly bounded. Further, the time derivative of $V_r(t)$ is obtained using Eq. (5.3), Eq. (5.5), and

Eq. (5.9) as follows

$$\begin{aligned}\dot{V}_r(t) &= \mathrm{tr}\left(\tilde{C}\dot{\hat{C}}\right) \\ &= \gamma \mathrm{tr}\left(\tilde{C}^T(\boldsymbol{y}\hat{\boldsymbol{y}}^T - \hat{\boldsymbol{y}}\boldsymbol{y}^T)\hat{C}\right) \\ &= -\gamma \boldsymbol{r}^T\left(I - C^T\hat{C}C^T\hat{C}\right)\boldsymbol{r} - \gamma \boldsymbol{v}^T C\left(I - C^T\hat{C}C^T\hat{C}\right)\boldsymbol{r} \\ &\leqslant -\frac{\gamma}{2}\|(I_{n\times n} - C^T\hat{C}C^T\hat{C})\boldsymbol{r}\|\left[\|(I_{n\times n} - C^T\hat{C}C^T\hat{C})\boldsymbol{r}\| - 2v_{\max}\right]. \end{aligned} \tag{5.11}$$

By the presence of measurement noise $\boldsymbol{v}(t)$, the sign indefinite term $\gamma \boldsymbol{v}^T C\left(I - C^T\hat{C}C^T\hat{C}\right)\boldsymbol{r}$ is introduced; thus, the convergence property of Eq. (5.6) is no longer valid. However, we may conclude that the residual set of $V_r(t)$ is governed by $v_{\max}$ based on the fact that $\dot{V}_r(t) \leq 0$ in Eq. (5.11) whenever $\|(I_{n\times n} - C^T\hat{C}C^T\hat{C})\boldsymbol{r}\| - 2v_{\max} \geq 0$. The foregoing robustness analysis of the proposed estimation algorithm confirms that while all the signals remain bounded, accuracy of estimated attitude values is deteriorated by measurement noise.

5.3.3 Comparison with Certainty Equivalence Framework

In this section, the proposed adaptive estimation algorithm in Theorem 6 and the conventional adaptive estimation algorithm based on certainty equivalence principle (CE)[39] are compared to explore the difference between them. In order to be consistent with the standard assumptions of the CE methodology, $C(t)$ is restricted to be a constant C^* (i.e., $\boldsymbol{\omega}(t) = 0$ in Eq. (5.2)). Benefits of the proposed estimation algorithm is originated from the fact that it preserves the proper and orthogonal structure of estimate $\hat{C}(t)$ along time t, while the conventional adaptive estimation schemes cannot. The reason for the foregoing fundamental difference is how to parameterize the unknown C^*. Utilizing the orthogonal structure of C^* as prior information results in the nonlinear parameterization of C^* in Eq. (5.1), which is not readily amenable to most existing CE-based formulations. On the other hand,

if we do not use an a priori information about C^*, then C^* is linearly parameterized and CE methods become feasible. However, the simplification due to the linear parameterization in CE methodologies requires over-parameterization and permitting estimates to be non-orthogonal matrices ($\notin SO(3)$) while $C^* \in SO(3)$, which means the poor estimation performance. For the case when $C(t) = C^*$, a simple CE-based formulation based on standard methods[39] may be obtained as given by

$$\dot{\hat{C}}(t) = -\gamma \boldsymbol{e}\boldsymbol{r}^T; \quad \text{any real } \gamma > 0, \text{ any } \hat{C}(0) \in \mathbb{R}^{n\times n} \tag{5.12}$$

where just as before, the output estimation error $\boldsymbol{e}(t)$ is defined by $\boldsymbol{e}(t) = \hat{\boldsymbol{y}}(t) - \boldsymbol{y}(t)$. Consider the following Lyapunov candidate function

$$V^{ce}(t) = \frac{1}{2}\mathrm{tr}\left(\tilde{C}^T\tilde{C}\right) \tag{5.13}$$

where $\tilde{C}(t)$ is defined in Eq. (5.4). The time derivative of $V^{ce}(t)$ along solutions of Eq. (5.12) is derived as follows

$$\begin{aligned}
\dot{V}^{ce}(t) &= \mathrm{tr}\left(\tilde{C}^T\dot{\tilde{C}}\right) = -\gamma\mathrm{tr}\left(\tilde{C}^T\boldsymbol{e}\boldsymbol{r}^T\right) \\
&= -\gamma\mathrm{tr}\left(\tilde{C}^T\tilde{C}\boldsymbol{r}\boldsymbol{r}^T\right) = -\gamma\boldsymbol{r}^T\tilde{C}^T\tilde{C}\boldsymbol{r} \\
&= -\gamma\|\tilde{C}\boldsymbol{r}\|^2 = -\gamma\|\boldsymbol{e}\|^2 \ \leq 0
\end{aligned} \tag{5.14}$$

Since $V^{ce}(t) \geq 0$ and $\dot{V}^{ce}(t) \leq 0$, $V^{ce}(t)$ is uniformly bounded and $V^{ce}_\infty \doteq \lim_{t\to\infty} V^{ce}(t)$ exists and is finite. Thus, $\hat{C}(t)$ and $\boldsymbol{e}(t)$ are also bounded from the boundedness of $V^{ce}(t)$. Further, based on $\dot{\boldsymbol{e}} = \dot{\tilde{C}}\boldsymbol{r} + \tilde{C}\dot{\boldsymbol{r}}$ whose terms are bounded, we have $\dot{\boldsymbol{e}} \in \mathcal{L}_\infty$. Thus, by using Barbalat's lemma, it is guaranteed that $\boldsymbol{e}(t) \to 0$ as $t \to \infty$.

Remark 6. The demonstrated CE-based method is applicable only to the case when unknown attitude matrix is a constant matrix as described in the foregoing analysis. In the proposed adaptive estimation method by Theorem 6, no such restriction

exists.

Remark 7. CE-based adaptive estimation methods have no mechanism to enforce orthogonality to attitude estimates at each time instant. Thus, even when one selects the initial guess $\hat{C}(0)$ as a proper orthogonal matrix, there is no guarantee that $\hat{C}(t)$ is orthogonal for all $t > 0$. Different from CE-based adaptive estimation methods, the proposed method guarantees that $\hat{C}(t)$ is orthogonal for all $t \geq 0$ by ensuring Poisson differential equation for $\hat{C}(t)$ update.

Remark 8. In the following sections, we show that the persistent excitation condition for the reference input of the proposed estimation method is less restrictive than that of CE-based estimation methods.

5.4 2-D Attitude Estimation

The simplified result of Theorem 6 specialized to a 2-dimensional attitude estimation problem is presented in this section. During the synthesis of adaptive estimator, we may define a precise condition for the persistency of reference signals in order for the estimation error $\tilde{C}$ to converge to zero.

For the 2-dimensional attitude matrix, it is possible to represent the attitude matrix $C(t)$ as a matrix parameterized by single scalar variable $\theta(t)$ and the corresponding estimate $\hat{C}(t)$ of an unknown attitude matrix is parameterized by $\hat{\theta}(t)$ as follows

$$C(t) = e^{J\theta(t)} = \begin{bmatrix} \cos\theta & -\sin\theta \\ \sin\theta & \cos\theta \end{bmatrix}, \quad \hat{C}(t) = e^{J\hat{\theta}(t)} = \begin{bmatrix} \cos\hat{\theta} & -\sin\hat{\theta} \\ \sin\hat{\theta} & \cos\hat{\theta} \end{bmatrix} \tag{5.15}$$

where J is the 2×2 matrix generalization of $\sqrt{-1}$ and is given by

$$J = \begin{bmatrix} 0 & -1 \\ 1 & 0 \end{bmatrix} \tag{5.16}$$

Corollary 1. *For the input-output system described by Eq. (5.1), with $n = 2$, if the initial value of the attitude estimate $\hat{C}(0) = e^{J\hat{\theta}(0)}$ is such that $\hat{\theta}(0) \in \Theta_s$ where*

$$\Theta_s = \{\phi \in \mathbb{R} : \phi - \theta(0) \neq (2k+1)\pi\}, \quad k = 0, \pm 1, \pm 2, \ldots$$

then the attitude estimate matrix $\hat{C}(t)$ generated through Eq. (5.5) exponentially converges to the unknown true value $C(t)$ for all non-zero (unit-vector) reference inputs $\boldsymbol{r}(t) \in \mathbb{R}^2$.

Proof. In addition to the boundedness of $V(t)$ in Eq. (5.7), we may characterize it further through the parameterization using $\theta(t)$ and $\hat{\theta}(t)$ of Eq. (5.15) as follows

$$\begin{aligned} V_F(t) &= \frac{1}{2}\mathrm{tr}(\tilde{C}^T(t)\tilde{C}(t)) = \frac{1}{2}\mathrm{tr}\left[(\hat{C}-C)^T(\hat{C}-C)\right] \\ &= \frac{1}{2}\mathrm{tr}\left[2I_{2\times 2} - (\hat{C}^T C + C^T\hat{C})\right] = \frac{1}{2}\mathrm{tr}\left[2I_{2\times 2} - e^{-J(\hat{\theta}-\theta)} - e^{J(\hat{\theta}-\theta)}\right] \\ &= 2\left[1 - \cos(\hat{\theta}-\theta)\right] = 4\sin^2\left(\frac{\hat{\theta}-\theta}{2}\right). \end{aligned} \tag{5.17}$$

From the last step of Eq. (5.17), we see that $0 \leq V_F(t) \leq 4$ for all $t \geq 0$ and $V_F(t) = 4$ at $\hat{\theta}(t) - \theta(t) = (2k+1)\pi$ for all integer k (simultaneously, $V_F(t) = 0$ at $\hat{\theta}(t) - \theta(t) = 2k\pi$ for all integer k). Moreover, from the differentiation of $V_F(t)$ with respect to $\tau \doteq \hat{\theta}(t) - \theta(t)$ given by

$$\begin{aligned} \frac{\partial}{\partial\tau}V_F &= \frac{\partial}{\partial\tau}4\sin^2\left(\frac{\tau}{2}\right) \\ &= 4\sin\left(\frac{\tau}{2}\right)\cos\left(\frac{\tau}{2}\right) \\ &= 0 \quad \text{at } \tau = 2k\pi,\ (2k+1)\pi \text{ for all integer } k \end{aligned} \tag{5.18}$$

it is clear that $\tau = 2k\pi,\ (2k+1)\pi$ are equilibria for V_F. Stability of those equilibria is obtained by the time derivative of $V_F(t)$. Since $C^T\hat{C}C^T\hat{C} = e^{J(2\hat{\theta}-2\theta)}$ based on

our notation, $\dot{V}_F(t)$ $(= \frac{d}{dt}V_F(t))$ is simplified as follows

$$\begin{aligned}
\dot{V}_F(t) &= -\gamma \boldsymbol{r}^T \left[I_{2\times 2} - e^{J(2\hat{\theta}-2\theta)} \right] \boldsymbol{r} \\
&= -\gamma \boldsymbol{r}^T \begin{bmatrix} 1-\cos(2\hat{\theta}-2\theta) & -\sin(2\hat{\theta}-2\theta) \\ \sin(2\hat{\theta}-2\theta) & 1-\cos(2\hat{\theta}-2\theta) \end{bmatrix} \boldsymbol{r} \\
&= -\gamma \left[1-\cos(2\hat{\theta}-2\theta) \right] \|\boldsymbol{r}\|^2 \\
&= -8\gamma \sin^2\left(\frac{\hat{\theta}-\theta}{2} \right) \cos^2\left(\frac{\hat{\theta}-\theta}{2} \right) \|\boldsymbol{r}\|^2 \\
&= -\frac{\gamma}{2} V_F(4-V_F) \|\boldsymbol{r}\|^2 \leq 0
\end{aligned} \tag{5.19}$$

Since $\|\boldsymbol{r}\|$ is unit from the reference signal definition, $\dot{V}_F(t) < 0$ except for equilibria and $V_F(t)$ is always monotonically decreasing. Therefore, we may conclude that $V_F(t) \to 0$ as $t \to \infty$ as long as $V_F(0) \neq 4$ as a direct result of Theorem 6. The foregoing analysis enables us to categorize two sets of equilibria based on their stability. One is the set of unstable equilibria defined by the condition $V_F = 4$ which corresponds to $\hat{\theta}(t) - \theta(t) = (2k+1)\pi$ for integer values of variable k. Thus, if $V_F(0) = 4$, then $V_F(t) = 4$ for all t. The other is the set of stable equilibria defined by the condition $V_F = 0$ which corresponds to $\hat{\theta}(t) - \theta(t) = 2k\pi$. If $\hat{\theta}(0) \in \Theta_s$, then $\hat{\theta}(t)$ converges to one of stable equilibria asymptotically. Properties of V_F and its equilibria discussed so far are depicted in Fig. 5.1. Furthermore, from Eq. (5.19) with $\|\boldsymbol{r}\| = 1$, we have

$$\dot{V}_F(t) = -\frac{\gamma}{2} V_F(t) \left[4 - V_F(t) \right] \tag{5.20}$$

whose solutions are obtained analytically as follows

$$V_F(t) = \frac{4ce^{-2\gamma t}}{1 + ce^{-2\gamma t}} \quad \text{for all } t \geq 0, \quad \text{where } c = \frac{V_F(0)}{4 - V_F(0)} \tag{5.21}$$

Therefore, it is guaranteed that any initial condition $\hat{\theta}(0) \in \Theta_s$ implying $V_F(0) < 4$

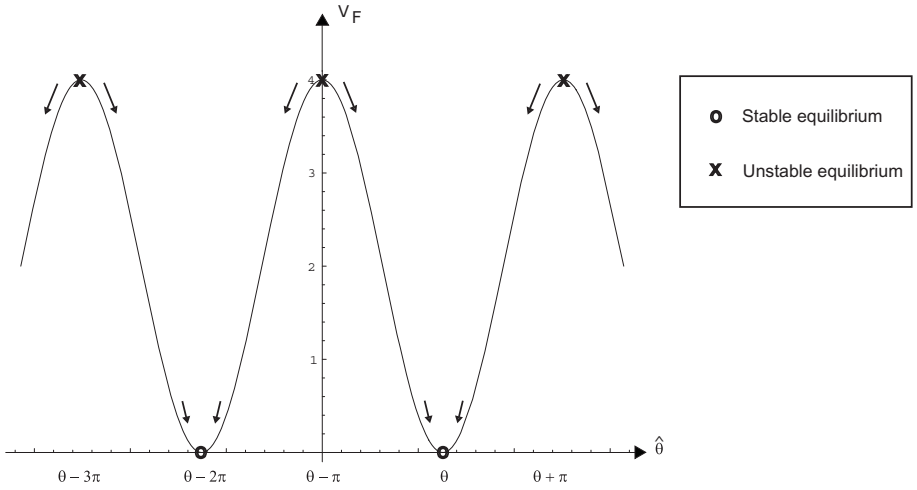

Figure 5.1: Plot showing variation of the bounded Lyapunov candidate function for flatland case $V_F(t)$ with respect to the estimated variable $\hat{\theta}(t)$.

leads to exponential convergence of $V_F(t)$ to zero. This means that if $\hat{\theta}(0) \in \Theta_s$, then $\hat{\theta}(t) - \theta(t) \to 2k\pi$ where integer k is determined by $\hat{\theta}(0)$, which is equivalent to that $\lim_{t\to\infty} \tilde{C}(t) = 0$ as claimed in Corollary 1. □

Remark 9. In 2-dimensional attitude problems, we eliminate an over-parameterization by updating $\hat{\theta}(t)$ instead of 2×2 matrix $\hat{C}(t)$. More specifically, instead of using Eq. (5.5), $\hat{C}(t)$ can be generated by using the identity $\hat{C}(t) = e^{J\hat{\theta}(t)}$ given from Eq. (5.15) as follows

$$\dot{\hat{\theta}}(t) = \omega(t) + \gamma \left[y_2(t)\hat{y}_1(t) - y_1(t)\hat{y}_2(t) \right] \tag{5.22}$$

where the scalar $\omega(t)$ is from the definition $\boldsymbol{\omega}(t) = \omega(t)\boldsymbol{e}_k$ in Eq. (5.2), and $\boldsymbol{e}_k$ is a unit vector normal to the plane defined by 2-dimensional basis vectors.

Remark 10. Corollary 1 states that $\tilde{C}(t)$ converges exponentially to zero as long as $\hat{\theta}(0) \in \Theta_s$. Thus $C(t)$ need not be a constant matrix and even $\boldsymbol{r}(t)$ need not be persistently exciting (i.e., $\boldsymbol{r}(t) = \boldsymbol{r}^*$ where $\boldsymbol{r}^*$ is any non-zero constant vector), which is impossible from the convention CE-based adaptive attitude estimation framework.

Remark 11. If the initial guess $\hat{\theta}(0)$ is one of unstable equilibria, then the proposed estimation method cannot make $\hat{\theta}(t)$ converge to $\theta(t)$ for all t. On the other hand, the perturbation from unstable equilibria ensures the exponential convergence of $\hat{\theta}(t)$ to $\theta(t)$ for all $t > t^*$ after some t^* no matter how small the applied perturbation is.

Remark 12. The robustness to the bounded measurement noise $\boldsymbol{v}(t)$ is obtained by considering the specialized version of the n-dimensional case in Eq. (5.11) given by

$$\begin{aligned}\dot{V}_r(t) &= -2\gamma \sin^2(\hat{\theta}-\theta)\|\boldsymbol{r}\|^2 - \gamma\left[\cos\theta - \cos(2\hat{\theta}-\theta)\right]\boldsymbol{v}^T\boldsymbol{r} \\ &\leq -2\gamma \sin^2(\hat{\theta}-\theta)\|\boldsymbol{r}\|^2 + 2\gamma \sin(\hat{\theta}-\theta)\boldsymbol{v}^T\boldsymbol{r} \end{aligned} \tag{5.23}$$

Since $\|\boldsymbol{r}(t)\| = 1$ as mentioned before, the last inequality is simplified further as

$$\dot{V}_r(t) \leq -2\gamma\,|\sin(\hat{\theta}-\theta)|\,\left[|\sin(\hat{\theta}-\theta)| - v_{\max}\right] \tag{5.24}$$

We see that $\dot{V}_r(t) \leq 0$ whenever $|\sin(\hat{\theta}-\theta)| - v_{\max} \geq 0$, which may provide an approximate upper bound on the estimation error for relatively low measurement noise (i.e.,$v_{\max}$ is small enough to satisfy $\sin(v_{\max}) \approx v_{\max}$). If $v_{\max} = 0$, then the proposed estimator recovers the exponential convergence immediately.

5.5 3-D Attitude Estimation

Before we proceed to the 3-dimensional attitude estimation problem, one thing should be mentioned here. So far, we consider the case that a single sensor generates measurements for the attitude estimator in Eq. (5.5) instead of multiple sensors. In a practical point-of-view, we may have more than one sensor for the system to increase the performance of the attitude estimator. The following analysis shows how to interpret the presence of multiple sensors within the proposed estimation

framework as an extension of Theorem 6. Suppose we have M number of sensors generating output measurements for the attitude estimator

$$\boldsymbol{y}_k(t) = C(t)\boldsymbol{r}_k(t), \quad k = 1, 2, \ldots, M \tag{5.25}$$

Then, Eq. (5.5) needs to be modified as follows

$$\dot{\hat{C}}(t) = -\left[S(\boldsymbol{\omega}) - \gamma \sum_{k=1}^{m} (\boldsymbol{y}_k \hat{\boldsymbol{y}}_k^T - \hat{\boldsymbol{y}}_k \boldsymbol{y}_k^T)\right] \hat{C}(t); \tag{5.26}$$

$$\text{any real } \gamma > 0, \text{ any proper orthogonal } \hat{C}(0) \in \mathbb{R}^{n \times n}$$

where $\hat{\boldsymbol{y}}_k$ denotes the k^{th} estimated output computed by

$$\hat{\boldsymbol{y}}_k(t) = \hat{C}(t)\boldsymbol{r}_k(t), \quad k = 1, 2, \ldots, M \tag{5.27}$$

From the definition of Lyapunov candidate Eq. (5.7) with a subscript M, we can derive the following time derivative of $V_M(t)$:

$$\begin{aligned}
\dot{V}_M(t) &= \text{tr}\left(-\tilde{C}^T S(\boldsymbol{\omega})\tilde{C} + \gamma \sum_{k=1}^{M} \tilde{C}^T (\boldsymbol{y}_k \hat{\boldsymbol{y}}_k^T - \hat{\boldsymbol{y}}_k \boldsymbol{y}_k^T)\hat{C}\right) \\
&= \gamma \text{tr}\left(\sum_{k=1}^{M} (-\boldsymbol{r}_k \boldsymbol{r}_k^T + C^T \hat{C} C^T \hat{C} \boldsymbol{r}_k \boldsymbol{r}_k^T)\right) \\
&= -\gamma \sum_{k=1}^{M} \left(\boldsymbol{r}_k^T (I_{n\times n} - C^T \hat{C} C^T \hat{C})\boldsymbol{r}_k\right) \\
&= -\frac{\gamma}{2} \sum_{k=1}^{M} \|(I_{n\times n} - C^T \hat{C} C^T \hat{C})\boldsymbol{r}_k\|^2
\end{aligned} \tag{5.28}$$

which recovers Eq. (5.8) when $M = 1$. Stability proof remains the same as Theorem 6 except for summation. One thing should be noted in Eq. (5.28) is that we can obtain the same effect from a single measurement device by tuning γ of Eq. (5.5)

instead of adopting M measurement devices. Given that all technical details remain unaltered with single or multiple measurements, to keep the notation simple, we retain the single measurement model while discussing all further implications of our proposed attitude estimation algorithm for 3-dimensions.

The unit-norm constrained quaternion is adopted to parameterize the attitude matrix without singularity in 3-dimensional form of Theorem 6. Thus, the true attitude matrix $C(t)$ is represented by the quaternion vector $\boldsymbol{q}(t) = [q_o(t), \boldsymbol{q}_v(t)]^T$ where the subscripts 'o' and 'v' respectively designate the scalar and vector parts of the quaternion representation. To obtain $C(t)$ from $\boldsymbol{q}(t)$, the following relationship is used

$$C(t) = I_{3\times 3} - 2q_o(t)S(\boldsymbol{q}_v(t)) + 2S^2(\boldsymbol{q}_v(t)) \tag{5.29}$$

where the 3×3 skew-symmetric matrix operator $S(\cdot)$ designates the vector cross product operation such that $S(\boldsymbol{a})\boldsymbol{b} = \boldsymbol{a} \times \boldsymbol{b}$ for all three-dimensional vectors $\boldsymbol{a}$ and $\boldsymbol{b}$. Corresponding $\hat{C}(t)$ is represented through the quaternion parameterization $\hat{\boldsymbol{q}}(t) = [\hat{q}_o(t), \hat{\boldsymbol{q}}_v(t)]^T$ so that we have

$$\hat{C}(t) = I_{3\times 3} - 2\hat{q}_o(t)S(\hat{\boldsymbol{q}}_v(t)) + 2S^2(\hat{\boldsymbol{q}}_v(t)) \tag{5.30}$$

In a similar way, the quaternion $\boldsymbol{z} = [z_o(t), \boldsymbol{z}_v(t)]^T$ parameterize the attitude matrix error defined by $C^T(t)\hat{C}(t)$ which is a proper orthogonal matrix in the following manner

$$C^T(t)\hat{C}(t) = I_{3\times 3} - 2z_o(t)S(\boldsymbol{z}_v(t)) + 2S^2(\boldsymbol{z}_v(t)) \tag{5.31}$$

where, by using the quaternion multiplication[34], the following identity holds

$$z_o(t) = \boldsymbol{q}^T(t)\hat{\boldsymbol{q}}(t). \tag{5.32}$$

In other words, if vectors $\boldsymbol{q}$ and $\hat{\boldsymbol{q}}$ are aligned in the same direction (i.e., if $\boldsymbol{q} = \pm\hat{\boldsymbol{q}}$

or in other words, $C = \hat{C}$), we have $z_o = \pm 1$ which from the unit vector constraint on the quaternion implies that $\|\boldsymbol{z}_v\| = 0$. Recalling the definition of the attitude estimation error matrix $\tilde{C}(t)$ in Eq. (5.4), it is obvious that $\tilde{C} = C(C^T\hat{C} - I_{3\times 3})$, and accordingly, we have $\tilde{C}(t) = 0$ whenever $C^T(t)\hat{C}(t) = I_{3\times 3}$ (i.e., $\boldsymbol{z}$ is a multiplicative matrix error definition, while $\tilde{C}$ is an additive matrix error definition). Thus, the vector $\boldsymbol{z}(t)$ has a relationship with $\tilde{C}(t)$ such that $z_o(t) = \pm 1 \iff \boldsymbol{z}_v(t) = 0$ if and only if matrix $C^T(t)\hat{C}(t) = I_{3\times 3} \iff \tilde{C}(t) = 0$. Note that the quaternion parameterization of $C^T(t)\hat{C}(t)C^T(t)\hat{C}(t)$ in Theorem 6 in terms of $\boldsymbol{z}$ is obtained by quaternion multiplication $\boldsymbol{z} \otimes \boldsymbol{z}$ where $\otimes$ denotes the quaternion multiplicative operator, and it is given by

$$C^T(t)\hat{C}(t)C^T(t)\hat{C}(t) = I_{3\times 3} - 2(2z_o^2(t) - 1)S(2z_o\boldsymbol{z}_v) + 2S^2(2z_o\boldsymbol{z}_v) \tag{5.33}$$

Based on the derived parameterization, the following 3-dimensional result and its stability proof are stated in quaternion space.

Corollary 2. *For the input-output attitude measurement system of Eq. (5.1) in the 3-dimensional case, suppose the true/unknown attitude matrix $C(t)$ evolving according to Eq. (5.2) is parameterized by the quaternion vector $\boldsymbol{q}(t)$ through Eq. (5.29). If the attitude estimate matrix $\hat{C}(t)$ is parameterized by the unit quaternion $\hat{\boldsymbol{q}}(t)$ according to Eq. (5.30) and is updated according to Eq. (5.5) subject to the condition that $\hat{\boldsymbol{q}}(0) \notin \Psi_u$ where*

$$\Psi_u = \left\{\boldsymbol{\eta} \in \mathbb{R}^4 : \|\boldsymbol{\eta}\| = 1; \boldsymbol{\eta}^T\boldsymbol{q}(0) = 0\right\}$$

then for all non-zero (unit-vector) reference inputs $\boldsymbol{r}(t) \in \mathbb{R}^3$ the following convergence condition holds asymptotically

$$\lim_{t\to\infty} \|\boldsymbol{r}(t) \times \boldsymbol{z}_v(t)\| = 0 \tag{5.34}$$

where $\boldsymbol{z}(t) = [z_o(t), \boldsymbol{z}_v(t)]^T$ *is a quaternion representation for the cascaded proper orthogonal matrix* $C^T(t)\hat{C}(t)$.

Proof. The following Lyapunov candidate function for the 3-dimensional case derived from Eq. (2.21) is used for the stability proof

$$V_o(t) = \frac{1}{2}\text{tr}\left(\tilde{C}^T\tilde{C}\right) = \frac{1}{2}\text{tr}\left(2I_{3\times 3} - (\hat{C}^T C + C^T\hat{C})\right) \tag{5.35}$$

In terms of the quaternion parameterization $\boldsymbol{z}(t)$ (corresponding to the multiplicative attitude error matrix $C^T(t)\hat{C}(t)$) defined by Eq. (5.31), $V_o(t)$ is written as follows

$$\begin{aligned} V_o(t) &= \frac{1}{2}\text{tr}\left[-2S^2(\boldsymbol{z}_v) - 2S^2(\boldsymbol{z}_v)\right] = -2\text{tr}\left[S^2(\boldsymbol{z}_v)\right] \\ &= -2\text{tr}\left[\begin{pmatrix} -z_3^2 - z_2^2 & z_1 z_2 & z_1 z_3 \\ z_1 z_2 & -z_1^2 - z_3^2 & z_2 z_3 \\ z_1 z_3 & z_2 z_3 & -z_2^2 - z_1^2 \end{pmatrix}\right] \\ &= 4(z_1^2 + z_2^2 + z_3^2) = 4\boldsymbol{z}_v^T\boldsymbol{z}_v \\ &= 4(1 - z_0^2) \end{aligned} \tag{5.36}$$

where $\boldsymbol{z}_v = [z_1, z_2, z_3]^T$. In the same way as in the 2-dimensional case, $V_o(t)$ is uniformly bounded for all $t \geq 0$ between 0 and 4. Based on Eq. (5.32), we may interpret the extrema of $V_o(t)$ in a geometric sense. If $\hat{\boldsymbol{q}}$ is on the hyperplane normal to $\boldsymbol{q}$ (i.e., $z_0 = \boldsymbol{q}^T\hat{\boldsymbol{q}} = 0$), then $V_o = 4$, its maximum value. On the other hand, if $\hat{\boldsymbol{q}}$ is aligned along $\boldsymbol{q}$ (i.e., $z_0 = 1$ or -1), then $V_o = 0$, its minimum value. Physically, $z_o = 0$ corresponds to an error in the Euler principal rotation angle (for the matrix $C^T\hat{C}$) given by $\pm\pi$ and therefore, the properties of $V_o(t)$ in the 3-dimensional case are very much analogous to the function $V_F(t)$ of the 2-dimensional case.

The time-derivative of Lyapunov candidate function $V_o(t)$ is derived following

each steps of Eq. (5.8). Using Eq. (5.33), the following simplified result is obtained

$$\begin{aligned}
\dot{V}_o(t) &= -\frac{\gamma}{2}\|(I_{3\times 3} - C^T\hat{C}C^T\hat{C})\boldsymbol{r}\|^2 \\
&= -\gamma \boldsymbol{r}^T\left[(1-2z_0^2)(2z_0)S(\boldsymbol{z}_v) - 8z_0^2 S^2(\boldsymbol{z}_v)\right]\boldsymbol{r} \\
&= -8\gamma z_0^2 \boldsymbol{r}^T S^T(\boldsymbol{z}_v)S(\boldsymbol{z}_v)\boldsymbol{r} \\
&= -8\gamma z_0^2 \|\boldsymbol{z}_v \times \boldsymbol{r}\|^2 \quad \leq 0
\end{aligned} \tag{5.37}$$

It is clear from the last inequality of Eq. (5.37) that Ψ_u is a set of equilibrium points for $V_o(t)$ at $t = 0$ (i.e., $z_o(0) = 0$); thus, if $V_o(0) = 4$, then $\dot{V}_o(t) = 0$ and $V_o(t) = 4$ for all $t \geq 0$. The stability of Ψ_u is characterized by the argument that if $z_o(0) \doteq \delta \neq 0$, with δ being arbitrarily small, then due to $\dot{V}_o(t) \leq 0$ from Eq. (5.37), we are guaranteed that $|\, z_o(t)\,| \geq |\, \delta\,|$ for all $t > 0$ and accordingly, there is no way for convergence $z_o(t) \to 0$ to happen as $t \to \infty$. Therefore, Ψ_u is a set of unstable equilibrium points for $V_o(t)$ at $t = 0$. Foregoing analysis is depicted in Fig. 5.2. On the other hand, by assuming $\hat{\boldsymbol{q}}(0) \notin \Psi_u$, we may preclude the case

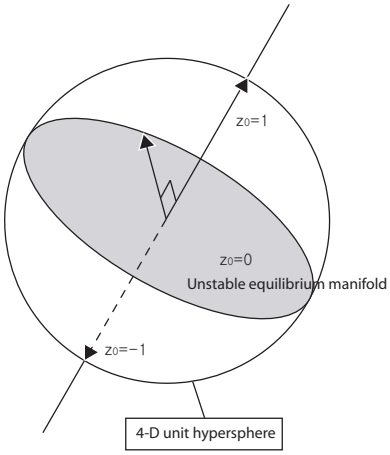

Figure 5.2: Illustration of the error quaternion vector $\boldsymbol{z} = [z_o, \boldsymbol{z}_v]^T$ representing the proper orthogonal matrix $C^T\hat{C}$. The hyperplane $z_o = 0$ represents an unstable equilibrium manifold.

that $\lim_{t\to\infty} z_o(t) = 0$. Thus, $\dot{V}_o(t) \leq 0$ and its combination with $V(t) \geq 0$ leads to

the fact that $\lim_{t\to\infty} V(t)$ exists and is finite, which means $\lim_{t\to\infty} \int_0^t \dot{V}_o(\sigma)d\sigma$ also exists and is finite. Further, we see that $\ddot{V}_o(t)$ is bounded by differentiating $\dot{V}_o(t)$ and thus, $\dot{V}_o(t)$ is uniformly continuous. By virtue of Barbalat's lemma, it is obtained that $\lim_{t\to\infty} \dot{V}_o(t) = 0$. Sine we ruled out $\lim_{t\to\infty} z_o(t) = 0$ by the assumption in Theorem 6, $\lim_{t\to\infty} \dot{V}_o(t) = 0$ is identical to $\lim_{t\to\infty} \|\boldsymbol{r}(t) \times \boldsymbol{z}_v(t)\| = 0$. This completes the proof. □

Remark 13. A direct consequence from Corollary 2 is the fact that whenever $\hat{\boldsymbol{q}}(0) \notin \Psi_u$, not only are we assured of convergence $\lim_{t\to\infty} \|\boldsymbol{r}(t) \times \boldsymbol{z}_v(t)\| = 0$ but in fact, the output estimation error $\boldsymbol{e}(t)$ also converges to zero as $t \to \infty$. This result can be easily established as follows: first, from Eq. (5.31) we note that $\boldsymbol{z}_v \times \boldsymbol{r} = S(\boldsymbol{z}_v)\boldsymbol{r} = 0$ implies $C^T\hat{C}\boldsymbol{r} = \boldsymbol{r}$; subsequently, starting with the definition of the output estimation error $\boldsymbol{e}(t)$, in the limit $t \to \infty$, we obtain

$$\boldsymbol{e}(t) = \hat{\boldsymbol{y}}(t) - \boldsymbol{y}(t) = \tilde{C}(t)\boldsymbol{r}(t) = C(t)[C^T(t)\hat{C}(t) - I_{3\times 3}]\boldsymbol{r}(t) = 0$$

which proves the stated assertion.

Remark 14. In the 2-dimensional attitude estimation case, we observe that there is an update law for a single parameter instead of the 2×2 matrix update law. This simplicity remains true for the 3-dimensional case by using a quaternion update law for $\hat{\boldsymbol{q}}(t)$ satisfying Eq. (5.30). First, it need to be recognized that 3-dimensional vectors $\boldsymbol{y}(t)$ and $\hat{\boldsymbol{y}}(t)$, the skew-symmetric matrix $\boldsymbol{y}\hat{\boldsymbol{y}}^T - \hat{\boldsymbol{y}}\boldsymbol{y}^T$ listed in Eq. (5.2) can be expressed in terms of the vector cross-product as follows

$$\gamma(\boldsymbol{y}\hat{\boldsymbol{y}}^T - \hat{\boldsymbol{y}}\boldsymbol{y}^T) = -S(\gamma\boldsymbol{y} \times \hat{\boldsymbol{y}}) \tag{5.38}$$

Accordingly, an update law for the unit-quaternion $\hat{\boldsymbol{q}}(t) = [q_o(t), \hat{\boldsymbol{q}}_v(t)]^T$ may be

expressed by

$$\dot{\hat{q}}_o(t) = -\frac{1}{2}\hat{\boldsymbol{q}}_v^T(\boldsymbol{\omega} + \gamma \boldsymbol{y} \times \hat{\boldsymbol{y}}); \quad \dot{\hat{\boldsymbol{q}}}_v(t) = \frac{1}{2}[\hat{q}_o I_{3\times 3} + S(\hat{\boldsymbol{q}}_v)](\boldsymbol{\omega} + \gamma \boldsymbol{y} \times \hat{\boldsymbol{y}}) \tag{5.39}$$

Remark 15. The dynamics of quaternion error $\boldsymbol{z}$ in Eq. (5.31) is expressed as

$$\dot{z}_o(t) = -\frac{1}{2}\boldsymbol{z}_v^T C^T(t)(\gamma \boldsymbol{y} \times \hat{\boldsymbol{y}}); \quad \dot{\boldsymbol{z}}_v(t) = \frac{1}{2}[z_o I_{3\times 3} + S(\boldsymbol{z}_v)]C^T(t)(\gamma \boldsymbol{y} \times \hat{\boldsymbol{y}}) \tag{5.40}$$

This can be further simplified by using the rotational invariance property of cross product

$$C^T(t)(\gamma \boldsymbol{y} \times \hat{\boldsymbol{y}}) = \gamma C^T(t)\boldsymbol{y} \times C^T(t)\hat{\boldsymbol{y}} = \gamma \boldsymbol{r} \times C^T(t)\hat{C}(t)\boldsymbol{r}$$

as follows

$$\dot{z}_o(t) = -\frac{\gamma}{2}\boldsymbol{z}_v^T[\boldsymbol{r} \times C^T(t)\hat{C}(t)\boldsymbol{r}]; \quad \dot{\boldsymbol{z}}_v(t) = \frac{\gamma}{2}[z_o I_{3\times 3} + S(\boldsymbol{z}_v)][\boldsymbol{r} \times C^T(t)\hat{C}(t)\boldsymbol{r}] \tag{5.41}$$

Remark 16. Starting from Corollary 2, it is possible to show that when $\hat{\boldsymbol{q}}(0) \notin \Psi_u$ together with $\dot{\boldsymbol{r}}(t) \neq 0$ (i.e., the reference input not a constant vector), then the attitude estimation error $\tilde{C}(t)$ asymptotically converges to zero. In Corollary 2 we proved that $\lim_{t\to\infty}[\boldsymbol{z}_v(t) \times \boldsymbol{r}(t)] = 0$. This result can be applied in Eq. (5.31) to infer that $C^T(t)\hat{C}(t)\boldsymbol{r}(t) = \boldsymbol{r}(t)$ as $t \to \infty$ which may further be substituted in Eq. (5.41) leading us to $\lim_{t\to\infty} \dot{\boldsymbol{z}}_v(t) = 0$. Further, from uniform continuity of $\boldsymbol{z}_v(t) \times \boldsymbol{r}(t)$, we have

$$\lim_{t\to\infty}[\boldsymbol{z}_v(t) \times \boldsymbol{r}(t)] = 0 \Longrightarrow \lim_{t\to\infty} \frac{\mathrm{d}}{\mathrm{dt}}[\boldsymbol{z}_v(t) \times \boldsymbol{r}(t)] = 0$$

which implies that $\lim_{t\to\infty}[\dot{\boldsymbol{z}}_v(t) \times \boldsymbol{r}(t) + \boldsymbol{z}_v(t) \times \dot{\boldsymbol{r}}(t)] = 0$ or $\lim_{t\to\infty}[\boldsymbol{z}_v(t) \times \dot{\boldsymbol{r}}(t)] = 0$. This means that as $t \to \infty$, $\boldsymbol{z}_v(t) \times \dot{\boldsymbol{r}}(t) \to 0$ and $\boldsymbol{z}_v(t) \times \boldsymbol{r}(t) \to 0$, i.e., the vector $\boldsymbol{z}_v(t)$ is simultaneously parallel to both $\boldsymbol{r}(t)$ and $\dot{\boldsymbol{r}}(t)$. It's possible only if $\boldsymbol{z}_v(t) = 0$ since

every unit vector $\boldsymbol{r}(t)$ satisfies $\boldsymbol{r}^T(t)\dot{\boldsymbol{r}}(t) = 0$, and therefore vectors $\boldsymbol{r}(t)$ and $\dot{\boldsymbol{r}}(t)$ remain normal to one other for all t. Now that we have $\lim_{t\to\infty} \boldsymbol{z}_v(t) = 0$, from Eq. (5.31), it is possible to conclude that $C^T(t)\hat{C}(t) \to I_{3\times 3}$ as $t \to \infty$ and accordingly, the asymptotic convergence result $\lim_{t\to\infty} \tilde{C}(t) = 0$ for the attitude estimation error matrix.

Remark 17. As a specialized case, we may consider the convergence properties of the attitude estimation algorithm for constant reference input, i.e., $\boldsymbol{r}(t) =_* \text{ for all } t \geq 0$. To analyze the evolving attitude error trajectory in terms of $\boldsymbol{z}$, the projection of $\dot{\boldsymbol{z}}_v(t)$ along $\boldsymbol{r}_*$ is derived as follows

$$\begin{aligned}
\boldsymbol{r}_*^T \dot{\boldsymbol{z}}_v(t) &= \frac{\gamma}{2} \boldsymbol{r}_*^T \left[z_o I_{3\times 3} + S(\boldsymbol{z}_v) \right] C^T(t)(\boldsymbol{y} \times \hat{\boldsymbol{y}}) \\
&= \gamma \boldsymbol{r}_*^T \left[z_o I_{3\times 3} + S(\boldsymbol{z}_v) \right] \left[z_o(\boldsymbol{z}_v \times \boldsymbol{r}_*) \times \boldsymbol{r}_* - (\boldsymbol{r}_*^T \boldsymbol{z}_v)(\boldsymbol{z}_v \times \boldsymbol{r}_*) \right] \\
&= \gamma (\boldsymbol{r}_*^T \boldsymbol{z}_v) \|\boldsymbol{z}_v \times \boldsymbol{r}_*\|^2
\end{aligned} \tag{5.42}$$

From the last equation in Eq. (5.42), two properties should be noted here. The first is that when the $\boldsymbol{z}_v(t)$ is orthogonal to $\boldsymbol{r}_*$, then $\boldsymbol{z}_v(t)$ will evolve restricted on the plane whose normal vector is aligned with $\boldsymbol{r}_*$. This implies that $\boldsymbol{z}_v(t) \to 0$ as $t \to \infty$ on the plane defined by the $\boldsymbol{r}_*$ vector whenever $\hat{\boldsymbol{q}}(0) \notin \Psi_u$, i.e., $z_o(0) \neq 0$ due to the fact that $\lim_{t\to\infty}[\boldsymbol{z}_v(t) \times \boldsymbol{r}_*] = 0$ as provided by Corollary 2. The other result of Eq. (5.42) is that any non-zero component of $\boldsymbol{z}_v(t)$ along $\boldsymbol{r}_*$ has the same sign as that of the component of $\dot{\boldsymbol{z}}_v(t)$ along $\boldsymbol{r}_*$. Thus, the absolute value of $\boldsymbol{r}_*^T \boldsymbol{z}_v(t)$ increases monotonically toward 1 so that $\boldsymbol{z}_v(t)$ never converges to zero. We may visualize the foregoing analysis using an unit sphere in 3-dimensions. Then, $\boldsymbol{z}_v(t)$ evolves on or inside the unit sphere whose poles are intersection between $\boldsymbol{r}_*$ and the unit sphere. Note that the equatorial plane is normal to $\boldsymbol{r}_*$. Depending on $\boldsymbol{z}_v(0)$ and corresponding $\boldsymbol{z}_o(0)$, we have the following convergence conditions:

(a) If $\boldsymbol{z}_v(0)$ is on the equator (i.e., $z_o(0) = 0$), and $\boldsymbol{z}_v(0)^T \boldsymbol{r}_* = 0$, then $\boldsymbol{z}_v(t)$ will

remain on the equator.

(b) If $\boldsymbol{z}_v(0)$ is on the equatorial plane but not on the equator (i.e., $z_o(0) \neq 0$), and $\boldsymbol{z}_v(0)^T \boldsymbol{r}_* = 0$, $\boldsymbol{z}_v(t)$ asymptotically converges to zero (the center of the sphere). Accordingly, the attitude estimation matrix $\tilde{C}(t)$ also converges to zero.

(c) If $\boldsymbol{z}_v(0)$ is inside the sphere but not on the equatorial plane, then $\boldsymbol{z}_v(t)$ will converge to a point on the axis towards the closest pole.

(d) If $\boldsymbol{z}_v(0)$ is on the surface of sphere but not on the equator, then $\boldsymbol{z}_v(t)$ will converge to one of closet poles. More precisely, if $\boldsymbol{z}_v(0)$ is in the Northern hemisphere, then $\boldsymbol{z}_v(t)$ converges to the North pole. Likewise for $\boldsymbol{z}_v(0)$ in the Southern hemisphere, $\boldsymbol{z}_v(t)$ converges to the South pole.

5.6 Numerical Simulations

This section supports the theoretical results developed so far by presenting numerical simulation results of the proposed attitude estimation algorithm. We focus on the 3-dimensional example from the simplified problem of estimating the attitude of a satellite stationed in a geosynchronous orbit. The reference input signal $\boldsymbol{r}(t)$, and angular velocity of the satellite $\boldsymbol{\omega}$ expressed in body frame are taken as follows

$$\boldsymbol{r}(t) = [\sin t, \cos t, 0]^T, \quad \boldsymbol{\omega} = [0, 0, 1]^T. \tag{5.43}$$

For our simulations, the true/unknown attitude matrix $C(0)$ is fixed and parameterized by the quaternion $\boldsymbol{q}(0) = [0.5, 0.5, 0.5, 0.5]^T$ based on Eq. (5.29).

Three cases are considered for simulations. For the first case, $\hat{\boldsymbol{q}}(0)$ parame-

terizing the initial estimate of the attitude matrix $\hat{C}(0)$ is selected to be

$$\hat{\boldsymbol{q}}(0) = [\sqrt{0.9}, \sqrt{0.1/3}, \sqrt{0.1/3}, \sqrt{0.1/3}]^T \tag{5.44}$$

It is clear that $\hat{\boldsymbol{q}}(0) \notin \Psi_u$ and therefore, $z_o(0) \neq 0$. Given that the reference input $\boldsymbol{r}(t)$ satisfies $\dot{\boldsymbol{r}}(t) \neq 0$ and by the consequence of Corollary 2, we know that the attitude estimation error $\tilde{C}(t)$ asymptotically converges to zero. This is shown in Fig. 5.3 where $\lim_{t\to\infty} \boldsymbol{z}_v(t) = \lim_{t\to\infty}[z_1(t), z_2(t), z_3(t)] = 0$ as expected.

A second case we consider is that the initial estimate $\hat{\boldsymbol{q}}(0)$ starts from $\hat{\boldsymbol{q}}(0) = [0.5\sqrt{2}, 0, -0.5\sqrt{2}, 0]^T \in \Psi_u$. Since $z_o(0) = \boldsymbol{q}^T(0)\hat{\boldsymbol{q}}(0) = 0$, we expect $\{z_o(t) = 0, \|\boldsymbol{z}_v(t)\| = 1\}$ for all $t > 0$ according to Corollary 2. However, from the fact that $z_o = 0$ is an unstable equilibrium manifold, we see in Fig. 5.4 that $\boldsymbol{z}_v(t)$ converges to zero after about 40 seconds of simulation time.

Finally, the robustness of the proposed attitude estimator to the measurement noise is considered. The measurement noise is modeled as a uniformly distributed random variable $\boldsymbol{v}(t) \in [-0.5,\ 0.5]$ at each time t. In this simulation, $\hat{\boldsymbol{q}}(0)$ is taken from Eq. (5.44). Simulation results are shown Fig. 5.5. As discussed before, $\boldsymbol{z}_v(t)$ no longer converges to zero because of the introduced measurement error $\boldsymbol{v}(t)$. However, we may recognize that each component of $\boldsymbol{z}_v(t)$ remains bounded so that the magnitude of $\|\boldsymbol{z}_v(t)\|$ is dictated by the magnitude of the measurement noise.

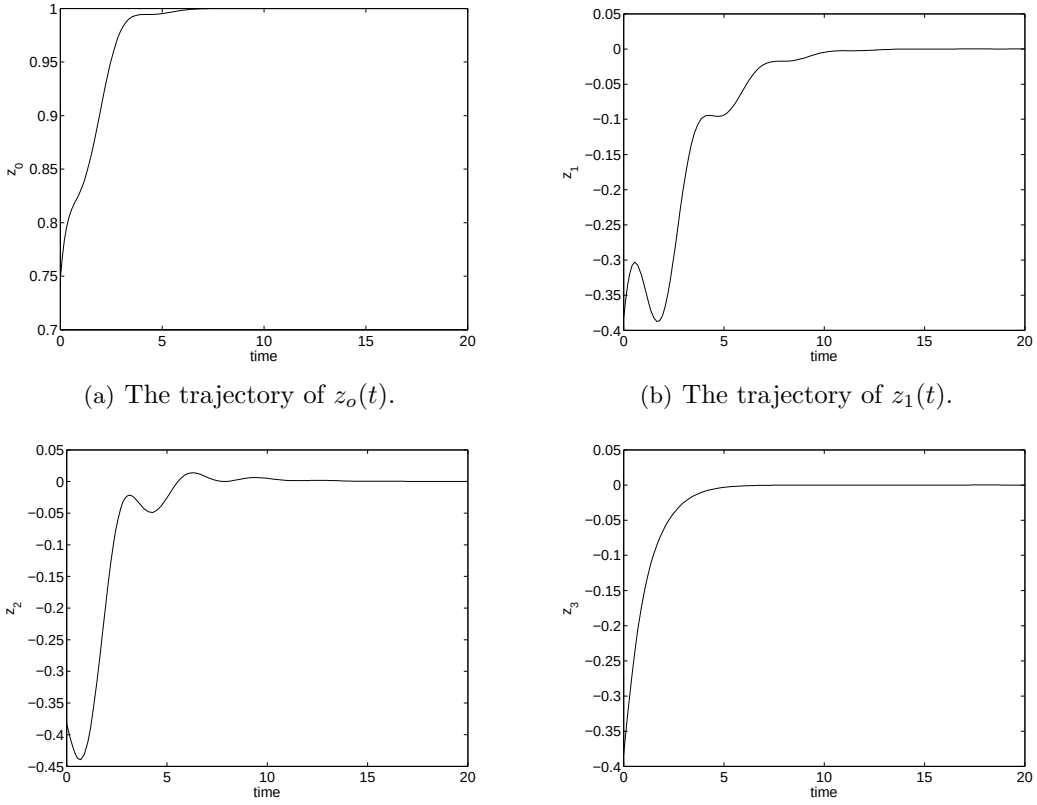

(a) The trajectory of $z_o(t)$.

(b) The trajectory of $z_1(t)$.

(c) The trajectory of $z_2(t)$.

(d) The trajectory of $z_3(t)$.

Figure 5.3: The trajectory of the error quaternion $\boldsymbol{z}(t)$ as a function of time t. The initial condition $\hat{\boldsymbol{q}}(0) \notin \Psi_u$ so that $z_o(0) \neq 0$.

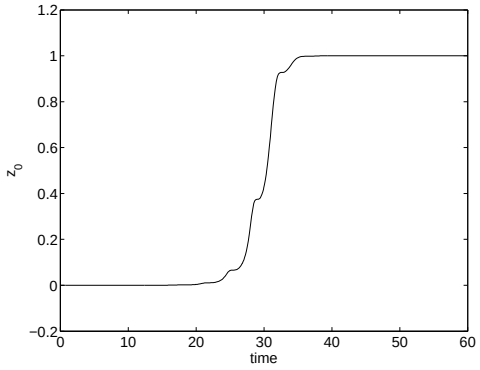

(a) The trajectory of $z_o(t)$.

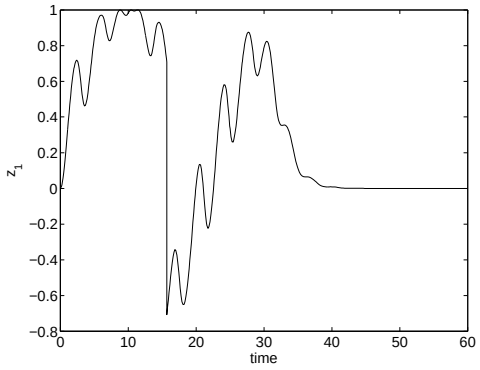

(b) The trajectory of $z_1(t)$.

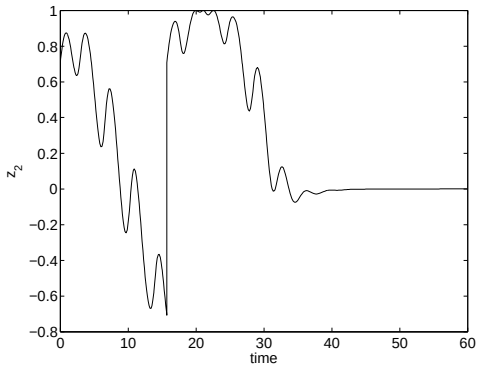

(c) The trajectory of $z_2(t)$.

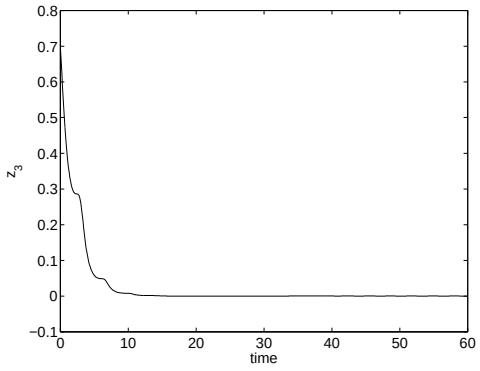

(d) The trajectory of $z_3(t)$.

Figure 5.4: The trajectory of the error quaternion $\boldsymbol{z}(t)$ as a function of time t. The initial condition $\hat{\boldsymbol{q}}(0) \in \Psi_u$ (the unstable equilibrium manifold) so that $z_o(0) = 0$. Accumulation of numerical round-off errors ultimately results in regulation of the attitude estimation error to zero.

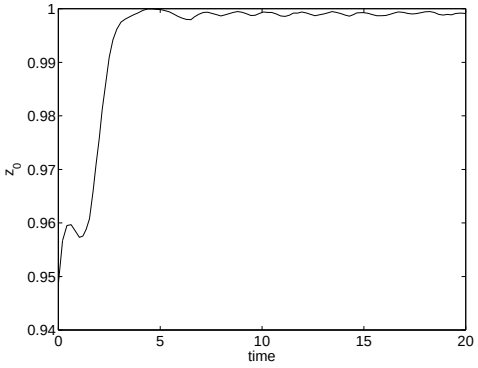

(a) The trajectory of $z_o(t)$.

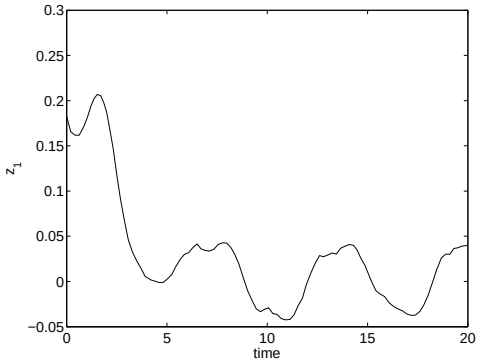

(b) The trajectory of $z_1(t)$.

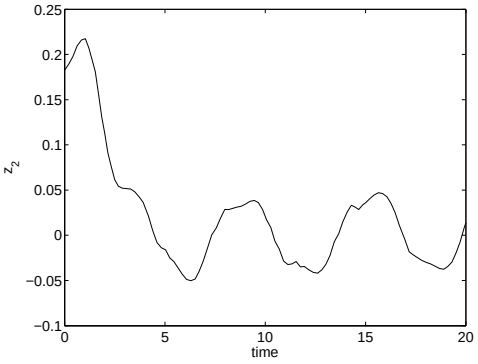

(c) The trajectory of $z_2(t)$.

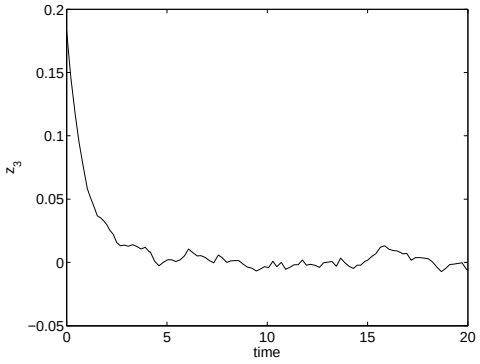

(d) The trajectory of $z_3(t)$.

Figure 5.5: The trajectory of the error quaternion $\boldsymbol{z}(t)$ as a function of time t. The initial condition $\hat{\boldsymbol{q}}(0) \notin \Psi_u$ Measurement noise is introduced as a signal having an uniform distribution between -0.05 and 0.05.

Chapter 6

Separation Property for the Rigid-Body Attitude Tracking Control Problem

Through the preceding chapters, we present a new control method and its applications including conventional robot-arm and attitude control systems. For the attitude control application, we develop a new attitude estimator based on the attracting manifold principle. In order for the proposed attitude control method to be implemented in real world, the stability of observer-based controller should be proved rigorously because it is inevitable to estimate current attitude information from sensor measurements. Although the separation principle provides the necessary foundation for linear observer-based control systems, there is no such principle for nonlinear systems due to the asymptotic convergence of estimates (generated by observer) to the true states. In this chapter, we propose the separation-like property for the proposed control scheme together with the state observer specialized to the attitude control problems.

6.1 Introduction

Proportional-derivative (PD) type attitude control systems for rigid spacecraft, i.e., rigid body rotational dynamics modeled by Euler's equations together with a suitable attitude parameterization, have been extensively studied during the past decades[32, 35–38, 40, 63–65]. More specifically, if the spacecraft is endowed with three independent torque actuators, then a complete (global) solution is available for both set-point and trajectory tracking control problems assuming availability of the full state vector comprising of the body angular rates and the globally valid (non-singular) quaternion vector. It is a well documented fact that the set of special group of rotation matrices that describe body orientation in three dimensions $SO(3)$ is not a contractable space and hence quaternion based formulations do not permit globally continuous stabilizing controllers[32, 33]. In this sense, we adopt the standard terminology/notion of (almost) global stability for this problem to imply stability over an open and dense set in $SO(3)$ as is usually seen in literature dealing with this problem[40].

When it comes to implementation of the PD type controllers, virtually all existing attitude control designs assume direct availability of the attitude (quaternion) vector for feedback implementations. However, the practical reality is that there exists no physical sensor that permits direct and exact measurement of the quaternion vector or any other representation of the body attitude. Motivated by this important practical consideration, there indeed exists a separate thread of research that bears several rich results addressing the development of attitude estimators (observers) formulated in terms of various attitude parameterizations[42]. These estimators are driven by measurements from rate-gyros, sun sensors, star sensors, earth sensors, magnetometers, and a host of other sensor candidates – essentially depending upon the particular application[44, 46, 47, 51, 66, 67], and their convergence proofs provide at best asymptotic (non-exponential) convergence to the true (actual) body

attitude.

Given that the governing dynamics are nonlinear and time-varying, any closed-loop stability result obtained from the PD type controller assuming exact measurement of the quaternion vector needs to be re-established all over again once the estimated quaternion is adopted. Therefore, a question of great theoretical and practical importance arises as to what can be said about closed-loop stability when the PD control implementation is modified so that the feedback uses attitude estimates generated by observers instead of the actual (true) attitude variables. Since the separation property[68] doesn't hold in general for nonlinear systems, this remains an open problem to our best knowledge for which no satisfactory solution currently exists. A key technical difficulty on this front is the fact that the closed-loop stability for the control problem is established through energy-type Lyapunov-like functions that aren't strict[32], i.e., their derivatives are only negative semi-definite involving only angular rate related terms. In such a setting, technical arguments involving LaSalle invariance (for stabilization or set-point regulation) and/or Barbalat's lemma (for trajectory tracking) are the common recourse for completing the closed-loop stability analysis. Not surprisingly, due to the non-strict nature of the Lyapunov-like functions in the full-state feedback control analysis, one encounters the formidable uniform detectibility obstacle[69] whenever PD based control designs are sought to be combined with attitude (quaternion) estimators.

In this chapter, we propose a novel methodology for design of a strict Lyapunov-like function in terms of the quaternion parameterization of the attitude such that the PD-type feedback controller ensures almost global closed-loop stability. Further, by making use of the proposed strict Lyapunov-like function construction, and thereby avoiding the detectability obstacle, we present a rigorous stability analysis for the PD based controller when it is combined with a suitable attitude quaternion observer (estimator).

The fundamental contribution is that if the reference signal for the attitude estimator possesses an easily verifiable persistence of excitation condition and the initial condition of the quaternion estimator $\hat{\boldsymbol{q}}(0)$ doesn't lie inside a hyperplane normal to the initial condition of the actual/true attitude quaternion $\boldsymbol{q}(0)$, i.e., $\hat{\boldsymbol{q}}^T(0)\boldsymbol{q}(0) \neq 0$, then we prove global stability and asymptotic convergence for the attitude tracking error with respect to any commanded attitude reference trajectory. Our results essentially imply that separate designs of the full-state feedback controller and the attitude estimator may be readily combined to ensure overall closed-loop stability. To our best knowledge, this is the first ever demonstration of separation property in the setting of the rigid-body attitude tracking control problem.

This chapter is organized as follows. In the following section, we develop a new full-state feedback controller derived through a strict Lyapunov function candidate and then prove the asymptotic stability of the closed-loop error dynamics. In section 6.3, we develop a new attitude observer since the true attitude values are assumed unavailable to the controller. The estimation error dynamics are derived based on the quaternion observer states. Section 4 presents the main results of this chapter for the combined estimator-controller closed-loop attitude tracking system. In section 5, numerical simulations are presented to describe the performance of the proposed theoretical results. We complete the chapter in section 6 with appropriate concluding statements.

6.2 Full-state Feedback Control with True Attitude Values

First, we develop a full-state feedback controller for the attitude tracking control system based on the true attitude values. The proposed control method provides

a strict Lyapunov candidate function in terms of the filtered angular velocity and the attitude values explicitly for all initial values (singularity[38] depending on the initial condition is removed). The introduced angular velocity filter is a simple low-pass filter and used only for the stability analysis, i.e., the implementation of the proposed control scheme does not depend on the angular velocity filter states. It will be clear in the later part of this section. To represent the attitude of the system, quaternion is adopted for nonsingular representation through all possible rotation angles[42]. To be consistent with Chapter 4, we denote the true attitude of the system as $\boldsymbol{q}$. Each quaternion vector obviously has four parameters where the first element, the scalar part of the quaternion, is represented by the subscript 'o' and the rest of them make up the vector part of the quaternion which is represented by the subscript '$\boldsymbol{v}$' with a bold face character, i.e., $\boldsymbol{q} = [q_o, \boldsymbol{q_v}]^T$. We also specify $\boldsymbol{q}_r$ to denote the reference attitude trajectory in terms of the quaternion parameterization.

The direction cosine matrix $C(\cdot)$ is considered as a mapping from the unit quaternion space, $\mathbb{R}^4$, to the proper orthogonal matrix space, $SO(3)$ as before (i.e., $C^TC = CC^T = I_{3\times 3}$, and $\det[C(\cdot)] = 1$). In the following development, three frames ($\mathcal{F}_N$, $\mathcal{F}_B$, and $\mathcal{F}_R$) are used to denote the relative attitude representation associated with $C(\cdot)$ as given in Eq. (4.13). Corresponding error quaternion between the body fixed frame $\mathcal{F}_B$ and the reference frame $\mathcal{F}_R$ is written again for the convenience as follows

$$C(\delta\boldsymbol{q}) = C(\boldsymbol{q})C^T(\boldsymbol{q}_r) \tag{6.1}$$

which is the same definition of multiplicative quaternion attitude error $\delta\boldsymbol{q}$ as Eq. (4.7).

In the sequel, for the sake of notational simplicity, the time argument 't' is left out except at places where it is noted for emphasis. Each following definition is already given and can be found in Chapter 4. We write them here for the reference only.

The kinematic evolution equation for quaternion $\boldsymbol{q}$ is expressed as

$$\dot{\boldsymbol{q}} = \frac{1}{2} E(\boldsymbol{q})\boldsymbol{\omega} \tag{6.2}$$

where $\boldsymbol{\omega}$ is the angular velocity with respect to the body fixed frame $\boldsymbol{B}$ and the quaternion operator $E(\cdot) : \mathcal{R}^4 \rightarrow \mathcal{R}^{4\times 3}$ is defined by

$$E(\boldsymbol{q}) = \begin{bmatrix} -\boldsymbol{q}_{\boldsymbol{v}}^T \\ q_o I_{3\times 3} + S(\boldsymbol{q}_{\boldsymbol{v}}) \end{bmatrix} \tag{6.3}$$

Here, the matrix operator $S(\cdot)$ denotes the skew-symmetric matrix that is equivalent to the vector cross product operation as follows [34]

$$S(\boldsymbol{a})\boldsymbol{b} = \boldsymbol{a} \times \boldsymbol{b} \quad \forall \boldsymbol{a}, \boldsymbol{b} \in \mathbb{R}^3. \tag{6.4}$$

The time evolution of the body angular velocity is described by the well known Euler differential equation for rotational motion and is given by

$$J\dot{\boldsymbol{\omega}} = -S(\boldsymbol{\omega})J\boldsymbol{\omega} + \boldsymbol{u} \tag{6.5}$$

where J is the 3×3 symmetric positive definite inertia matrix and $\boldsymbol{u}$ is the control torque vector.

In terms of the direction cosine matrix $C(\cdot)$, the analogous matrix version of Eq. (6.2) can be derived as follows[34]

$$\frac{d}{dt} C(\boldsymbol{q}) = -S(\boldsymbol{\omega})C(\boldsymbol{q}) \tag{6.6}$$

which of course is the well known Poisson differential equation. The true angular

velocity error $\delta\boldsymbol{\omega}$ is defined through

$$\delta\boldsymbol{\omega} = \boldsymbol{\omega} - C(\delta\boldsymbol{q})\boldsymbol{\omega}_r \tag{6.7}$$

where $\boldsymbol{\omega}_r(t)$ represents the bounded reference angular velocity with bounded time derivatives and is prescribed with respect to the reference frame $\boldsymbol{R}$.

In order to derive the governing dynamics for the attitude error $C(\delta\boldsymbol{q})$, the following steps are taken starting from Eq. (6.1)

$$\begin{aligned}
\frac{d}{dt}C(\delta\boldsymbol{q}) &= -S(\boldsymbol{\omega})C(\boldsymbol{q})C^T(\boldsymbol{q}_r) + C(\boldsymbol{q})C^T(\boldsymbol{q}_r)S(\boldsymbol{\omega}_r) \\
&= -S(\boldsymbol{\omega})C(\delta\boldsymbol{q}) + C(\delta\boldsymbol{q})S(\boldsymbol{\omega}_r) \\
&= -S(\boldsymbol{\omega})C(\delta\boldsymbol{q}) + S(C(\delta\boldsymbol{q})\boldsymbol{\omega}_r)C(\delta\boldsymbol{q}) \\
&= -S(\boldsymbol{\omega} - C(\delta\boldsymbol{q})\boldsymbol{\omega}_r)C(\delta\boldsymbol{q}) \\
&= -S(\delta\boldsymbol{\omega})C(\delta\boldsymbol{q})
\end{aligned} \tag{6.8}$$

Detailed derivation of the preceding relationship is given in Eq. (4.9) The attitude matrix version of the tracking error kinematics are represented by Eq. (6.8). Differentiating Eq. (6.7) along Eq. (6.8) and Eq. (6.5) provides the the angular rate tracking error dynamics for the rigid-body rotational motion. Consequently the overall attitude tracking error dynamics and kinematics (expressed in terms of the quaternion attitude tracking error $\delta\boldsymbol{q}$) are as follows[34]

$$\delta\dot{\boldsymbol{q}} = \frac{1}{2}E(\delta\boldsymbol{q})\delta\boldsymbol{\omega} \tag{6.9}$$

$$J\delta\dot{\boldsymbol{\omega}} = -S(\boldsymbol{\omega})J\boldsymbol{\omega} + \boldsymbol{u} + J\bar{\boldsymbol{\eta}} \tag{6.10}$$

wherein the quantity $\bar{\boldsymbol{\eta}}$ is defined for notational convenience to represent the following

$$\bar{\boldsymbol{\eta}} = S(\delta\boldsymbol{\omega})C(\delta\boldsymbol{q})\boldsymbol{\omega}_r - C(\delta\boldsymbol{q})\dot{\boldsymbol{\omega}}_r \tag{6.11}$$

We note here that regulation of $\lim_{t\to\infty}[\delta\boldsymbol{q_v}(t), \delta\boldsymbol{\omega}(t)] = 0$ obviously also goes on to achieve our desired attitude tracking control objective.

We now present the following proposition.

Proposition 1 (Full-state Feedback)**.** *For the attitude tracking system given by Eq. (6.9), Eq. (6.10), and Eq. (6.11), consider the control torque* $\boldsymbol{u}$ *to be computed as follows*

$$\boldsymbol{u} = -k_v J\delta\boldsymbol{\omega} + S(\boldsymbol{\omega})J\boldsymbol{\omega} - J\bar{\boldsymbol{\eta}} - k_p J\left[\alpha\delta\boldsymbol{q_v} + \frac{1}{2}\left(\delta q_o I_{3\times 3} + S(\delta\boldsymbol{q_v})\right)\delta\boldsymbol{\omega}\right] \tag{6.12}$$

where $k_p > 0$, $k_v > 0$, $\alpha = k_p + k_v$. *Then, all closed-loop signals remain bounded and the attitude tracking control objective,* $\lim_{t\to\infty}[\delta\boldsymbol{q_v}(t), \delta\boldsymbol{\omega}(t)] = 0$, *is achieved globally (for all possible initial conditions) and asymptotically.*

Proof. For the sake of analysis, we introduce an angular velocity filter state $\boldsymbol{\omega}_f$ governed through the stable linear differential equation

$$\dot{\boldsymbol{\omega}}_f = -\alpha\boldsymbol{\omega}_f + \delta\boldsymbol{\omega}, \quad \text{any } \boldsymbol{\omega}_f(0) \in \mathcal{R}^3 \tag{6.13}$$

Differentiating both sides of the filter dynamics in Eq. (6.13) followed by substitution of the angular velocity error dynamics Eq. (6.10) along with Eq. (6.12), we have

$$\frac{d}{dt}\left[\dot{\boldsymbol{\omega}}_f + k_v\boldsymbol{\omega}_f + k_p\delta\boldsymbol{q_v}\right] = -\alpha\left[\dot{\boldsymbol{\omega}}_f + k_v\boldsymbol{\omega}_f + k_p\delta\boldsymbol{q_v}\right] \tag{6.14}$$

which obviously has the following analytical solution

$$\dot{\boldsymbol{\omega}}_f = -k_v\boldsymbol{\omega}_f - k_p\delta\boldsymbol{q_v} + \boldsymbol{\varepsilon}e^{-\alpha t} \tag{6.15}$$

where the exponentially decaying term $\mathbf{w}(t) \doteq \boldsymbol{\varepsilon}e^{-\alpha t}$ on the right hand side of the

preceding equation is characterized by

$$\dot{\mathbf{w}} = -\alpha \mathbf{w}; \quad \mathbf{w}(0) = \boldsymbol{\varepsilon} = \{\dot{\boldsymbol{\omega}}_f(0) + k_v \boldsymbol{\omega}_f(0) + k_p \delta \boldsymbol{q_v}(0)\} \tag{6.16}$$

Next, consider the following lower bounded Lyapunov-like candidate function V_t given by

$$V_t = \frac{1}{2}\boldsymbol{\omega}_f^T \boldsymbol{\omega}_f + [(\delta q_o - 1)^2 + \delta \boldsymbol{q_v}^T \delta \boldsymbol{q_v}] + \frac{\lambda}{2}\mathbf{w}^T\mathbf{w}; \quad \lambda > \max\left(\frac{1}{k_p^2}, \frac{1}{k_v^2}\right) \tag{6.17}$$

By taking the time derivative of V_t along trajectories generated by Eq. (6.9), Eq. (6.15), and Eq. (6.16), we have the following

$$\begin{aligned}
\dot{V}_t &= \boldsymbol{\omega}_f^T(-k_v\boldsymbol{\omega}_f - k_p\delta\boldsymbol{q_v} + \mathbf{w}) + \delta\boldsymbol{q_v}^T\delta\boldsymbol{\omega} - \lambda\alpha\mathbf{w}^T\mathbf{w} \\
&= -k_v\|\boldsymbol{\omega}_f\|^2 - k_p\boldsymbol{\omega}_f^T\delta\boldsymbol{q_v} + \boldsymbol{\omega}_f^T\mathbf{w} + \delta\boldsymbol{q_v}^T(\dot{\boldsymbol{\omega}}_f + \alpha\boldsymbol{\omega}_f) - \lambda\alpha\mathbf{w}^T\mathbf{w} \\
&= -k_v\|\boldsymbol{\omega}_f\|^2 - k_p\boldsymbol{\omega}_f^T\delta\boldsymbol{q_v} + \boldsymbol{\omega}_f^T\mathbf{w} + \delta\boldsymbol{q_v}^T(-k_v\boldsymbol{\omega}_f - k_p\delta\boldsymbol{q_v} + \mathbf{w} + \alpha\boldsymbol{\omega}_f) - \lambda\alpha\mathbf{w}^T\mathbf{w} \\
&= -k_v\|\boldsymbol{\omega}_f\|^2 - k_p\|\delta\boldsymbol{q_v}\|^2 - \lambda\alpha\|\mathbf{w}\|^2 + \boldsymbol{\omega}_f^T\mathbf{w} + \delta\boldsymbol{q_v}^T\mathbf{w} \\
&\leq -\frac{k_v}{2}\|\boldsymbol{\omega}_f\|^2 - \frac{k_p}{2}\|\delta\boldsymbol{q_v}\|^2 - \frac{\lambda\alpha}{2}\|\mathbf{w}\|^2 - \frac{k_v}{2}\|\boldsymbol{\omega}_f - \frac{1}{k_v}\mathbf{w}\|^2 - \frac{k_p}{2}\|\delta\boldsymbol{q_v} - \frac{1}{k_p}\mathbf{w}\|^2 \\
&\leq -\frac{k_v}{2}\|\boldsymbol{\omega}_f\|^2 - \frac{k_p}{2}\|\delta\boldsymbol{q_v}\|^2 - \frac{\lambda\alpha}{2}\|\mathbf{w}\|^2 \leq 0
\end{aligned} \tag{6.18}$$

which is negative semidefinite and thus, the Lyapunov candidate function V_t is *strict*[69] due to presence of non-positive terms of $\boldsymbol{\omega}_f$ and $\delta\boldsymbol{q_v}$ in $\dot{V}_t$. Moreover, since V_t is lower bounded and monotonic, the integral $\int_0^\infty \dot{V}_t(s)ds$ exists and is finite, which implies $\boldsymbol{\omega}_f, \delta\boldsymbol{q_v} \in \mathcal{L}_2 \cap \mathcal{L}_\infty$. This also implies boundedness of $\dot{\boldsymbol{\omega}}_f, \ddot{\boldsymbol{\omega}}_f$, and $\delta\dot{\boldsymbol{q}}_{\boldsymbol{v}}$ from Eq. (6.9) and Eq. (6.15). Therefore, using Barbalat's lemma, we can guarantee $\lim_{t\to\infty}[\boldsymbol{\omega}_f(t), \delta\boldsymbol{q_v}(t)] = 0$. Finally, from the stable linear filter Eq. (6.13), it follows that $\lim_{t\to\infty}\delta\boldsymbol{\omega}(t) = 0$ thereby completing the proof. □

It needs to be emphasized that the filter dynamics from Eq. (6.13) are re-

quired only for analysis as part of the stability proof. This observation is highlighted by the fact that the control law given in Eq. (6.12) is independent of the filter variables $\boldsymbol{\omega}_f$ which therefore need not be computed in the actual controller implementation. Additionally, it is also always possible to introduce the filter states such that $\mathbf{w}(t) = 0$ for all $t \geq 0$ by letting $\mathbf{w}(0) = 0$ based on the proper choice of initial filter states such that $\boldsymbol{\omega}_f(0) = (\delta\boldsymbol{\omega}(0) + k_p\delta\boldsymbol{q_v}(0))/k_p$ as can be seen in Eq. (6.16). Even otherwise, if the filter initial conditions are such that $\mathbf{w}(0) \neq 0$, it is obvious from our demonstration thus far that the exponentially decaying signal $\mathbf{w}(t)$ present in Eq. (6.15) can be neglected without any loss because it plays no role whatsoever on the stability analysis[10, 11]. Accordingly, the exponentially decaying term $\mathbf{w}(t)$ is eliminated hereon from filtered angular velocity error dynamics in Eq. (6.15) to provide

$$\dot{\boldsymbol{\omega}}_f = -k_v\boldsymbol{\omega}_f - k_p\delta\boldsymbol{q_v}. \tag{6.19}$$

and analogously, the term $\mathbf{w}^T\mathbf{w}/2$ from the Lyapunov-like candidate function in Eq. (6.17) may be dropped to simplify the stability analysis with no impact whatsoever on the overall asymptotic convergence results assured by the proposed controller.

In contrast to most conventional PD-type quaternion based formulations for rigid-body attitude control wherein Lyapunov candidate functions are at best negative semi-definite involving only the angular rate error terms, the proposed control method succeeds in introducing an additional negative definite term $-k_p\|\delta\boldsymbol{q_v}\|^2$ in Eq. (6.18) which makes V_t a strict Lyapunov function[69]. The importance of the extra negative definite term consisting of the quaternion tracking error is discussed in the sequel.

6.3 Attitude Observer Design

In many practical applications, full-state feedback attitude control is not readily applicable due to the fact that the true attitude quaternion measurement is typically not available to the controller for feedback purposes. Thus, feedback control signals are sought to be based on the estimated attitude quaternion values that are obtained from the observer (attitude estimator) which in turn is driven by the measured (output) signals. In this section, first we provide a brief presentation of a very recent stability and convergence proof for an attitude estimator[67] and subsequently introduce certain new Lyapunov-like function constructions in the context of the attitude observer convergence analysis that ultimately enable establishment of the nonlinear separation property.

We assume the measurement model and its estimator to be specified in the following fashion

$$\boldsymbol{y}(t) = C(\boldsymbol{q}(t))\boldsymbol{x}(t) \tag{6.20}$$

$$\hat{\boldsymbol{y}}(t) = C(\hat{\boldsymbol{q}}(t))\boldsymbol{x}(t) \tag{6.21}$$

where the output signal $\boldsymbol{y}$ indicating the true attitude measurements and the estimated measurements $\hat{\boldsymbol{y}}$ in the body fixed frame. The reference signal $\boldsymbol{x}$ is the unit vector governing the inertial direction of the observation and $\dot{\boldsymbol{x}}$ is assumed to be bounded with time. We replace $\boldsymbol{r}(t)$ with $\boldsymbol{x}(t)$ to avoid the confusion between the attitude reference trajectory and the observation reference signal in Chapter 5. From a practical standpoint, in three-dimensions, the measurement model Eq. (6.20) is typical for single input-output type unit vector measurement sensors such as star trackers, sun sensors and magnetometers[70]. More specific examples of sensor modeling in attitude determination problems can be found in the literatures[58–61]. Discrete-time analogues of the attitude estimation problem routinely arise within

the field of spacecraft attitude determination. In such cases, Eq. (6.20) can be interpreted as that $\boldsymbol{x}$ is the star catalog value with respect to the inertial frame and $\boldsymbol{y}$ is the corresponding star tracker measurement. Vector quantities $\hat{\boldsymbol{y}}$ and $\hat{\boldsymbol{q}}$ are the interpreted to be estimates of $\boldsymbol{y}$ and $\boldsymbol{q}$ respectively. Obviously, both $\boldsymbol{y}$ and $\hat{\boldsymbol{y}}$ are unit vectors in this model.

In the following proposition, we briefly review the convergence result of an adaptive attitude estimator recently introduced in Akella, *et al*[67].

Proposition 2 (Attitude Observer)**.** *If the attitude quaternion estimate $\hat{\boldsymbol{q}}(t)$ is updated through*

$$\dot{\hat{\boldsymbol{q}}} = \frac{1}{2}E(\hat{\boldsymbol{q}})(\boldsymbol{\omega} + \gamma \boldsymbol{y} \times \hat{\boldsymbol{y}}); \quad \gamma > 0 \tag{6.22}$$

subject to the condition that $\hat{\boldsymbol{q}}(0) \in \Psi_s$ where

$$\Psi_s = \left\{ \boldsymbol{\eta} \in \mathbb{R}^4 : \|\boldsymbol{\eta}\| = 1; \boldsymbol{\eta}^T \boldsymbol{q}(0) \neq 0 \right\} \tag{6.23}$$

then, for all unit-vector reference signals $\boldsymbol{x}(t) \in \mathbb{R}^3$ that are not constant with time with bounded derivatives, the following asymptotic convergence condition holds

$$\lim_{t \to \infty} C(\hat{\boldsymbol{q}}(t)) - C(\boldsymbol{q}(t)) = 0 \tag{6.24}$$

which essentially accomplishes the attitude estimation objective.

Proof. We define a new quaternion error $\boldsymbol{z}(t) = [z_o(t), \boldsymbol{z_v}(t)]^T$ to parameterize $C(\boldsymbol{z}(t)) \doteq C^T(\boldsymbol{q}(t))C(\hat{\boldsymbol{q}}(t))$ which has the following identity[34]

$$C^T(\boldsymbol{q}(t))C(\hat{\boldsymbol{q}}(t)) = I_{3\times 3} - 2z_o(t)S(\boldsymbol{z_v}(t)) + 2S^2(\boldsymbol{z_v}(t)), \tag{6.25}$$

It is obvious from Eq. (6.25) that $\boldsymbol{z_v} \to 0$ ($z_o \to \pm 1$) implies $C(\hat{\boldsymbol{q}}) \to C(\boldsymbol{q})$. Now, we derive dynamics of $\boldsymbol{z_v}$ by following similar steps described in Eq. (6.8). Differentiating $C^T(\boldsymbol{q})C(\hat{\boldsymbol{q}})$ with respect to time along with Eq. (6.6) and Eq. (6.22) leads

to[67]

$$\frac{d}{dt}C(\boldsymbol{z}) = -S\left(\gamma C^T(\boldsymbol{q})(\boldsymbol{y}\times\hat{\boldsymbol{y}})\right)C(\boldsymbol{z}) \tag{6.26}$$

Thus, we have the corresponding quaternion dynamics for $\boldsymbol{z}$ given by

$$\dot{\boldsymbol{z}} = \frac{\gamma}{2}E(\boldsymbol{z})C^T(\boldsymbol{q})(\boldsymbol{y}\times\hat{\boldsymbol{y}}) \tag{6.27}$$

Further, from Eq. (6.20), Eq. (6.21) and Eq. (6.25) the following algebraic identity may be established

$$\boldsymbol{y}\times\hat{\boldsymbol{y}} = C(\boldsymbol{q})\left[2z_o(\boldsymbol{z_v}\times\boldsymbol{x})\times\boldsymbol{x} - 2(\boldsymbol{x}^T\boldsymbol{z_v})(\boldsymbol{z_v}\times\boldsymbol{x})\right] \tag{6.28}$$

and thus, we can express Eq. (6.27) as follows

$$\dot{z}_o = \gamma z_o\|\boldsymbol{z_v}\times\boldsymbol{x}\|^2; \quad \dot{\boldsymbol{z}}_{\boldsymbol{v}} = \gamma\left[z_o^2(\boldsymbol{z_v}\times\boldsymbol{x})\times\boldsymbol{x} - (\boldsymbol{x}^T\boldsymbol{z})S(\boldsymbol{z_v})(\boldsymbol{z_v}\times\boldsymbol{x})\right] \tag{6.29}$$

Next, consider the following bounded (from above and below) Lyapunov-like candidate function

$$V_e = \frac{1}{2}\boldsymbol{z}_{\boldsymbol{v}}^T\boldsymbol{z_v} = \frac{1}{2}(1-z_o^2) \tag{6.30}$$

By taking the time derivative of V_e along the trajectory of $\boldsymbol{z_v}$ in Eq. (6.29), we obtain the following result

$$\begin{aligned}
\dot{V}_e(t) &= \boldsymbol{z}_{\boldsymbol{v}}^T\dot{\boldsymbol{z}}_{\boldsymbol{v}} \\
&= -\gamma\boldsymbol{z}_{\boldsymbol{v}}^T\left[z_o^2(\boldsymbol{z_v}\times\boldsymbol{x})\times\boldsymbol{x} - (\boldsymbol{x}^T\boldsymbol{z})S(\boldsymbol{z_v})(\boldsymbol{z_v}\times\boldsymbol{x})\right] \\
&= -\gamma z_o^2\boldsymbol{z}_{\boldsymbol{v}}^T\left[(\boldsymbol{z_v}\times\boldsymbol{x})\times\boldsymbol{x}\right] \\
&= -\gamma z_o^2\|\boldsymbol{z}_v\times\boldsymbol{x}\|^2 \quad \leq 0.
\end{aligned} \tag{6.31}$$

From $V_e \geq 0$ and $\dot{V}_e \leq 0$, $\lim_{t\to\infty}V_e(t) = V_{e_\infty}$ exists and is finite which leads to the fact that $\int_0^\infty \dot{V}_e(t)dt$ also exists and is finite. Further, from boundedness of

$\ddot{V}_e(t)$ (shown by differentiating Eq. (6.31)), $\dot{V}_e(t)$ is uniformly continuous. As a consequence, we have $\lim_{t\to\infty} \dot{V}_e(t) = 0$. From Eq. (6.29) and Eq. (6.31), we notice that $z_o = 0$ defines one of equilibrium manifolds (i.e., $z_o(0) = 0 \implies z_o(t) = 0$ for all $t \geq 0$). Since $z_o(t) = \hat{\boldsymbol{q}}^T(t)\boldsymbol{q}(t)$ for all $t \geq 0$ from Eq. (6.25)[34], $z_o(0) = 0$ is implied from $\hat{\boldsymbol{q}}(0) \notin \Psi_s$. In other words, if $\hat{\boldsymbol{q}}(0) \in \Psi_s$, then $z_o(0) \neq 0$ and from Eq. (6.29), it is immediately obvious that $z_o(t) \neq 0$ for all $t \geq 0$. In this case, $\lim_{t\to\infty} \dot{V}_e(t) = 0$ implies $\lim_{t\to\infty}[\boldsymbol{z}_v(t) \times \boldsymbol{x}(t)] = 0$. Again from Eq. (6.29), it means $\lim_{t\to\infty} \dot{\boldsymbol{z}}_{\boldsymbol{v}}(t) = 0$. Moreover, from uniform continuity of $[\boldsymbol{z}_v(t) \times \boldsymbol{x}(t)]$, we have

$$\lim_{t\to\infty}[\boldsymbol{z}_v(t) \times \boldsymbol{x}(t)] = 0 \Longrightarrow \lim_{t\to\infty} \frac{\mathrm{d}}{\mathrm{dt}}[\boldsymbol{z}_v(t) \times \boldsymbol{x}(t)] = 0 \tag{6.32}$$

which implies that $\lim_{t\to\infty}[\dot{\boldsymbol{z}}_v(t) \times \boldsymbol{x}(t) + \boldsymbol{z}_v(t) \times \dot{\boldsymbol{x}}(t)] = 0$ or $\lim_{t\to\infty}[\boldsymbol{z}_v(t) \times \dot{\boldsymbol{x}}(t)] = 0$. Thus, it is shown that $\boldsymbol{z}_v(t) \times \dot{\boldsymbol{x}}(t) \to 0$ and $\boldsymbol{z}_v(t) \times \boldsymbol{x}(t) \to 0$ as $t \to \infty$ simultaneously. This can be possible only if $\boldsymbol{z}_v(t) = 0$ since every unit vector $\boldsymbol{x}(t)$ satisfies $\boldsymbol{x}^T(t)\dot{\boldsymbol{x}}(t) = 0$ (i.e., vectors $\boldsymbol{x}(t)$ and $\dot{\boldsymbol{x}}(t)$ remain normal to one other for all t). This completes the proof with the fact that $\lim_{t\to\infty} \boldsymbol{z}_v(t) = 0$ is equivalent to $\lim_{t\to\infty} C^T(\boldsymbol{q}(t))C(\hat{\boldsymbol{q}}(t)) = I_{3\times 3}$ from Eq. (6.25).

□

In addition, the following important observations are in order.

1. The equilibrium manifold $z_o = 0$ that results whenever $\hat{\boldsymbol{q}}^T(0)\boldsymbol{q}(0) = 0$ happens can actually be shown to be unstable. From Eq. (6.30), V_e belongs to the closed interval $[0,\ 1/2]$ with $V_e = 0$ whenever $z_o = \pm 1$ and $V_e = 1/2$ whenever $z_o = 0$. If $z_o(0) \doteq \xi \neq 0$ (i.e., $V_e(0) < 1/2$) with arbitrary small ξ, then $|z_o(t)| \geq |\xi|$ for all $t > 0$ from Eq. (6.29) and thereby, it is impossible that $z_o(t) \to 0$ as $t \to \infty$. Consequently, equilibrium $z_o = 0$ defines an unstable manifold.

2. The convergence result of Proposition 2 can also be established by the following

new Lyapunov-like candidate function V_o defined as follows

$$V_o = \frac{\boldsymbol{z_v}^T \boldsymbol{z_v}}{2\gamma z_o^2}; \quad \gamma > 0 \tag{6.33}$$

which is well defined and a bounded function whenever $\hat{\boldsymbol{q}}(0) \in \Psi_s$ or in other words, $z_o(t) \neq 0$ for all $t \geq 0$. By differentiating V_o with respect to time along Eq. (6.29), we can show that

$$\begin{aligned} \dot{V}_o &= \frac{1}{\gamma z_o^4} \left(z_o^2 \boldsymbol{z_v}^T \dot{\boldsymbol{z}}_{\boldsymbol{v}} - z_o \dot{z}_o \boldsymbol{z_v}^T \boldsymbol{z_v} \right) \\ &= -|\boldsymbol{z_v} \times \boldsymbol{x}\|^2 - \frac{\|\boldsymbol{z_v} \times \boldsymbol{x}\|^2}{z_o^2} \boldsymbol{z_v}^T \boldsymbol{z_v} \\ &\leqslant -\|\boldsymbol{z_v} \times \boldsymbol{x}\|^2. \end{aligned} \tag{6.34}$$

We can follow the same steps described in the proof of Proposition 2 and thus, the asymptotic convergence $C(\hat{\boldsymbol{q}}) \to C(\boldsymbol{q})$ is again guaranteed.

3. The modification from V_e to V_o is a crucial development in the context of the results being sought in this chapter because this new construction for candidate function V_o helps in the production of the term $\|\boldsymbol{z_v} \times \boldsymbol{x}\|^2$ in $\dot{V}_o(t)$ as seen from Eq. (6.34) which is independent of z_o. Detailed derivations in to be presented in the sequel will further illustrate how this modification can help compensate for the closed-loop attitude tracking and estimation errors when the attitude estimator of Eq. (6.22) is adopted as part of a feedback control algorithm.

4. From Proposition 2, the group of initial conditions $\hat{\boldsymbol{q}}(0)$ corresponding to the condition $\hat{\boldsymbol{q}}(0)^T \boldsymbol{q}(0) = 0$ are categorized as an unstable initial condition (belonging to unstable manifold $z_o(t) = 0$ for all $t \geq 0$) for the attitude estimator. The effects of initializing the attitude estimator while satisfying the condition $\hat{\boldsymbol{q}}(0)^T \boldsymbol{q}(0) = 0$ will be demonstrated in numerical simulations section.

5. Having the unit-vector reference signal $\boldsymbol{x}(t)$ that drives the observer to be not constant with time is shown to be sufficient for ensuring that the attitude estimate matrix $C(\hat{\boldsymbol{q}})$ converges to the actual attitude matrix $C(\boldsymbol{q})$, of course whenever $\hat{\boldsymbol{q}}(0) \in \Psi_s$. In effect, this condition ensures satisfaction of "persistence of excitation" so far as the attitude observer design is concerned. More importantly, verifying whether this condition holds or not is as simple a matter as determining if the reference signal $\boldsymbol{x}$ is constant with time or not.

6.4 Separation Property of Observer-based Attitude Control

Analogous to the separation principle of linear control theory, we develop here a closed-loop stability result for the nonlinear rigid-body attitude tracking control system by carefully combining two separately designed control components: (a) the full-state feedback part (as if the true quaternion exactly determined); and (b) the attitude observer that estimates the quaternion using measured signals. In the following, we first derive the attitude tracking error dynamics based on the estimated attitude information $\hat{\boldsymbol{q}}$ from the attitude observer Eq. (6.22).

We start by defining the observer-based attitude tracking error $\delta\hat{\boldsymbol{q}}$ through the following implicit relationship

$$C(\delta\hat{\boldsymbol{q}}) = C(\hat{\boldsymbol{q}})C^T(\boldsymbol{q}_r), \tag{6.35}$$

Next, we introduce the estimated body frame $\mathcal{F}_E$ in association with the estimated quaternion $\hat{\boldsymbol{q}}$ which satisfies the following relationships:

$$\begin{aligned} \mathcal{F}_N \xrightarrow{\hat{\boldsymbol{q}}} \mathcal{F}_E \implies \hat{\boldsymbol{e}} = C(\hat{\boldsymbol{q}})\hat{\boldsymbol{n}} \\ \mathcal{F}_R \xrightarrow{\delta\hat{\boldsymbol{q}}} \mathcal{F}_E \implies \hat{\boldsymbol{e}} = C(\delta\hat{\boldsymbol{q}})\hat{\boldsymbol{r}} \end{aligned}$$

where $\hat{\boldsymbol{e}}$ represents the unit vector triad in the estimated body frame $\mathcal{F}_E$. By following the same steps taken in deriving Eq. (6.8), the time derivative of Eq. (6.35) is obtained by

$$\frac{d}{dt}C(\delta\hat{\boldsymbol{q}}) = -S(\delta\hat{\boldsymbol{\omega}} + \gamma\boldsymbol{y}\times\hat{\boldsymbol{y}})C(\delta\hat{\boldsymbol{q}}) \tag{6.36}$$

where $\delta\hat{\boldsymbol{\omega}}$ is defined by

$$\delta\hat{\boldsymbol{\omega}} = \boldsymbol{\omega} - C(\delta\hat{\boldsymbol{q}})\boldsymbol{\omega}_r \tag{6.37}$$

The quaternion realization of Eq. (6.36) is represented as[34]

$$\delta\dot{\hat{\boldsymbol{q}}} = \frac{1}{2}E(\delta\hat{\boldsymbol{q}})\left(\delta\hat{\boldsymbol{\omega}} + \gamma\boldsymbol{y}\times\hat{\boldsymbol{y}}\right). \tag{6.38}$$

Similarly, by taking the time derivative of Eq. (6.37), and using the Euler differential equation from Eq. (6.5), we derive the following observer-based angular velocity error dynamics

$$J\delta\dot{\hat{\boldsymbol{\omega}}} = -S(\boldsymbol{\omega})J\boldsymbol{\omega} + \boldsymbol{u} + J\boldsymbol{\eta} \tag{6.39}$$

wherein $\boldsymbol{\eta}$ is defined by

$$\boldsymbol{\eta} = S(\delta\hat{\boldsymbol{\omega}} + \gamma\boldsymbol{y}\times\hat{\boldsymbol{y}})C(\delta\hat{\boldsymbol{q}})\boldsymbol{\omega}_r - C(\delta\hat{\boldsymbol{q}})\dot{\boldsymbol{\omega}}_r \tag{6.40}$$

It is possible to interpret the overall tracking error dynamics as given by Eq. (6.38) and Eq. (6.39), so that our control objective for the attitude tracking problem is to specify the control signal $\boldsymbol{u}(t)$ in such a way to achieve $\lim_{t\to\infty}[\delta\hat{\boldsymbol{q}}_{\boldsymbol{v}}(t), \delta\hat{\boldsymbol{\omega}}(t)] = 0$ along with $\lim_{t\to\infty}[C(\hat{\boldsymbol{q}}(t)) - C(\boldsymbol{q}(t))] = 0$.

We now present the main contribution of this chapter, a separation property of the rigid-body attitude tracking control problems based on the new observer-based attitude tracking control method.

Theorem 7. *For the attitude tracking error dynamics described through Eq. (6.38)*

and Eq. (6.39), suppose the control input $\boldsymbol{u}(t)$ *is computed by*

$$\boldsymbol{u} = -k_v J\delta\hat{\boldsymbol{\omega}} + S(\boldsymbol{\omega})J\boldsymbol{\omega} - J\boldsymbol{\eta} - k_p J\left[\alpha\delta\hat{\boldsymbol{q}}_{\boldsymbol{v}} + \frac{1}{2}\left(\delta\hat{q}_o I_{3\times 3} + S(\delta\hat{\boldsymbol{q}}_{\boldsymbol{v}})\right)\left(\delta\hat{\boldsymbol{\omega}} + \gamma\boldsymbol{y}\times\hat{\boldsymbol{y}}\right)\right] \tag{6.41}$$

where $k_p > 0$, $k_v > 0$, $\alpha = k_p + k_v$. *Further, suppose the attitude estimate* $\hat{\boldsymbol{q}}(t)$ *is computed from Eq. (6.22) under the assumptions of Proposition 2 governing the reference signal* $\boldsymbol{x}$ *(i.e., unit vector* $\boldsymbol{x}(t)$ *is not a constant with respect and has bounded time derivatives). If* $\hat{\boldsymbol{q}}(0)$ *satisfies* $\hat{\boldsymbol{q}}(0)^T\boldsymbol{q}(0) \neq 0$, *then the attitude tracking control objective,* $\lim_{t\to\infty}[\delta\boldsymbol{q}_{\boldsymbol{v}}(t), \delta\boldsymbol{\omega}(t)] = 0$, *is guaranteed (almost) globally and asymptotically. On the other hand, if the attitude estimator is initiated such that the initial value of the estimated quaternion* $\hat{\boldsymbol{q}}(0)$ *satisfies* $\hat{\boldsymbol{q}}(0)^T\boldsymbol{q}(0) = 0$, *then all closed-loop signals remain bounded with no further assurance of asymptotic convergence of the tracking errors.*

Proof. Suppose $\hat{\boldsymbol{q}}^T(0)\boldsymbol{q}(0) \neq 0$ and accordingly, $z_o(t) \neq 0$ for all $t \geq 0$. We consider a composite Lyapunov-like candidate function that is motivated from the results and discussion presented under Proposition 1 and 2 and is defined as follows

$$V = V_c + V_o = \underbrace{\frac{1}{2}\hat{\boldsymbol{\omega}}_f^T\hat{\boldsymbol{\omega}}_f + [(\delta\hat{q}_o - 1)^2 + \delta\hat{\boldsymbol{q}}_{\boldsymbol{v}}^T\delta\hat{\boldsymbol{q}}_{\boldsymbol{v}}]}_{\text{V}_\text{c}\text{ (controller part)}} + \underbrace{\frac{\lambda\boldsymbol{z}_{\boldsymbol{v}}^T\boldsymbol{z}_{\boldsymbol{v}}}{2z_o^2}}_{\text{V}_\text{o}\text{ (observer part)}} \tag{6.42}$$

where $\lambda = 16\gamma^2/k_p$. The construction V_c is motivated by Eq. (6.17) and involves a new filter state $\hat{\boldsymbol{\omega}}_f$ driven by the angular velocity error $\delta\hat{\boldsymbol{\omega}}$ in Eq. (6.37) as follows

$$\dot{\hat{\boldsymbol{\omega}}}_f = -\alpha\hat{\boldsymbol{\omega}}_f + \delta\hat{\boldsymbol{\omega}} \tag{6.43}$$

Differentiating both sides of Eq. (6.43) with respect to time and making a substitu-

tion from Eq. (6.39) and Eq. (6.41), filtered error dynamics can be seen to satisfy

$$\dot{\hat{\boldsymbol{\omega}}}_f = -k_v \hat{\boldsymbol{\omega}}_f - k_p \delta\hat{\boldsymbol{\omega}} \tag{6.44}$$

wherein we have already neglected an exponentially decaying term which can be justified though arguments identical to those presented earlier that led to establishment of Eq. (6.19). The time derivative of the Lyapunov-like candidate function V taken along Eq. (6.27), Eq. (6.38), and Eq. (6.44) yields the following

$$\dot{V} = \dot{V}_c + \dot{V}_o = -k_v\|\hat{\boldsymbol{\omega}}_f\|^2 - k_p\|\delta\hat{\boldsymbol{q}}_{\boldsymbol{v}}\|^2 + \gamma\delta\hat{\boldsymbol{q}}_{\boldsymbol{v}}^T(\boldsymbol{y}\times\hat{\boldsymbol{y}}) - \lambda\|\boldsymbol{z}_{\boldsymbol{v}}\times\boldsymbol{x}\|^2 - \lambda\frac{\|\boldsymbol{z}_{\boldsymbol{v}}\times\boldsymbol{x}\|^2}{z_o^2} \tag{6.45}$$

we can further simplify $\dot{V}$ from Eq. (6.45) to obtain

$$\begin{aligned}
\dot{V} =& -k_v\|\hat{\boldsymbol{\omega}}_f\|^2 - k_p\|\delta\hat{\boldsymbol{q}}_{\boldsymbol{v}}\|^2 + \gamma\delta\hat{\boldsymbol{q}}_{\boldsymbol{v}}^T C(\boldsymbol{q})\left[2z_o(\boldsymbol{z}_{\boldsymbol{v}}\times\boldsymbol{x})\times\boldsymbol{x} - 2(\boldsymbol{x}^T\boldsymbol{z}_{\boldsymbol{v}})(\boldsymbol{z}_{\boldsymbol{v}}\times\boldsymbol{x})\right] \\
&- \lambda\|\boldsymbol{z}_{\boldsymbol{v}}\times\boldsymbol{x}\|^2 - \lambda\frac{\|\boldsymbol{z}_{\boldsymbol{v}}\times\boldsymbol{x}\|^2}{z_o^2} \\
\leqslant& -k_v\|\hat{\boldsymbol{\omega}}_f\|^2 - k_p\|\delta\hat{\boldsymbol{q}}_{\boldsymbol{v}}\|^2 + 4\gamma\|\delta\hat{\boldsymbol{q}}_{\boldsymbol{v}}\|\|\boldsymbol{z}_{\boldsymbol{v}}\times\boldsymbol{x}\| - \lambda\|\boldsymbol{z}_{\boldsymbol{v}}\times\boldsymbol{x}\|^2 \\
\leqslant& -k_v\|\hat{\boldsymbol{\omega}}_f\|^2 - \frac{k_p}{2}\|\delta\hat{\boldsymbol{q}}_{\boldsymbol{v}}\|^2 - \frac{\lambda}{2}\|\boldsymbol{z}_{\boldsymbol{v}}\times\boldsymbol{x}\|^2 \\
&- \frac{k_p}{2}\left[\|\delta\hat{\boldsymbol{q}}_{\boldsymbol{v}}\|^2 - \frac{8\gamma}{k_p}\|\delta\hat{\boldsymbol{q}}_{\boldsymbol{v}}\|\|\boldsymbol{z}_{\boldsymbol{v}}\times\boldsymbol{x}\| + \frac{\lambda}{k_p}\|\boldsymbol{z}_{\boldsymbol{v}}\times\boldsymbol{x}\|^2\right] \\
\leqslant& -k_v\|\hat{\boldsymbol{\omega}}_f\|^2 - \frac{k_p}{2}\|\delta\hat{\boldsymbol{q}}_{\boldsymbol{v}}\|^2 - \frac{\lambda}{2}\|\boldsymbol{z}_{\boldsymbol{v}}\times\boldsymbol{x}\|^2
\end{aligned} \tag{6.46}$$

wherein the last inequality follows from the choice of $\lambda = 16\gamma^2/k_p$. Following essentially same steps as on the proof of Proposition 2, we now can conclude boundedness of all the all closed-loop signals. Further, it also follows that $\dot{\hat{\boldsymbol{\omega}}}_f, \dot{\delta\hat{\boldsymbol{q}}}_{\boldsymbol{v}}$, and $\dot{\boldsymbol{z}}_{\boldsymbol{v}}$ are $\mathcal{L}_\infty$. In addition, integrating both sides of Eq. (6.46), we readily establish $\|\hat{\boldsymbol{\omega}}_f\|, \|\delta\hat{\boldsymbol{q}}_{\boldsymbol{v}}\|$, and $\|\boldsymbol{z}_{\boldsymbol{v}}\times\boldsymbol{x}\|$ are $\mathcal{L}_2\cap\mathcal{L}_\infty$. Thus, by Barbalat's lemma, $[\|\hat{\boldsymbol{\omega}}_f(t)\|, \|\delta\hat{\boldsymbol{q}}_{\boldsymbol{v}}(t)\|, \|\boldsymbol{z}_{\boldsymbol{v}}(t)\times\boldsymbol{x}(t)\|] \to 0$ as $t\to\infty$ which is equivalent to $[\delta\hat{\boldsymbol{\omega}}(t), \delta\hat{\boldsymbol{q}}_{\boldsymbol{v}}(t), \boldsymbol{z}_{\boldsymbol{v}}(t)] \to 0$ as $t\to\infty$ given the filter definition Eq. (6.43) and the fact that the unit-vector reference signal $\boldsymbol{x}$ is

not constant with time. Consequently, we guarantee that $\lim_{t\to\infty}[\delta\boldsymbol{\omega}(t), \delta\boldsymbol{q_v}(t)] = 0$ along with $\lim_{t\to\infty}[C(\hat{\boldsymbol{q}}(t)) - C(\boldsymbol{q}(t))] = 0$.

Next, for the case $\hat{\boldsymbol{q}}^T(0)\boldsymbol{q}(0) = 0$, (i.e., $z_o(0) = 0$), we consider the following lower bounded Lyapunov-like candidate function

$$V_u = V_c + V_e = \underbrace{\frac{1}{2}\hat{\boldsymbol{\omega}}_f^T\hat{\boldsymbol{\omega}}_f + [(\delta\hat{q}_o - 1)^2 + \delta\hat{\boldsymbol{q}}_{\boldsymbol{v}}^T\delta\hat{\boldsymbol{q}}_{\boldsymbol{v}}]}_{V_c} + \underbrace{\frac{\boldsymbol{z}_{\boldsymbol{v}}^T\boldsymbol{z}_{\boldsymbol{v}}}{2}}_{V_e} \tag{6.47}$$

Then, the time derivative of V_u is given as follows

$$\dot{V}_u(t) = -k_v\|\hat{\boldsymbol{\omega}}_f\|^2 - k_p\|\delta\hat{\boldsymbol{q}}_{\boldsymbol{v}}\|^2 + \gamma\delta\hat{\boldsymbol{q}}_{\boldsymbol{v}}^T(\boldsymbol{y}\times\hat{\boldsymbol{y}}) - \gamma z_o^2\|\boldsymbol{z}_{\boldsymbol{v}}\times\boldsymbol{x}\|^2 \tag{6.48}$$

Since $z_o(t) = 0$ for all $t \geq 0$ as long as $z_o(0) = 0$ from Eq. (6.29), we can simplify Eq. (6.48) further as follows

$$\begin{aligned}\dot{V}_u(t) &= -k_v\|\hat{\boldsymbol{\omega}}_f\|^2 - k_p\|\delta\hat{\boldsymbol{q}}_{\boldsymbol{v}}\|^2 + \gamma\delta\hat{\boldsymbol{q}}_{\boldsymbol{v}}^T(\boldsymbol{y}\times\hat{\boldsymbol{y}}) \\ &\leq -k_v\|\hat{\boldsymbol{\omega}}_f\|^2 + c_1; \quad c_1 \doteq \sup_{t\geq 0}\left\{k_p\|\delta\hat{\boldsymbol{q}}_{\boldsymbol{v}}\|^2 + \gamma\|\delta\hat{\boldsymbol{q}}_{\boldsymbol{v}}^T(\boldsymbol{y}\times\hat{\boldsymbol{y}})\|\right\}\end{aligned} \tag{6.49}$$

where c_1 is the well defined finite positive constant consisting of norms of the bounded quaternion element $\delta\hat{\boldsymbol{q}}_{\boldsymbol{v}}$ and the quantity $\boldsymbol{y}\times\hat{\boldsymbol{y}}$ (vector cross product between unit vectors). Similarly, from Eq. (6.47), we can represent upper bounding function for V_u as follows

$$V_u \leq \frac{1}{2}\|\hat{\boldsymbol{\omega}}_f\|^2 + c_2; \quad c_2 \doteq \sup_{t\geq 0}\left\{[(\delta\hat{q}_o - 1)^2 + \delta\hat{\boldsymbol{q}}_{\boldsymbol{v}}^T\delta\hat{\boldsymbol{q}}_{\boldsymbol{v}}] + \frac{\boldsymbol{z}_{\boldsymbol{v}}^T\boldsymbol{z}_{\boldsymbol{v}}}{2}\right\} \leq \frac{5}{2} \tag{6.50}$$

Based on Eq. (6.49) and Eq. (6.50), $\dot{V}_u$ is bounded from above by

$$\dot{V}_u \leq -2k_vV_u + c_3; \quad c_3 = 2k_vc_2 + c_1 \tag{6.51}$$

which shows that V_u is bounded and in turn, $\hat{\boldsymbol{\omega}}_f$ is bounded from Eq. (6.47). Since $\hat{\boldsymbol{\omega}}_f$ is bounded, $\delta\hat{\boldsymbol{\omega}}$ is also bounded from the definition of filter dynamics in Eq. (6.43) because the rest of closed-loop signals are already bounded quaternion elements ($\delta\hat{\boldsymbol{q}}$ and $\boldsymbol{z}$). Further, $\boldsymbol{\omega}$ is bounded from Eq. (6.37). Therefore, every closed-loop signal is bounded and likewise, the control torque is bounded from Eq. (6.41). This completes the proof for all stated assertions. □

6.5 Numerical Simulations

To demonstrate the performance of the attitude estimator (observer) combined with the proposed controller, we perform simulations. The reference signal $\boldsymbol{x}(t)$ for the attitude observer is taken to be $\boldsymbol{x}(t) = [\cos t, \sin t, 0]^T$. The commanded attitude reference trajectory taken from the literature [38] is given as $\boldsymbol{\omega}_r = \omega_r(t) \times [1,1,1]^T$ where $\omega_r(t) = 0.3\cos t(1 - e^{-0.01t^2}) + (0.08\pi + 0.006\sin t)te^{-0.01t^2}$. We assume initial conditions $\boldsymbol{q}(0) = [\frac{2\sqrt{2}}{3}, \frac{1}{3\sqrt{3}}, \frac{1}{3\sqrt{3}}, \frac{1}{3\sqrt{3}}]^T$, $\hat{\boldsymbol{q}}(0) = [\frac{\sqrt{3}}{2}, \frac{1}{2\sqrt{3}}, \frac{1}{2\sqrt{3}}, \frac{1}{2\sqrt{3}}]^T$, $\boldsymbol{q}_r(0) = [1,0,0,0]^T$, and $\boldsymbol{\omega}(0) = [0,0,0]$ (i.e., the body is initially at rest). The inertia matrix J is chosen as

$$J = \begin{bmatrix} 20 & 1.2 & 0.9 \\ 1.2 & 17 & 1.4 \\ 0.9 & 1.4 & 15 \end{bmatrix} \tag{6.52}$$

and control gains γ, k_p and k_v are all set to unity.

In Fig. 6.1, we show results from two sets of simulations wherein in one case, the controller is given by Eq. (6.41) by using the attitude estimator, and the second case corresponds to the controller from Eq. (6.12) that assumes instantaneous availability of the actual true quaternion $\boldsymbol{q}(t)$. It is clear from Fig. 6.1(a) and Fig. 6.1(b) that the overall performance (speed of tracking error convergence) for the controller that assumes availability of the true attitude quaternion is slightly faster compared

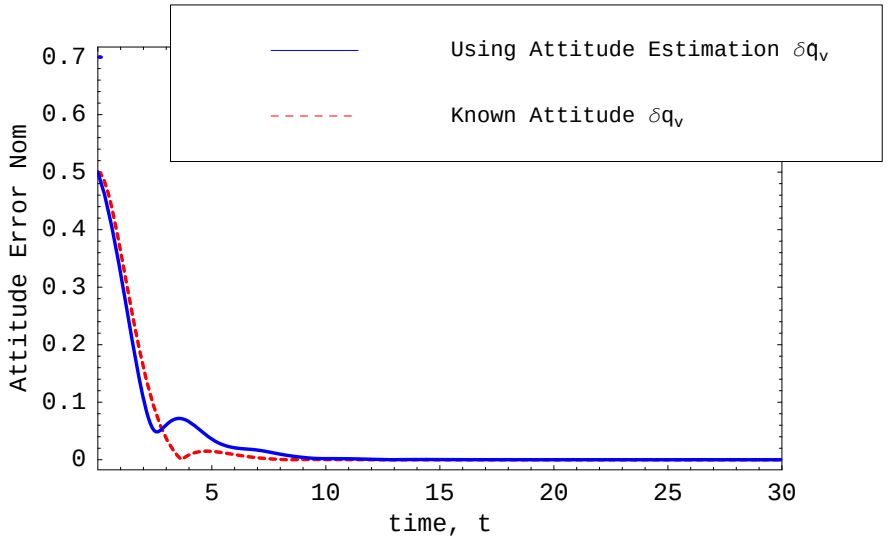

(a) Quaternion attitude error

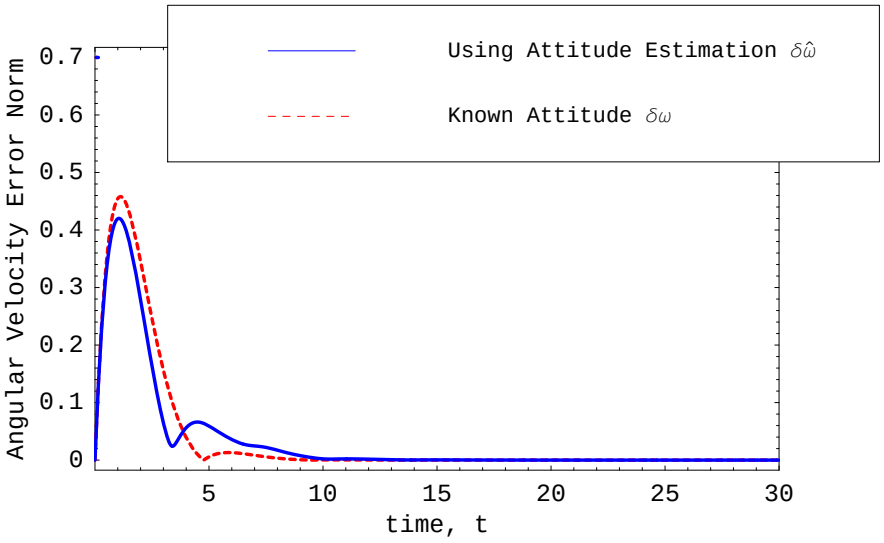

(b) Angular velocity error

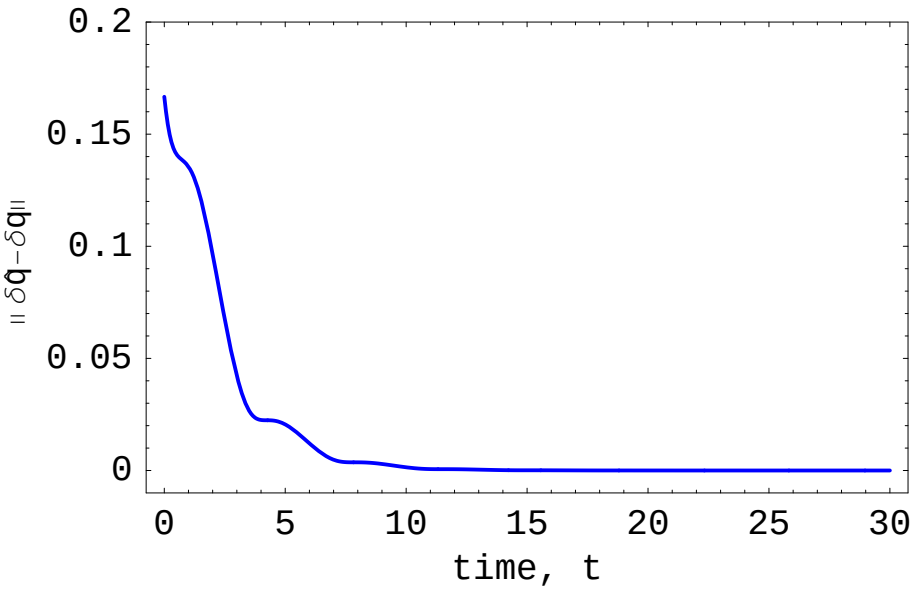

(c) Attitude estimator performance

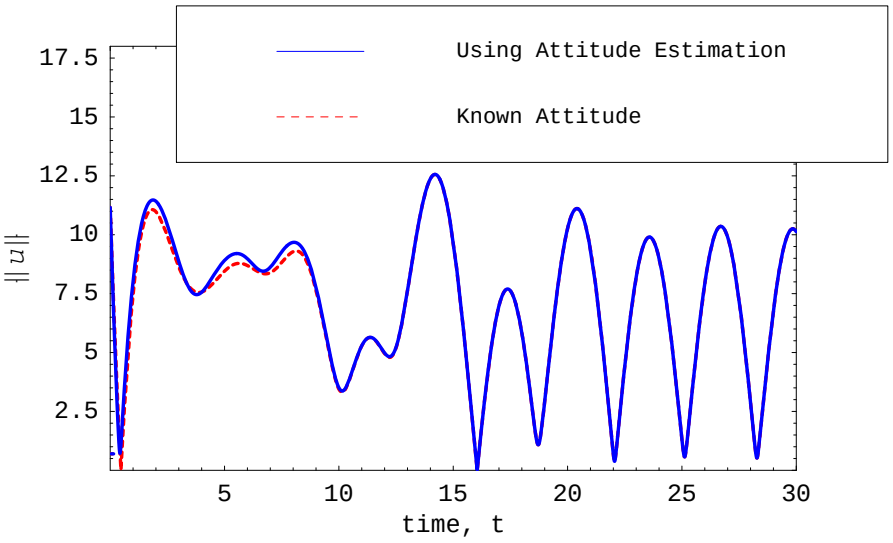

(d) Control torque

Figure 6.1: Closed-loop simulation results comparing performance of the controller from Eq. (6.41) (adopting the attitude estimator) with controller from Eq. (6.12) that assumes direct availability of attitude variables (no estimation required).

to the controller that needs to perform the additional task of attitude estimation while attending to the underlying tracking objective. Of course, this is quite reasonable and bound to happen because the controller based on the attitude estimator needs to apply additional effort toward compensating the difference between the estimated attitude value and the true attitude value as shown in Fig. 6.1(c) (note that origin in this plot is slightly off-set to the "first quadrant" in order to help better visualization) and Fig. 6.1(d). Once the attitude estimates converge to the true attitude values, the control norms of either controller become virtually identical and they remain essentially non-zero to ensure the body maintains the prescribed attitude tracking motion. This happens after about 10 seconds into the simulation and is shown in Fig. 6.1(d).

Next, we simulate the case where the initial condition for the attitude estimator $\hat{\boldsymbol{q}}(0)$ is deliberately chosen such that the condition $z_o(0) = 0$ is identically satisfied. In Fig. 6.2, we show the simulation results that compare the closed-loop performance of the controllers from Eq. (6.41) and Eq. (6.12). It is evident from these results that the attitude estimation error converges to zero after about 60 seconds which is much slower compared to the convergence rates documented in Fig. 6.1. Correspondingly, control efforts commanded by the controller to enable attitude tracking are also greater as seen in Fig. 6.2(c). Since the initial condition for the estimator in these simulations corresponds to an unstable manifold [67], the attitude estimator expectedly converges to the actual attitude state within our simulations after going through an initial transient.

It needs to be emphasized that there is no special significance to the time instant $t \sim 50$ seconds except for the fact that in the case of this particular simulation, it took about 50 seconds for the numerical integration errors to sufficiently build up and drive the attitude estimator away from the unstable equilibrium manifold corresponding to $z_o = 0$. It is perhaps more important to note that during

the time the attitude estimator is stuck within the unstable equilibrium manifold (for $t \leq 50$ seconds), the control torque and all other closed-loop trajectories remain bounded just as it is assured by our theoretical results.

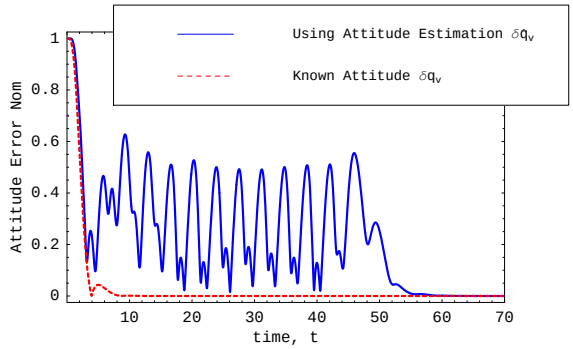

(a) Quaternion attitude error

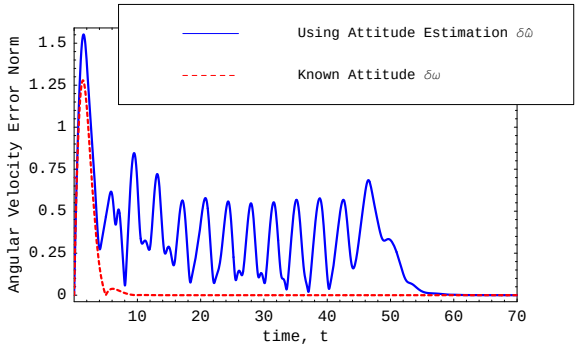

(b) Angular velocity error

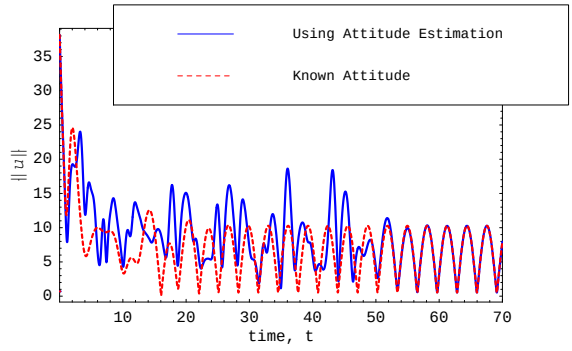

(c) Control torque

Figure 6.2: Closed-loop simulation results comparing performance of the controller from Eq. (6.41) (adopting the attitude estimator) with controller from Eq. (6.12) that assumes direct availability of attitude variables (no estimation required). The attitude estimator is initialized in such a way that $\hat{\boldsymbol{q}}(0)$ exactly satisfies condition $\hat{\boldsymbol{q}}(0)^T \boldsymbol{q}(0) = 0$.

Chapter 7

Conclusions

This research brings together the fields of nonlinear system analysis, system identification, adaptive control techniques, and observation algorithms. More specifically, a novel adaptive control method is developed and applied to actual systems, which is enabled by designing an attracting manifold for adaptation. The proposed adaptive control method improves the closed-loop system response and it is implemented on both robot and spacecraft control systems. Especially in the attitude estimation and control field, the developed adaptive control scheme is applied to a spacecraft attitude control problem and attitude estimation algorithm is also developed and combined with the proposed adaptive control method to demonstrate the possibility of independent designs for an observer-based nonlinear control system.

7.1 Contributions

Detailed contributions of the presented work are in the following order:

1. **A novel adaptive control method** for nonlinear systems is developed on the basis of a non-certainty equivalence principle. The proposed control method utilizes an attracting manifold in adaptation, which is enabled by introducing

an regressor filter. This regressor filter technique succeeds in eliminating an integrability obstacle that is addressed as a constraint in [6]. Further, the presented adaptive control method generalizes the result in [9]. By virtue of an attracting manifold, a closed-loop system performance is significantly improved without demanding increased control efforts compared with conventional certainty equivalence framework (MRAC). As a result of an attracting manifold, two properties are introduced to the closed-loop dynamics. First, parameter estimates stay locked at true parameter values after they hit true parameter values. For example, if initial estimates are equal to true values incidentally, then the proposed adaptive control method act as a deterministic controller while the MRAC method makes estimates deviate from true values. Second, the closed-loop error dynamics always mimic the dynamics of deterministic control system (i.e., control system without uncertain parameters), which is independent of estimation errors.

2. **Application** to actual systems shows the improvement on the system performance. Especially, in the spacecraft attitude tracking application, the restriction on an initial quaternion error in [38] is removed.

3. **An attitude estimator/observer** is developed and applied to a spacecraft attitude control problem jointly with the proposed adaptive control method. The developed attitude estimator enforces the orthogonal structure to estimated attitude matrices using Poission update law, while other attitude estimation algorithm can not generate orthogonal attitude matrices; thus, the attitude estimator fully utilizes the a priori information of the system structure and thereby no longer requires an overparameterization. Since the non-overparameterizing algorithm is validated in n-dimensional space, the attitude estimation algorithm in 3-dimensional space (i.e., subspace of n-dimensional space) is implemented through a quaternion update law but a matrix update

law.

4. **A separation property for nonlinear attitude control problems** is established and demonstrated using numerical simulation. The presented separation property is proved based on the fact that the deterministic version of the proposed control method provides a strict Lyapunov function, which is not possible when the conventional proportional-derivative type controller is implemented. Consequently, an observer and a controller can be designed independently and combined later for the observer-based attitude control system as it is done in the linear systems.

7.2 Recommendations for Future Research

In this dissertation, we do not mention certain possibilities that the proposed control methods may provide on the basis of the following aspects:

1. In order to implement the proposed adaptive control method, we assume that full-state feedback is available. It is worth investigating the use of the proposed controller to the observer-based output feedback control systems, which may leads to the performance improvement of overall system dynamics.

2. Although the attracting manifold serves as a sink for uncertain parameter effects in the closed-loop dynamics, it does not guarantee the convergence of each estimate to a true parameter value and still requires a persistence excitation condition for the reference input. If we can explicitly include a reference in the attracting manifold dynamics, then it will guarantee the convergence of estimates to the true parameter values.

3. In the attitude observer design, the angular velocity is assumed to be exactly measured, which is not true in practical sense. Thus, there exits some solutions

that relieve this assumption and introduce a constant gyro bias. However, present results are not applicable to n-dimensional problems. Therefore, it should be studied to extend the proposed result to n-dimensional attitude estimation problems with a bias in the angular velocity (or angular-velocity-like quantity).

Bibliography

[1] K. J. Åström. Adaptive control around 1960. *IEEE Control Systems Magazine*, 16(3):44–49, 1996.

[2] B. Wittenmark. A survey of adaptive control applications. In *Dynamic Modeling Control Applications for Industry Workshop*, pages 32–36, Vancouver, BC, Canada, 1997. IEEE Industry Applications Socity.

[3] D. E. Seborg, T. F. Edgar, and S. L. Shah. Adaptive control strategies for process control:a survey. *AlChE*, 32:881–913, 1986.

[4] Brian D. O. Anderson. Failures of adaptive control theory and their resolution. *Communications in Information and Systems*, 5:1–20, 2005.

[5] G. Tao. *Adaptive Control Design and Analysis*, chapter 1. Wiley, 2003.

[6] A. Astolfi and R. Ortega. Immersion and invariance: A new tool for stabilization and adaptive control of nonlinear systems. *IEEE. Trans. on Automatic Control*, 48:590–606, 2003.

[7] A. Astolfi, H. Liu, M. S. Netto, and R. Ortega. Two solutions to the adaptive visual servoing problem. *IEEE Trans. on Robotics and Automation*, 18:387–392, 2002.

[8] D. Karagiannis, A. Astolfi, and R. Ortega. Two results for adaptive output feedback stabilization of nonlinear systems. *Automatica*, 39:857–866, 2003.

[9] R. Ortega, L. Hsu, and A. Astolfi. Immersion and invariance adaptive control of linear multivariable systems. *Systems & Control Letters*, 49(1):37–47, 2003.

[10] P. Ioannou and J. Sun. *Robust Adaptive Control*, pages 200–201. Prentice Hall, 1996.

[11] R. Ortega, L. Hsu, and A. Astolfi. Immersion and Invariance Adaptive Control of Linear Multivariable Systems. *Systems and Control Letters*, 49(1), 2003.

[12] A. Astolfi. A remark on an example by teel-hespanha with applications to cascaded systems. *IEEE Trans. on Automatic Control*, 54:289–293, 2007.

[13] P. Ioannou and J. Sun. *Robust Adaptive Control*. Prentice-Hall, Englewood Cliffs, NJ, 1996.

[14] J. T. Spooner, M. Maggiore, R. Ordó nez, and K. M. Passino. *Stable Adaptive Control and Estimation for Nonlinear Systems*. Wiely, New York, 2002.

[15] M. Krstic, I. Kanellakopoulos, and P. Kokotivic. *Nonlinear and Adaptive Control Design*. Wiley, New York, 1995.

[16] S. Sastry and M. Bodson. *Adaptive Control: Stability, Convergence, and Robustness*. Prentice-Hall, Englewood Cliffs, NJ, 1989.

[17] J. B. Pomet and L. Praly. Adaptive nonlinear regulation: Estimation from lyapunov equation. *IEEE Trans. on Automatic Control*, 37:729–740, 1992.

[18] Z. Cai, M. S. de Queiroz, and D. M. Dawson. A sufficiently smooth projection operator. *IEEE Trans. on Automatic Control*, 51:135–139, 2006.

[19] M. R. Akella. Adaptive control-a departure from the certainty-equivalence paradigm. *J. Astronautical Sciences*, 52:75–91, 2004.

[20] M. Spong and M. Vidyasagar. *ROBOT DYNAMICS AND CONTROL*. John Wiley, New York, NY, 1989.

[21] S. Lin. Dynamics of the manipulator with closed chains. *IEEE Trans. on Robotics and Automation*, 6:496–501, 1990.

[22] H. Takeuchi, K. Kosuge, and K. Furuta. Motion control of a robot arm using joint torque sensors. *IEEE Trans. on Robotics and Automation*, 6:258–263, 1990.

[23] J. Craig, J. Hsu, Pl, and S. Sastry. Adaptive control of mechanical manipulators. San Francisco, CA, Mar. 1986. IEEE Int. Conf. on Robotics and Automation.

[24] M. W. Spong and R. Ortega. On adaptive inverse dynamics control of rigid robots. *IEEE Trans. on Automatic Control*, 35:92–95, 1990.

[25] M. Amestegui, R. Ortega, and J. M. Ibarra. Adaptive linearizing-decoupling robot control: A comparative study of different parameterizations. In *Proc. 5th Yale Workshop on Applications of Adaptive Systems Theory*, New Haven, Conn, 1987.

[26] R. H. Middleton and G. C. Goodwin. Adaptive computed torque for rigid link manipulators. *Systems & Control Letters*, 10:9–16, 1988.

[27] J. J. Slotine and W. Lie. On the adaptive control of robot manipulators. In *ASME Winter Annual Meeting*, Anaheim, CA, 1986.

[28] N. Sadegh and R. Horowitz. Stability analysis of an adaptive controller for

robotic manipulators. In *IEEE Int. Conf. on Robotics and Automation*, Raleigh, NC, 1987.

[29] R. Kelly, R. Ortega, and R. Carelli. Adaptive motion control design of robot manipulators: An input-ouput approach. In *IEEE Int. Conf. on Robotics and Automation*, Philadelphia, 1988.

[30] R. Ortega and M. W. Spong. Adaptive motion control of rigid robots: A tutorial. Austin, TX, Dec. 1988. IEEE Proc. Conf. on Decision and Control.

[31] P. R. Pagilla and M. Tomizuka. An adaptive output feedback controller for robot arms:stability and experiments. *Automatica*, 37:983–995, 2001.

[32] J. T. Wen and K. Kreutz-Delgado. The attitude control problem. *IEEE Trans. on Automatic Control*, 36(10):1148–1162, 1991.

[33] S. P. Bhat and D. S. Bernstein. A topological obstruction to continuous global stabilization of rotational motion and the unwinding phenomenon. *Systems & Control Letters*, 39:63–70, 2000.

[34] H. Schaub and J. L. Junkins. *Analytical Mechanics of Space Systems*, chapter 3. AIAA Education Series, 2003.

[35] M. Krstić and P. Tsiotras. Inverse optimal stabilization of a rigid spacecraft. *IEEE Trans. on Automatic Control*, 44:1042–1049, 1999.

[36] J. L. Junkins, M. R. Akella, and R. D. Robinett. Nonlinear adaptive control of spacecraft maneuvers. *J. Guicance, Control, and Dynamics*, 20(6):1104–1110, 1997.

[37] H. Schaub, M. R. Akella, and J. L. Junkins. Adaptive control of nonlinear attitude motions realizing linear closed-loop dynamics. *J. Guidance, Control, and Dynamics*, 24:95–100, 1999.

[38] B. T. Costic, D. M. Dawson, M. S. de Queiroz, and V. Kapila. Quaternion-based adaptive attitude tracking controller without velocity measurements. *J. Guidance, Control, and Dynamics*, 24(6):1214–1222, 2001.

[39] S. Sastry and M. Bodson. *Adaptive Control: Stability, Convergense, and Robustness*, chapter 3. Prentice Hall, 1989.

[40] P. Tsiotras. Further passivity results for the attitude control problem. *IEEE Trans. on Automatic Control*, 43:1597–1600, 1998.

[41] S. R. Marandi and V. J. Modi. A preferred coordinate system and the associated orientation representation in attitude dynamics. *Acta Astronaut*, 15(11):833–843, 1987.

[42] M. D. Shuster. A survey of attitude representations. *J. Astronautical Sciences*, 41(4):439–517, 1993.

[43] H. Schaub and J. L. Junkins. Stereographic orietation parameters for attitude dynamics: a generalization of the rodrigues parameters. *J. Astronautical Sciences*, 44(1):1–19, 1996.

[44] Y. Li, M. Murata, and B. Sun. New approach to attitude determination using global positioning system carrier phase measurements. *J. Guidance, Control, and Dynamics*, 25:130–136, 2002.

[45] A. Cayley. On the motion of rotation of a solid body. *Cambridge Mathematics J.*, 3:224–232, 1843.

[46] M.D. Shuster and S.D. Oh. Attitude determination from vector observations. *J. Guidance, Control, and Dynamics*, 4(1):70–77, 1981.

[47] F.L. Markley. Attitude determination from vector observations: A fast optimal matrix algorithm. *J. Astronautical Sciences*, 41(2):261–280, 1993.

[48] G. Wahba. A least-squares estimate of satellite attitude. *SIAM Review*, 7(3):409, 1965.

[49] G.M. Lerner. Three-axis attitude determination. In J.R. Wertz, editor, *Spacecraft Attitude Determination and Control*, pages 420–428. D. Reidel Publishing Co., Dordrecht, The Netherlands, 1978.

[50] M. D. Shuster. Attitude determination in higher dimensions. *J. Guidance, Control, and Dynamics*, 16(2):393–395, 1993.

[51] J.L. Farrell. Attitude determination by kalman filter. *Automatica*, 6(5):419–430, 1970.

[52] D. Chu and E. Harvie. Accuracy of the erbs definitive attitude determination system in the presence of propagation noise. In *Proc. Flight Mechanics/Estimation Theory Symposium*, pages 97–114, Greenbelt, MD, 1990. NASA-Goddard Space Flight Center.

[53] I.Y. Bar-Itzhack and J.K. Deutschmann. Extended kalman filter for attitude estimation of the earth radiation budget satellite. In *Proc. AAS Astrodynamics Conference*, AAS Paper #90-2964, pages 786–796, Portland, OR, 1990.

[54] M.S. Challa, G.A. Natanson, D.E. Baker, and J.K. Deutschmann. Advantages of estimating rate corrections during dynamic propagation of spacecraft rates-applications to real-time attitude determination of sampex. In *Proc. Flight Mechanics/Estimation Theory Symposium*, pages 481–495, Greenbelt, MD, 1994. NASA-Goddard Space Flight Center.

[55] M.S. Challa. Solar, anomalous, and magnetospheric particle explorer (sampex) real-time sequential filter (rtsf). Technical report, NASA-Goddard Space Flight Center, Greenbelt, MD, April 1993.

[56] J.C. Kinsey and L.L. Whitcomb. Adaptive identification on the group of special orthogonal matrices. Technical report, The Johns Hopkins University, 2005.

[57] J. R. Wertz. *Spacecraft attitude determination and control*, chapter 6,7. Springer, 1978.

[58] J. L. Crassidis. Angular velocity determination directly from star tracker measurements. *J. Guidance, Control, and Dynamics*, 25:1165–1168, 2002.

[59] P. Singla, J. L. Crassidis, and J. L. Junkins. Spacecraft angular rate estimation algorithms for a star tracker mission. In *Paper AAS 03-191*, Ponce, Puerto-Rico, Feb. 2003. AAS/AIAA Space Flight Mechanics Meeting.

[60] M. L. Psiaki. Global magnetometer-based spacecraft attitude and rate estimation. *J. Guidance, Control, and Dynamics*, 27:240–250, 2004.

[61] M. L. Psiaki, E. M. Klatt, P. M. Kintner Jr., and S. P. Powell. Attitude estimation for a flexible spacecraft in an unstable spin. *J. Guidance, Control, and Dynamics*, 25:88–95, 2002.

[62] H. Schaub, P. Tsiotras, and J. L. Junkins. Principal rotation representations of proper nxn orthogonal matrices. *Int. J. Engineering Science*, 33:2277–2295, 1995.

[63] F. Lizarralde and J. Wen. Attitude control without angular velocity measurement: a passivity approach. *IEEE Trans. on Automatic Control*, 41(3):468–472, 1996.

[64] F. Caccavale and L. Villani. Output feedback control for attitude tracking. *Systems & Control Letters*, 38:91–98, 1999.

[65] M. R. Akella. Rigid body attitude tracking without angular velocity feedback. *Systems & Control Letters*, 42(4):321–326, 2001.

[66] J. Tsinias. Observer design for nonlinear control systems. *Systems & Control Letters*, 13(2):135–142, 1989.

[67] M. R. Akella, D. Seo, and R. Zanetti. Attracting manifolds for attitude estimation in flatland and otherlands. *J. Astronautical Sciences*, 2007.

[68] W. J. Rugh. *LINEAR SYSTEM THEORY*, chapter 6,15. Prentice Hall, 1996.

[69] E. Panteley, R. Ortega, and P. Moya. Overcoming the detectability obstacle in certainty equivalence adaptive control. *Automatica*, 38(7):1125–1132, 2002.

[70] J. R. Wertz. *Spacecraft Attitude Determination and Control*, chapter 6,7. Springer, 1978.

Vita

Dong Eun Seo was born on Ausgust 3, 1973 in Jinju, Korea to Young Soon Han and Pan Jung Seo. He received Bachelor of Engineering degree in mechanical engineering from Korea Advanced Institute of Science and Technology (KAIST), Korea in February 1997, and Master of Science degree in mechanical engineering from Korea Advanced Institute of Science and Technology (KAIST), Korea in February 1999. He worked for Dasol Inc. in Seoul, Korea as a chief research engineer from 1999 to 2001. He enrolled in graduate school at The University of Texas at Austin in Fall 2001. While his education in Aerospace Engineering and Engineering Mechanics, Dong Eun worked as both teaching assistant and graduate research assistant.

Permanent Address: Daechang Sen city Apt. #102 - 702
Bulgwang-2 dong, Eunpyung-gu, 122-042
Seoul, Korea

This dissertation was typeset with LaTeX 2_ε[1] by the author.

[1] LaTeX 2_ε is an extension of LaTeX. LaTeX is a collection of macros for TeX. TeX is a trademark of the American Mathematical Society. The macros used in formatting this dissertation were written by Dinesh Das, Department of Computer Sciences, The University of Texas at Austin, and extended by Bert Kay, James A. Bednar, and Ayman El-Khashab.